ANALYSIS OF ENGINE INDUCED VIBRATIONS OF MOTORCYCLES

By

Prashanth Dalawai

M/E/2004/M
D15a

DEPARTMENT OF MECHANICAL ENGINEERING

Indian Institute of Technology, Kanpur

FEBRUARY, 2004

ANALYSIS OF ENGINE INDUCED VIBRATIONS OF MOTORCYCLES

A Thesis Submitted

in Partial Fulfillment of the Requirements

for the Degree of

MASTER OF TECHNOLOGY

by

PRASHANTH DALAWAI

to the

DEPARTMENT OF MECHANICAL ENGINEERING

INDIAN INSTITUTE OF TECHONOLOGY, KANPU

FEBRUARY, 2004

M.E.
पुरुषोत्तम विनायक केलकर पुस्तकालय
भारतीय प्रौद्योगिकी संस्थान कानपुर
अवाप्ति क्र० A 148432

th
ME/2005/M
D15C

A148432

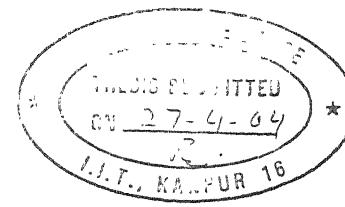

CERTIFICATE

It is certified that the work contained in the thesis entitled ***"ANALYSIS OF ENGINE INDUCED VIBRATIONS OF MOTORCYCLES "***, *by " Prashanth Dalawai"*, has been carried out under our supervision and that this work has not been submitted elsewhere for a degree.

DINESH KUMAR
(General Manager)
Department: Research and Development.
L.M.L Ltd., Kanpur

N.S. VYAS
(Professor)
Department: Mechanical Engineering.
I.I.T. Kanpur

6/2/04

February 2004

ABSTRACT

Name of the Student: PRASHANTH DALAWAI Roll No: Y110524
Degree for which submitted: M. Tech Department: Mechanical Engineering.
Thesis Title: ANALYSIS OF ENGINE INDUCED VIBRATIONS OF MOTORCYCLES
Name of the thesis supervisors: 1. Dr. N.S. VYAS,
2. Mr. DINESH KUMAR
Month and Year of thesis submission: February, 2004

A study involving computational simulation and experiments on motorcycles (110 cc to 150 cc) has been carried out to understand their vibration behavior and suggest modifications on a specific component for reduction in levels of vibration.

Finite element technique is used as a computational modeling tool. Geometry, modal damping and engine shaking force spectrum are the parameters needed in building a model for a comprehensive dynamic analysis of the vehicle. Free and forced vibration structural models have been built and resonant acceleration levels and stresses are computed. Experimental investigations involve tests on four motorcycles of different makes. Tests are carried out under identical conditions over full range of engine excitation. The vibration signatures are measured at selected locations and dynamic characteristics in the form of natural frequencies, damping factors, critical speeds and the vibration harmonics are identified. A comparison between the vehicles is carried out to explore the vibratory characteristics and overall information about vehicle conditions. For the sake of simplicity and practical possibility the experiments were performed in the laboratory. A comparison is also made between results from the finite element model and experimental results. The steering bar of a specific vehicle is selected for further modeling and suggesting the modification in reduction of vibration levels. Passive vibration control techniques such as change in stiffness, localized addition of masses (alteration of location, material and size), and combination of these are investigated through finite element simulation and the results of various possibilities are compared.

STATEMENT OF THESIS PREPARATION

1. Thesis Title	"ANALYSIS OF ENGINE INDUCED VIBRATIONS OF MOTORCYCLES "
2. Degree for which submitted	Master of Technology
3. The thesis guide was referred to for thesis preparation	Yes
4. Specifications regarding thesis format have been closely followed	Yes
5. The contents of the thesis was organized according to the guidelines	Yes

(Signature of the Student)

Name: Prashanth Dalawai

Roll No.: Y110524

Department: Mechanical Engg.

ACKNOWLEDGEMENTS

I would like to express my gratitude and sincere thanks to my thesis supervisors Dr. N. S. Vyas and Mr. Dinesh Kumar for their guidance, suggestions and encouragement. I am also thankful to them for introducing me to the experimental and computational aspects of vehicular vibration and its importance in real situations.

I am indebted to Mr P. S. Ashok, Mr. Sumant Pathak and the management of LML Limited for their support in taking up the M.Tech course and providing me the vehicles and other facilities to accomplish this work.

I am grateful to Mr. T. J. Christopher and Mr. R. M. Alagu - whose contribution has been crucial - for their tips and suggestions on motorcycle measurements and design. Special thanks are due to Mr. S. K. Mishra, Mr. Imran Khan and Mr. Rohith Reja for helping me carry out the on-road and laboratory experiments. I am thankful to Mr G. M. Marathe for helping me in deciding the engine shaking force. I am also thankful to Mr. Ankur Saini, Mr. C. Arun Sankar and Dr. V. Raghuram for their help in using MAT lab, ANSYS and FFT analyzer effectively. I appreciate Mr. S. P. Sinha and Mr. J. P. Verma for their help in sorting out system and hardware problems, Mr. R. K. Pal, Mr. S. Srikanth, Mr. H. Chelladuri, Mr. R. K. Singh and Mr. N. R. K. Reddy for their co-operation in weight measurement, typing and material collection. I also thankful others who helped in the course of this work.

CONTENTS

NOMENCLATURES

1. SYMBOLS

A	Area, mm^2
a	Acceleration, g
D	Cylinder bore, mm
d	Displacement, mm
F	Force, Newton
g	Gravitational acceleration, 9.81 m per $second^2$
L	Piston stroke, mm
l	Connecting rod length, mm
M	Moment, Newton - mm
m	Mass, kg
N	Crankshaft rotational speed, rpm
p	Resonant frequency, cycles per second
	Cylinder pressure, MPa
R	Reaction, Newton
r	Radius, m
T	Torque, Newton - mm
V	Volume, in mm^3
v	Velocity, mm per second
β	Angular position of counter weight, degree
θ	Crank angle, degree
ω	Excitation frequency, radians per second
ζ	Modal damping, decimal

2. ABBREVIATIONS

ALI	Automotive Lift Institute
BC	Bottom - Center
CA	Cylinder Axis
CDI	Capacitor Discharged Ignition
CSA	Crank Shaft Axis
CR	Compression Ratio
FEM	Finite Element Model
FFT	Fast Fourier Transform
FRF	Frequency Response Function
ISO	International Organization for Standardization
mep	Mean effective pressure
ohc	Over head camshaft
o-p	Zero to peak of measured value
RMS	Root - Mean - Square
TC	Top - Center

3. NOTATIONS

[i]	i^{th} reference number
x_i	i^{th} direction on variable x
x_r	Resultant of variable x

LIST OF FIGURES

LIST OF TABLES

Chapter - 1

INTRODUCTION

Increasing demands of safety and reliability on motorcycles either defined by government regulations or generated through the demands of consumers have created new challenges for dynamic analysis of such vehicles. Better understanding of dynamic properties and vibration response of vehicles using analytical, computational or experimental means or a combination of them is crucial to the challenges posed by these demands.

Contemporary designs of vehicles require them to become increasingly lighter, flexible and stronger. These demands on the vehicle structures often result in making them more susceptible to unwanted vibrations. The vibrations lead to discomfort and fatigue to the driver and pillion-rider, damage of mating components and deteriorate the machine performance. They also cause hazardous noise pollution. The competition between rival automobiles manufactures means that the vehicle with most vibration and noise can lose the market. The design of vehicles to ensure vibration comfort is often made using finite element analysis as a computer modeling approach. This computational analysis requires rigorous theoretical guidance to ascertain meaningful outcomes in relation to structural dynamics and this computer modeling alone cannot determine completely the dynamic behavior of structures, because certain structural properties such as damping and non linearity do not conform to traditional modeling treatment. The computational modeling needs the additional help in resolving the boundary condition uncertainties. The experimental techniques have complemented modeling in determination of structural properties.

A vibration analysis generally follows four steps. First, the structure is identified with its mounting and loading locations. Second, the dynamic properties are determined. Third dynamic loads are estimated and in fourth, these loads are applied to an analytical or computational modal to determine its response.

1.1 Vehicle Vibration and Exposure

Vibrations on a vehicle can be classified as road-induced vibrations, engine-induced vibrations and wind-induced vibrations. The unevenness of road profile generates the impact loads during accelerating, braking or cornering of the ride. The crank unbalance, combustion load and misalignment in the driveline shake the engine, which causes the vibration in the vehicle. Wind causes a high frequency fluctuating drag load that causes vehicle components to flutter. Road and wind-induced vibrations are occasionally periodic and always random. However, engine-induced vibrations are mainly periodic. These can be decomposed to harmonic components to understand their effect and contribution. Wind-induced vibrations are small in magnitude in a two-wheeler especially at normal driving speeds. The road-induced vibrations are high amplitude, low frequency type of the order 20 Hz. The engine-induced vibrations can be observed up to ten times of the running frequency or at frequencies even greater than 1 kHz.

The combined road, engine and wind-induced vibrations are of great interest because these represent the true dynamic performance of the vehicle. However obtaining good resolution data and identifying individual harmonics in a single spectrum containing low and high-order vibrations is difficult. The vibration on the super-structure makes the signal more complex. The reliability of data and repeatability on road condition is even more difficult. As far as the vibration level assessment of vehicles on road is concerned, all vehicles have to be exposed to same loading environment. Hence, the vehicle geometry, damping, and engine-shaking spectrum are sufficient to assess the vibration levels.

Vehicles possess wide range of critical speeds. Generally the suspension critical lies between 1 and 5 Hz; the steering system critical between 20 and 60 Hz; frame critical between 20 and 50 Hz; crank cases critical between 50 and 100 Hz and the crank shaft critical between 1.5 and 2 kHz. The excitation frequency lies in the range 25 Hz and 175 Hz. The vehicle exhibits different damping in different directions.

Table 1.1 gives the summary of vehicle vibrations, characteristics and common actions.

TABLE 1.1 - **Vehicle vibrations**

Parameter	**Road - Induced**	**Engine - Induced**	**Wind - Induced**
Nature	Random	Periodic	Random
Amplitude	Low order	Medium	Low at low speeds
Frequency	Up to 20 Hz	Up to 500 Hz	Up to 1kHz
Source	Road undulation Impact load	Net shaking torque due to combustion drive train, Inertia, power train and fraction	Fluctuating drag load
Effect and causes	•Dangerous to human body and creates discomfort •Creates road-noise	•Damage and deterioration of vehicle components •Creates engine-noise	•Decreases the stability of ride •Decreases the fuel economy and increases engine cooling •Creates wind-noise
Primary Action	Active isolation	Minimization of shaking torque	Aerodynamic design

The human body is very sensitive to the vibrations of the frequency range 0.5 Hz to 80 Hz. Most of whole body resonant lies in the range from 2 to 8 Hz. The vibrations that lead the discomfort are whole-body, hand-arm, seat, seat-back vibrations and feet-vibrations. Whole body vibrations occur due to gross unsteady motion of the vehicle. These are transmitted to the body as a whole, through the supporting surface and hand-arm vibrations are the vibrations, which are transmitted to hand and arm. A summary of vibration exposure, characteristics and common primary actions are given in the Table 1.2

TABLE 1.2 - **Vibration exposure**

Exposure	**Whole Body**	**Hand / Leg arm**	**Eye**
Through	Seat	Steering bar/Foot rest	Retina
Amplitude	High	Medium	Small
Frequency	1 to 80 Hz	5 to 1500 Hz	2 to 20 Hz
Affects	Entire body	Fingers, arm mussels	Eye ball
Effects causes and Losses	•Physical damage •Circulatory or urological system •Headache and shakiness •Decrease the performance	•Sensation •white finger attacks •grip strength •damage to blood vessels and nerves •light touch	•Vision blurred
Primary Action	Active Isolation	•Increase Mass •Reduce Force	Increase the viewing distance

Vibrations on a vehicle lead to a noisy environment, which cases hearing interference with speech and annoyance. The vehicle noise can be classified similar to vehicle

vibrations. The engine noise are of high amplitude up to 90 dB(A), the tire and wind noise can be seen up to 80 dB(A). The threshold human ears level is 130 dB(A). The ears are sensitive for high frequency noise with the range between 1 to 5 kHz.

In the current chapter, the Indian motorcycle market, available standards for vibration evaluation on human and machine and their limits for damage and discomfort are reviewed.

1.2 Objective and Standards

The objective of this study is to compare the different motorcycles in the range of 110 cc to 150cc for vibration levels and determining the presence of any malfunction due to abnormal operation of the engine. The abnormal malfunction causes the damage of the respective component or leads to discomfort, fatigue and impairment of the passenger. The accelerations associated with occupational exposure to hand-arm vibrations normally range from 2-50m/s^2 RMS, while those encountered in whole-body vibration range from 0.1 - 40m/s^2. The severer vibrations that can come on the engines are up to 15mm/s RMS velocity at running frequency. The total occupational noise level is limited to 85 dB(A).

1.2.1 Indian Motorcycle Industry 2002-03

The market trend has showed that the two-wheeler industry should close fiscal 2002-03 with a total of 5.1 million units. According to the data from motorcycle makers on an average 4,24,800 units of two-wheelers are sold every month in Indian market of which 3,15,300 (representing 74 %) are motorcycles.

Motorcycle segment is divided in to three sectors as shown in Fig. 1.1, viz the economy category, executive class and performance category. The economy motorcycles constitute 32% of total Indian motorcycle pie. Here the simplicity, pricing and fuel efficiency are the prime factors driving the sale. The other end is the premium segment. This is a niche market share with 14% of the pie, where style and performance are major factors. The executive segment alone accounts for the remaining 54% where the sales are defined by mileage from economy with performance from premium segment for mid range price.

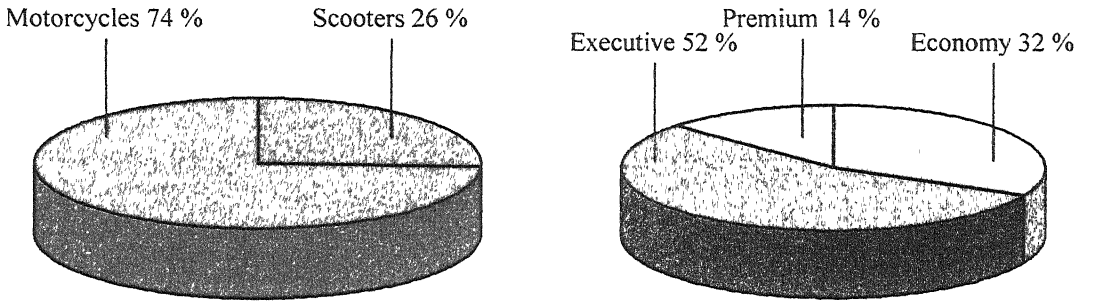

(a) : **Two-wheeler pie** (b) : **Motorcycle pie**

FIGURE 1.1 - **Indian two - wheeler pie diagrams**

1.2.2 ISO Evaluation for Human and Vehicle Vibration

The available ISO standards for evaluating the human and vehicle vibration are;

(i) Human and Machine Vibration Evaluation: ISO standards assess the vibration on human body based on the equivalent acceleration value; the various frequencies, which make up the vibration; the direction of excitation; and the time of exposure. This standard distinguishes the vibrations based on the working efficiency, health or safety, comfort and predicts the number of years for developing the passable syndromes.

ISO 2631: Guide for the evaluation of human exposure to whole body vibration.

ISO 5349: Measurement and assessment of human exposure to hand transmitted vibration.

ISO 7096: Laboratory evaluation of operator's seat vibration.

ISO 2372: Evaluation of vibration of general machines.

ISO 3945: Evaluation of vibration of large machines based on the foundation.

(ii) Human and Machine Noise Evaluation: ISO standard classifies the noise severity based on the size of the machine. These standard determines the acceptable noise levels in the specified frequency range.

ISO 1999: Assessment of occupational noises.

ISO 362: Measurement of noise emitted by vehicles.

1.3 Common Malfunctions in a Reciprocating Machinery

Machinery malfunctions provide reliable information in estimating the severity, product life, diagnosing the faults and helping forecast the future failures of the machinery.

The exact time for the fatigue occurrence or the endurance limit is predicated based on the maximum stress and relevant fatigue data of material for the components. The vibration velocities, accelerations and displacements are used in predicating the life of the product. The successful use of these vibration techniques in determining the health of rotating machinery has motivated their use in reciprocating machines. Unlike rotating machines, the reciprocating machines house wide number of revolving, sliding and intermittent-motion parts. Careful understanding of their dynamic behavior and identifying their source of vibration can help in determining the health of reciprocating machine. This section reviews the currently available strategies for assessing the overall condition of machinery. The references can be made the research made by Eisenmann and Eisenmann (1997), deBotton et al (1999) and Rao (2000).

Combustion Process: Since in a four-stroke single cylinder engine for every two revolution of crankshaft one firing occurs, hence this malfunction is characterized by half the frequency of engine running speed. This malfunction is predominant near the combustion chamber. When the engine misfires, this leads the uneven state of operation and excites the vibrations in the driveline. This process is identified by the presence of lower amplitude malfunctions at sub-harmonic and massive reduction in the engine rpm. The early and late combustion processes are observed by the dispersion the firing frequency amplitude to sub-harmonics. Under no load or less loaded conditions, all the integer harmonics are present with one per revaluation component.

Unbalance: Unbalance forces arise due to eccentricities between the mass and geometric centers either present in the design stage or caused by manufacturing effects or damage during the operation. This malfunction prominently occurs at frequency corresponding to running speed of engine.

Bearing Defects: Bearings are deigned to operate in a very close clearance with bearing race and rolling element. They provide very high stiffness and very low damping. Under the application of shock or repetitive cyclic loads the internal clearance and wear will increase results in bearing failure. The presence of high clearance or wear in the bearing will exhibit at higher order harmonics or sub-harmonics.

Mechanical Looseness: Looseness of rotating and sliding components such as flywheels, sleeves, thrust collars, crank pins, piston pins and structure mounting cause internal friction problem. These malfunctions are characterized by vibration at shaft critical speed for rotating elements and striking frequency for sliding members. Loose assembly of bearings give rise to sub-harmonic at half or one-third of running frequency.

Misalignment: The coupling misalignment causes friction and deflection forces, which cause the shaft bearing system to deflect, creating secondary phenomena such as harmonic resonance. These malfunctions are observed at twice the running speed, some times third and forth running speed.

Structural Resonance: When the base structure or the component itself exited near its resonant frequency it gives rise to very large amplitude vibrations. These malfunctions general occur any where at sub harmonics or higher order harmonics.

Gear Trains: The shafts in a gear train generate malfunctions equal to the running speed or multiple of running speed of the shaft. The gear teeth meshing frequencies are also prominent in a gear train. These show higher amplitudes when the gear tooth is broken or worn out.

Shaft Rubbing: The contact of shaft with any other mechanical elements cause the rubbing and leads to frictional losses. Most of these rubbing malfunctions occur at twice the running speed but some times lower and higher running speed are also observed.

1.4 Literature Review

Whipple is known to have carried out the first theoretical study on the stability of single-track vehicle in 1899. He studied the stability of a bicycle while modeling the tire as a rigid element. The first quantitative work in motorcycle vibrations was made by Sharp (1971) who investigated motorcycle oscillations due to road undulations and cornering. He described conditions on particular road, which cause severe steering oscillations. Koenen and Pacejka (1980) studied the vibration modes of Motorcycle in curves. Nishimi et al. (1985) studied the rider behavior using a passive model. Bayer (1988) experimentally investigated the influence of design parameter on the damping of suspension vibrations. Hucho (1987) studied the importance of aerodynamics and wind induced vibrations in road vehicles. Sujatha and Ramamurthi (1999) carried out a computational analysis of motor vehicles. They investigated various modal techiniques in computation of vehicle vibrations. The studies made by Senthil and Sethi (1999) give guidance evaluation of ride quality.

The vibration signature analysis of various rotating machines has been summarized by Eisenmann (1997). Macian et al. (1998) have measured the vibrations of a reciprocating engine and concluded that the vibration signature of the engine block provide useful information regarding the malfunctions in the cylinder. deBotton et al. (1998) performed a series of experiments and measured the vibrations of an engine block while the engine is running under normal and abnormal conditions. They found that the vibration level of the engine provides reliable information regarding the engine condition and gives source of the malfunction.

1.5 Present Study

The objective of present work is to carry out modeling and experiments on motorcycles to understand their vibration behavior and suggest modifications on a specific component for reduction in levels of vibration.

Standard finite element package has been employed to carry out structural modeling of a selected vehicle. Free vibration characteristics have been obtained in terms of natural frequencies and mode shape. Excitation forces arising from the engine, in the form of combustion forces and inertia forces have been computed analytically and fed as input to the forced vibration analysis. Damping is determined from experimental results, using two different techniques and also fed as input to the program to theoretically establish forced vibration levels in terms of g-levels and von-Mises stresses.

For experimental work, four different motorcycles from different manufactures in the range of 110 cc to 150 cc are selected and tested for vibration response in identical conditions over full range of engine excitation. The vibrations are measured at the engine cylinder head and mounting, and human interface locations like the steering bar tip, foot rest bar tip and seat mounting. Frequency domain analysis is carried out. The dynamic characteristics of the vehicle in the form of natural frequencies, damping factors, critical speeds and the vibration harmonics are identified and a comparison between various vehicles is carried out.

Further modeling is carried out to improve the vibration characteristics of the steering bar. Passive vibration control techniques such as structural design change, localized mass additions (Various location, material and size) and combination of these are investigated.

Vehicle modeling and simulation has been described in Chapter 2. Experimental investigations are discussed in Chapter 3. A brief description of vibration control techniques is followed by modeling of suggested modifications to steering bar, in Chapter 4. Conclusions and scope for the future work are given in Chapter 5.

CHAPTER - 2

COMPUTATIONAL MODELLING OF VEHICLES

Computer aided design and analysis have made vehicle testing and evaluation a virtual, persistent and cost-effective process. In this chapter development of the Finite Element model of the vehicle and the subsequent free and forced vibration analysis is described. The model essentially involves the steering assembly, frame, engine supports, footrest and swing bar assembly. A combination of three-dimensional beam, shell and brick elements is employed.

Sources of vibration in a motorcycle engine include unbalance force components and moments from reciprocating and rotating parts, internal impulsive forces due to the combustion in the cylinder, drive train load from the wheel, power train load, internal friction and misalignment and clearances in rotating or reciprocating unit.

These excitation forces are calculated for a sample case and employed for forced vibration response computation.

2.1 Vehicle Model Description

The motorcycle chosen for modeling is a 110 cc vehicle shown in Fig. 2.1. The vehicle belongs to the executive segment of the market with specifications are given in Table 2.1 (a – d).

Table 2.1 (a) : **Engine details**

Type	Single cylinder, 4-stroke, air cooled
Valve Train	2 valve, ohc
Displacement	109.15cc
Bore x Stroke	53mm x 49.5mm
Comp Ratio	9.0:1
Max Power	8.5bhp@7750rpm
Max Torque	10.5Nm@4500rpm
Power to Weight	75.89 bhp/ton
Ignition	CDI electronic

Table 2.1 (b) : **General details**

Kerb Weight	112kg
Max Payload	130kg
Wheelbase	1230mm
Length	2010mm
Width	NA
Height	1080mm
Ground. Clearance	165mm
Minimum Turning Radius	NA
Fuel Tank Capacity	12.2liters

Table 2.1 (c) : **Gear - box details**

Clutch	Wet multi plate
Primary Reduction	3.579 Gear Drive
Final Reduction	2.859 Chain Drive
Gear Box	4-speed constant mesh
Gear Ratio	3083, 1.882 1.318, 1.041

Table 2.1 (d) : **Chassis details**

Type	Tubular single cradle
Fr. Suspension	Telescopic forks
Rear Suspension	Adjustable Swing arm
Wheel size F/R	1.6 X 18 / 1.6 X 18
Tires F/R	2.75 X 18 / 3.00 X 18
Type	Tubular single cradle

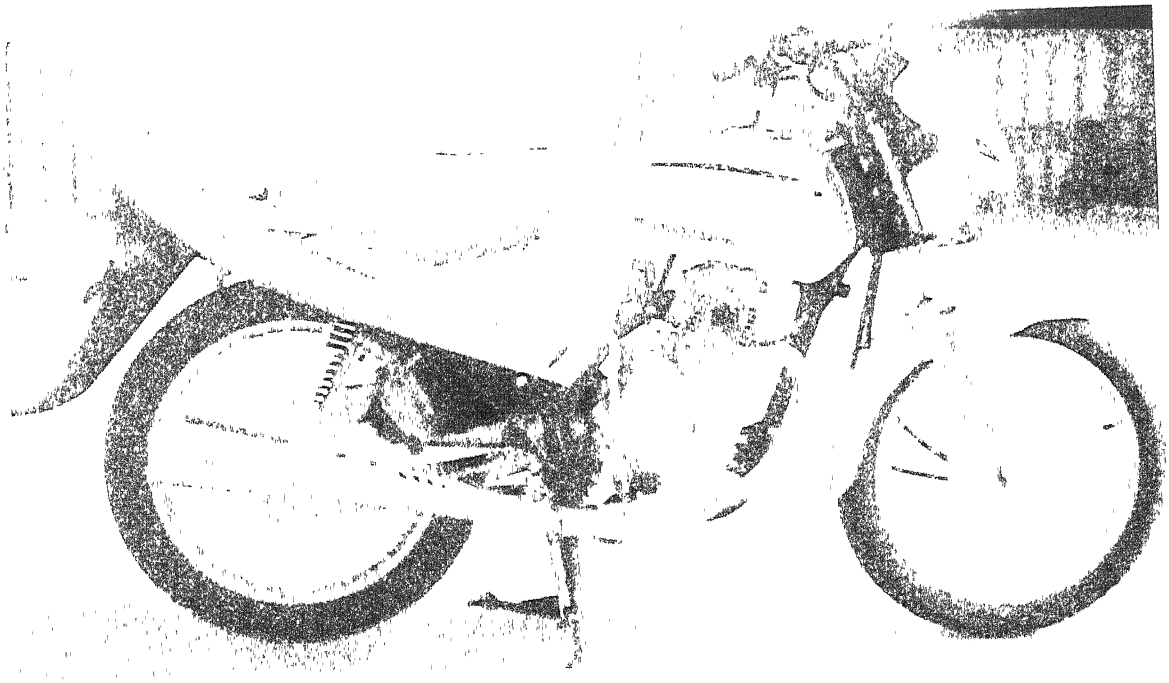

FIGURE 2.1 - **Photograph of the study vehicle**

Vehicle Coordinate System

The coordinate system employed for vehicle analysis is shown in Fig. 2.2, with the user co-ordinate system (UCS) located at mid location of swing arm pin. X-axis (Lateral direction) being parallel to the crankshaft axis in horizontal plane; Y-axis (Vertical direction) is perpendicular to crankshaft axis in vertical plane; and the Z –axis (Longitudinal direction) is perpendicular to crankshaft axis in horizontal plane. The orthogonal planes X, Y, Z are defined as per the ISO 6725 standard. Table 2.2 gives the dimensional extremis, with reference to Fig.2.1, of the two-wheeler chosen for analysis.

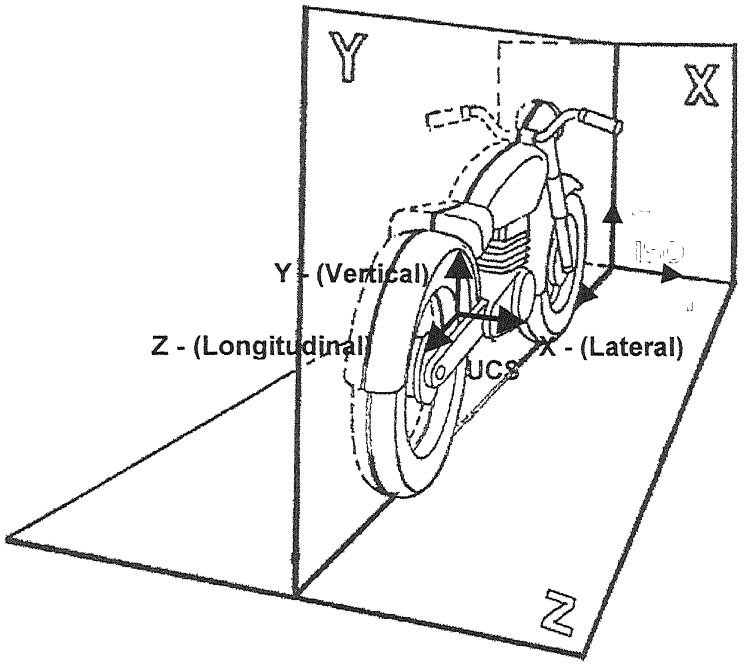

FIGURE 2.2 - **Vehicle coordinate systems**

TABLE 2.2 - **Model extremis**

Axis	+ Direction, mm	- Direction, mm
X	351.02	351.02
Y	594.19	165.00
Z	753.84	764.80

Engine Center of Gravity

The engine center of gravity is measured as per the Automotive Lift Institute (ALI) specifications. The engine was suspended using the hydraulic engine hoist through an engine mount and the plane passing through the engine center of gravity was determined. The test was repeated for other mounting points, also. Table 2.3 gives the co-ordinates thus determined.

Table 2.3 - **Engine center of gravity**

Axis	Direction, mm
X	0.0
Y	53.73
Z	-201.95

2.2 Model Development

The vehicle has been discretised as shown in Fig 2.3. The model represents the steering assembly, frame, engine mount, footrest and swing bar assembly. The frame tubes, front forks and footrest bar are modeled using three dimensional (six degree of freedom per node) linear beam elements with respective cross section along the centerline. The footrest plates, stiffening bracket of frame and bridge fork top plates are modeled using linear shell elements (six degree of freedom per node). The shell elements are modeled at the middle plane with respective thick nesses. The steering bar tube is modeled with linear shell element at average radius, while steering bar holder pieces are represented using eight-noded brick elements. The steering bar accessory and adjustable footrest pad masses are modeled using mass element at their respective center of gravity. Adjustable swing bar is modeled using three dimensional beam elements. The front and rear axles are modeled using rigid elements.

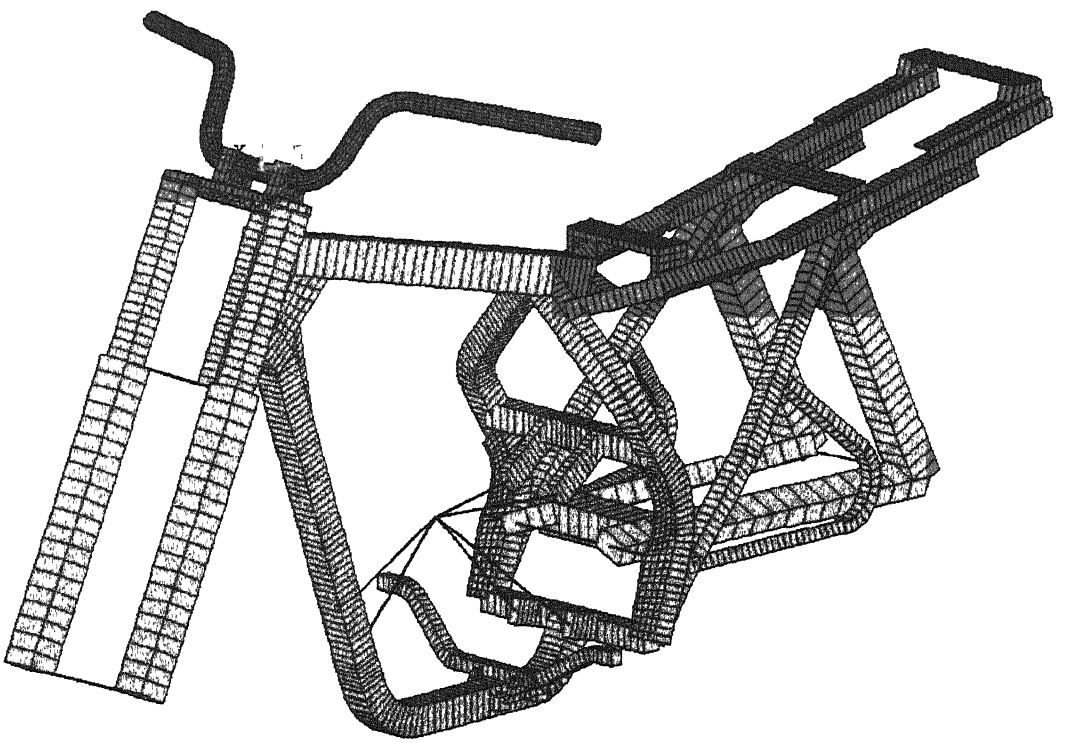

FIGURE 2.3 - **FEM model of a motorcycle structure (With tube extremes)**

The engine is modeled using a lumped mass at the engine center of gravity. This mass is connected to the engine mounting locations using rigid elements. In the loaded condition the mass of the rider has been lumped appropriately on the seat frame at seat resting locations. Table 2.4 gives the summary of the finite element statistics.

TABLE 2.4 (a) : **FE statistics**

Type	Element	Number
1	Shell	3419
2	Beam	983
3	Solid	128
4	Rigid	74
5	Mass	5

TABLE 2.4 (b) : **FE model size**

Type	Quantity	Number
1	Elements	4609
2	Nodes	4758
3	DOF	28050

Mass Compression Between Measured and Analysis

For a comparison the vehicle structural sub assemblies mass is measured and compared with the total mass of the FE model. Table 2.5 gives the summary of the component weights and finite element mass distribution.

TABLE 2.5 (a) : **Actual mass**

Type	Actual component mass	
	Component	Mass, kg
1	Steering bar asm	09.001
2	Frame	16.694
3	Swing asm	06.498
4	Foot rest asm	01.276
5	Engine asm	32.250
	Total	**65.971**

TABLE 2.5 (b) : **FE mass distribution**

Type	Finite element mass	
	Element	Mass, kg
1	Shell	03.896
2	Beam	24.750
3	Solid	00.146
4	Mass	36.095
	Total	**64.887**

There is some difference between the actual measured weight of the vehicle and the FE model weight. This is due to the unaccounted welding, small brackets and manufacturing deviations.

2.3 Vehicle Mounting Conditions

The structural assembly rests on the front and rear wheels during the engine excitation. This was approximated as simply supported conditions at both ends; so the front wheel center node rear wheel center nodes are arrested in all directions.

2.4 Vehicle Laden Conditions

Vehicle is modeled as carrying a rider weighing 68 kg. The rider weight was distributed at the rider-seat, footrest and steering bar (making use of ISO 6549 standard H point machine elements and mass distribution).

2.5 Free Vibration Characteristics

First ten fundamental modes are computed for un-laden and laden conditions and tabulated in the Table 2.6 Figure 2.4 (a-j) shows the first ten fundamental mode shapes with laden conditions. These modes shapes lies in the in the range of zero to 100 Hz. While there is a correspondence between the natural frequencies of the vehicle in un-laden and laden conditions, it can be seen that the system is significantly altered with consideration of the rider mass. For, example in the un-laden condition the first mode of vibration has a natural frequency of 43.97 Hz. This mode corresponds primarily to the bending of the bottom portion of the frame in the lateral direction. In the case of the laden vehicle the frame can be seen to vibrate in two bending modes - at natural frequencies 37.77 Hz and 45.29 Hz. While the first mode corresponds to predominantly top portion vibration, the second mode corresponds to a predominantly bottom portion vibration. It can be seen that the predominantly top portion mode does not exist for the un-laden vehicle. This is due to the fact that for this condition the top-portion mass is not significant enough for this mode to get registered.

It can also be seen from Table 2.6 that, as expected, with laden condition, there is a reduction in the values of the natural frequencies in comparison the un-laden condition, for corresponding modes.

TABLE 2.6 - **Resonant frequencies and modes**

Sl No	Un-laden condition		Laden condition	
	Frequency In Hz	Mode	Frequency In Hz	Mode
1	43.97	Frame central bottom portion lateral bending	37.77	Frame central top portion lateral bending
2	54.06	Steering bar I lateral bending	45.29	Frame central bottom portion lateral bending
3	56.18	Steering bar I vertical bending	53.99	Steering bar I lateral bending
4	57.83	Steering bar I longitudinal bending	56.17	Steering bar I vertical bending
5	65.02	Steering bar II vertical bending	57.87	Steering bar I longitudinal bending
6	83.92	Frame back portion lateral bending	58.78	Frame back +central portion in phase vertical bending
7	106.79	Frame back +central portion in phase vertical bending	65.02	Steering bar II vertical bending
8	115.56	Foot Rest Right vertical bending	76.08	Frame back portion lateral bending
9	120.69	Frame back portion vertical bending + footrest longitudinal	80.11	Frame back + central portion out of phase lateral bending
10	124.43	Foot Rest Right vertical bending	87.80	Frame back +central portion out of phase vertical bending

The mode shapes are shown in Figs. 2.4 (a-j). These plots can be employed for identifying the regions, which would be more susceptible to vibrations at specific natural frequencies.

Mode I : 37.77 Hz

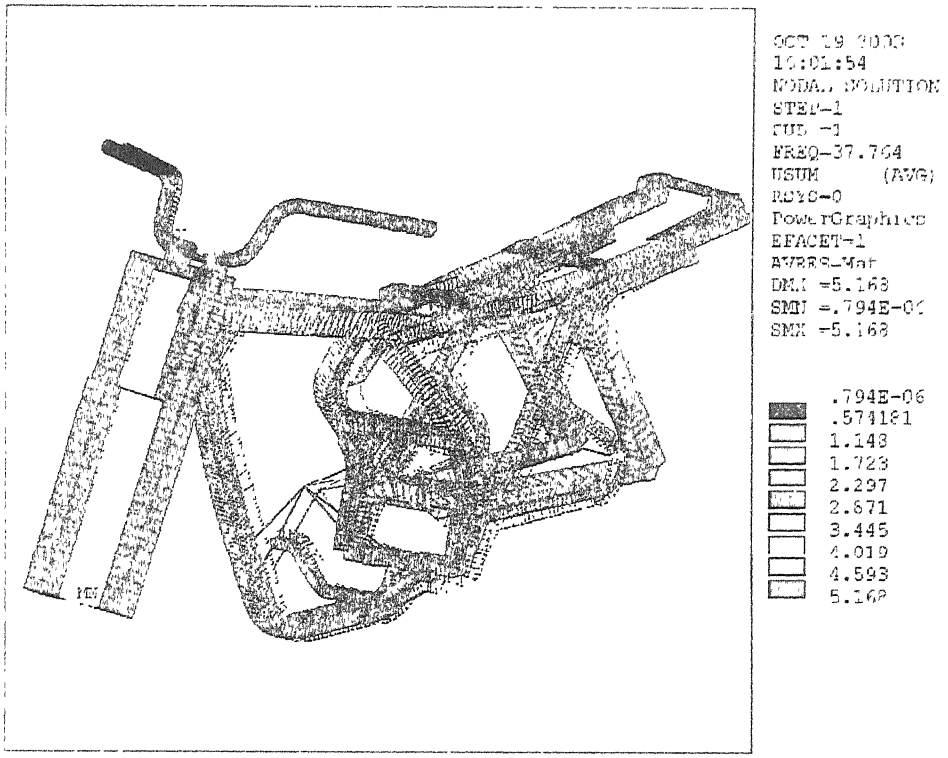

(a) : **Frame central top portion lateral bending**

Mode II : 45.29 Hz

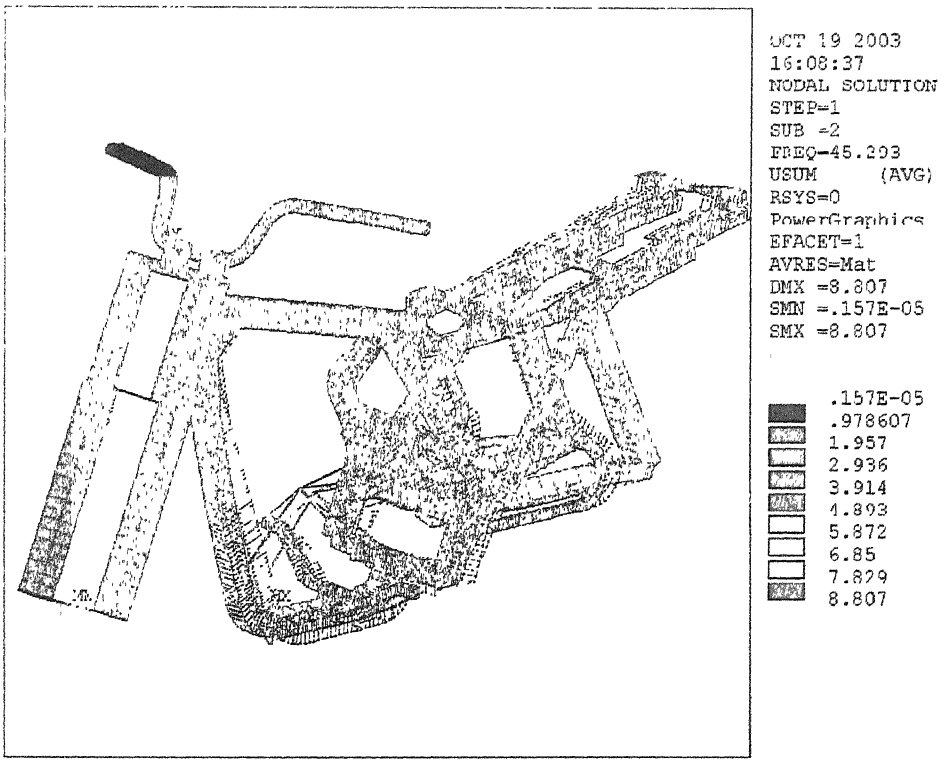

(b) : **Frame central bottom portion lateral bending**

FIGURE 2.4 (a & b) - **Vehicle mode shapes**

Mode III : 53.99 Hz

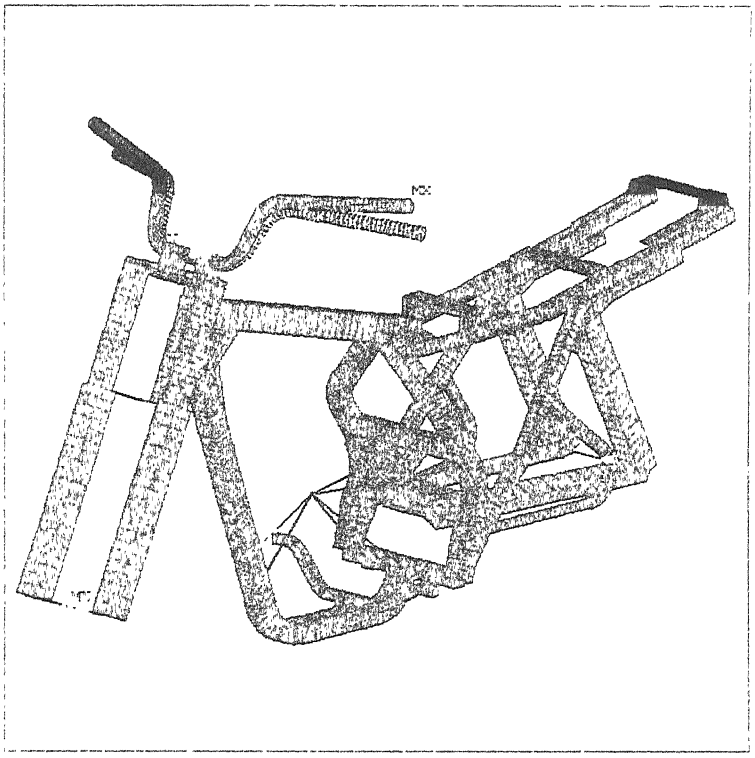

(c) : **Steering bar I lateral bending**

Mode IV : 56.18 Hz

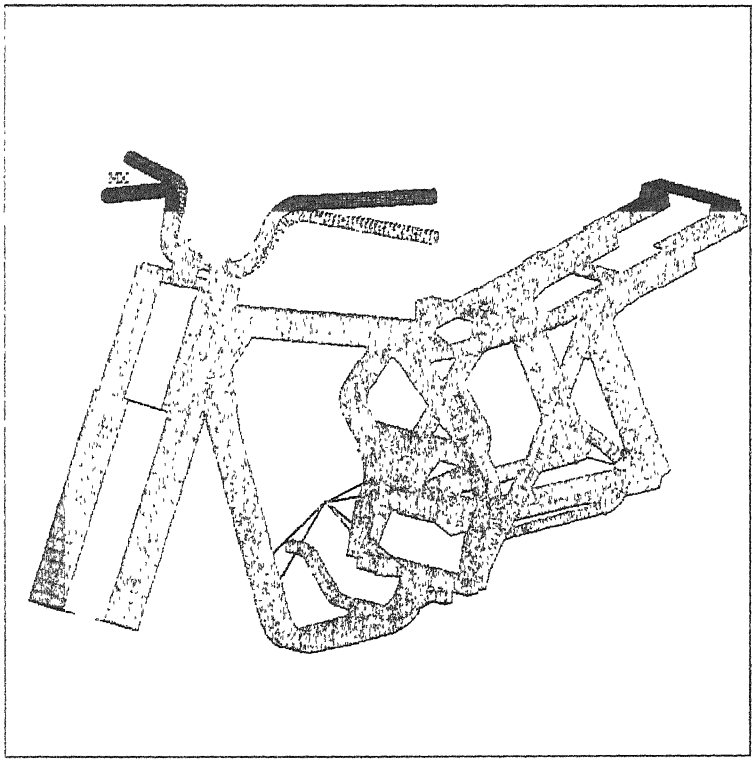

(d) : **Steering bar I vertical bending**

FIGURE 2.4 (c & d) - **Vehicle mode shapes**

Mode V : 57.86 Hz

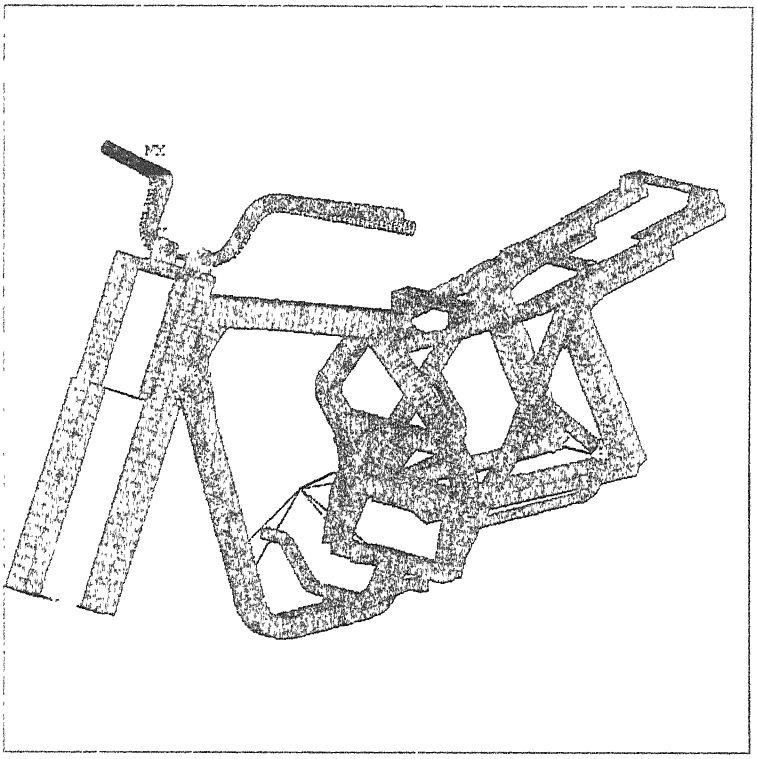

(e) : **Steering bar I longitudinal bending**

Mode VI : 58.76 Hz

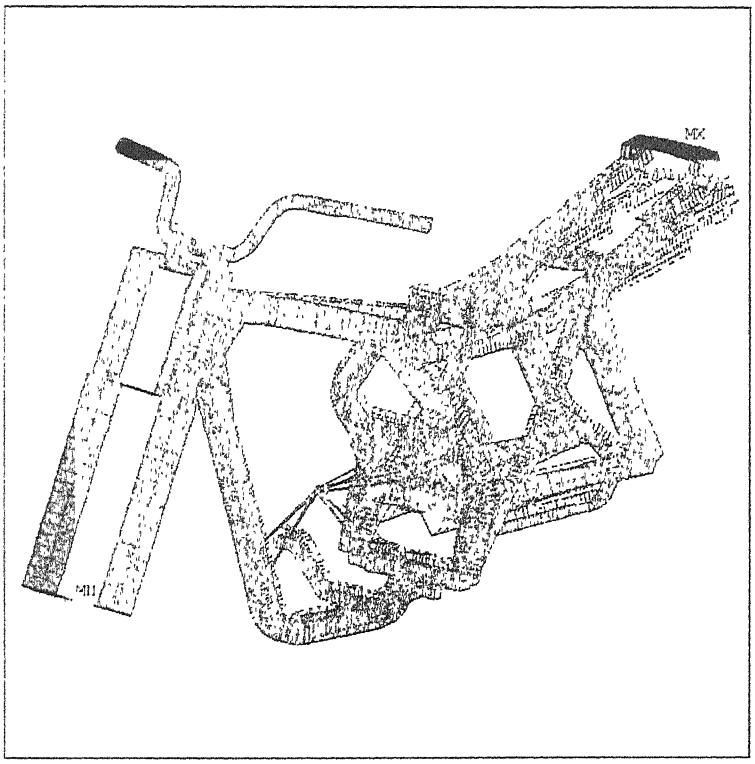

(f) : **Frame back +central portion in phase vertical bending**

FIGURE 2.4 (e & f) - **Vehicle mode shapes**

Mode VII : 65.02 Hz

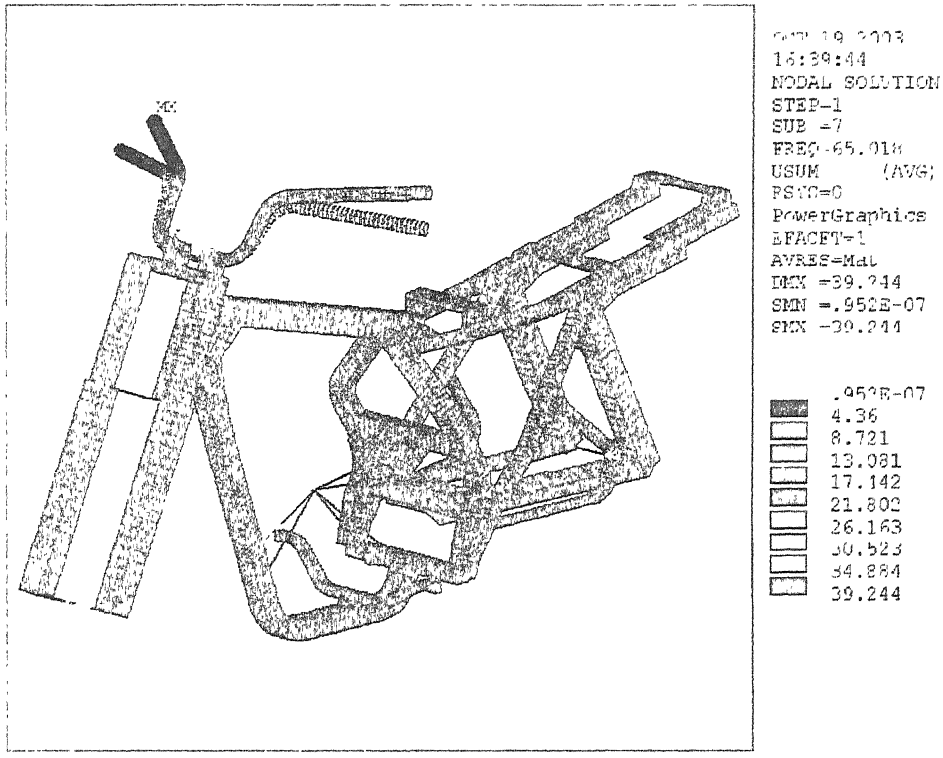

(g) : **Steering bar II vertical bending**

Mode VIII : 76.07 Hz

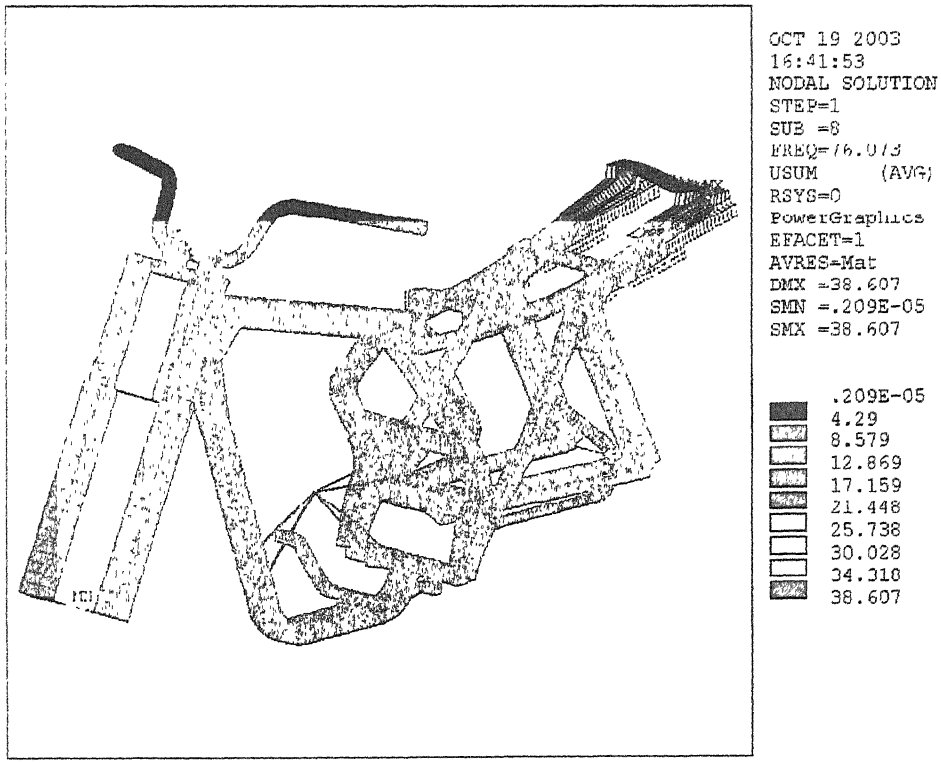

(h) : **Frame back portion lateral bending**

FIGURE 2.4 (g & h) - **Vehicle mode shapes**

Mode IX : 80.10 Hz

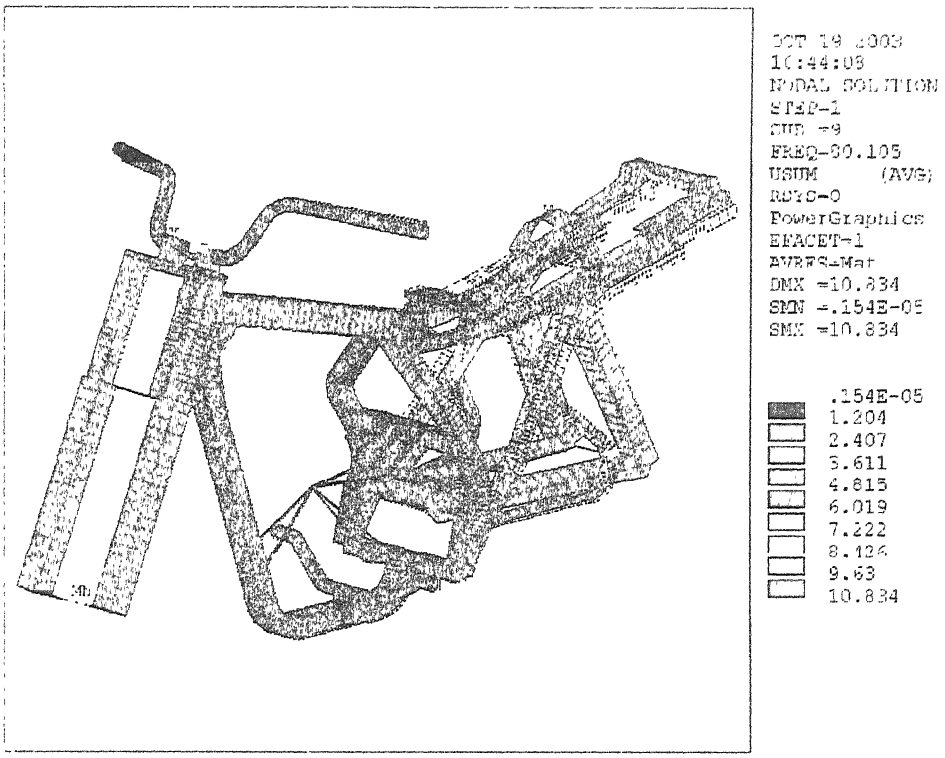

(i) : Frame back + central portion out of phase lateral bending

Mode X: 87.80 Hz

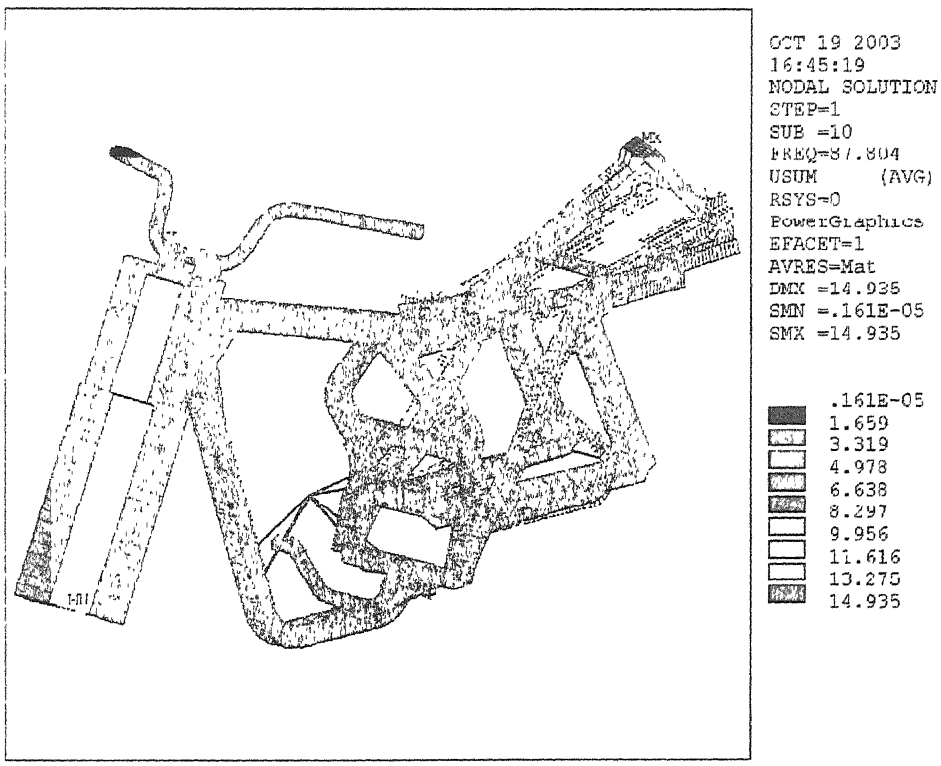

(j) : Frame back +central portion out of phase vertical bending

FIGURE 2.4 - **Vehicle mode shapes**

2.6 Campbell Diagram

The free vibration analysis has been further employed to construct a Campbell diagram for the vehicle under analysis. A Campbell diagram is commonly employed in Rotor dynamic analysis. It is a plot between the running speed of the machine and the natural frequencies and is employed to compute the critical speeds. The machine is under resonant vibrations at these critical speeds and running the vehicle at these speeds for long durations should be avoided.

The Campbell diagram is shown in Fig. 2.5 and the critical engine speed and the corresponding critical vehicle speeds are given in Table 2.7

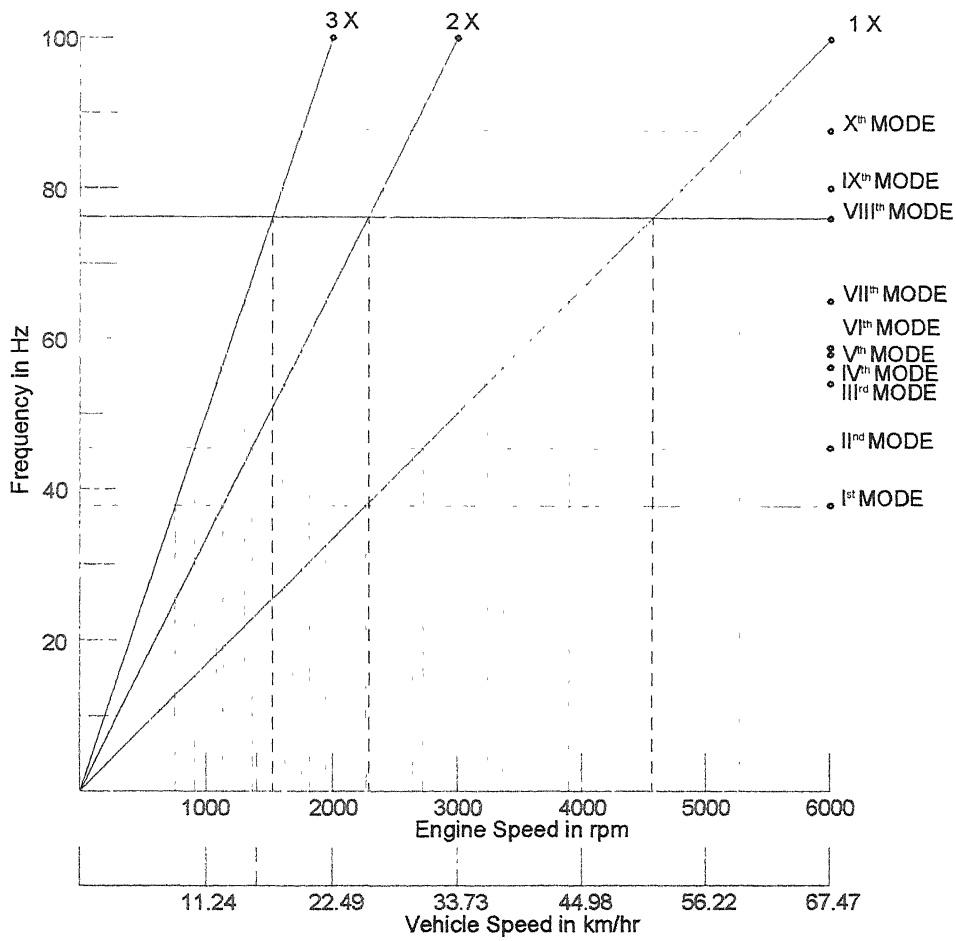

FIGURE 2.5 - **Campbell diagram for the vehicle**

TABLE 2.7 – **Critical speeds of the vehicle**

SL. No.	FREQ in Hz	MODE SHAPE	1 X		2 X		3 X	
			rpm	kmph	rpm	kmph	rpm	kmph
1	37.77	Frame central top portion lateral bending	2266.02	25.47	1133.01	12.74	755.34	8.49
2	45.41	Frame central bottom portion lateral bending	2724.36	30.62	1362.18	15.31	908.12	10.21
3	54.00	Steering bar I lateral bending	3239.82	36.42	1619.91	18.21	1079.94	12.14
4	56.19	Steering bar I vertical bending	3371.16	37.89	1685.58	18.95	1123.72	12.63
5	57.87	Steering bar I longitudinal bending	3471.90	39.02	1735.95	19.51	1157.30	13.01
6	58.78	Frame back +central portion in phase vertical bending	3526.68	39.64	1763.34	19.82	1175.56	13.21
7	65.02	Steering bar II vertical bending	3901.08	43.85	1950.54	21.92	1300.36	14.62
8	76.08	Frame back portion lateral bending	4564.74	51.31	2282.37	25.65	1521.58	17.10
9	80.11	Frame back + central portion out of phase lateral bending	4806.36	54.02	2403.18	27 01	1602.12	18.01
10	87.81	Frame back +central portion out of phase vertical bending	5268.30	59.22	2634.15	29.61	1756.10	19.74

2.7 Damping Estimation

The dynamic analysis of the vehicle needs the suspension modal damping. In absence of an analytical model for determining the modal damping, an experimental approach has been employed.

Two different methods were used for estimation of damping in the vehicle mounting. Mounting includes the vehicle suspension system, wheel and the tire. In the first method, Logarithmic decrement formula [12] (equation 2.1) was applied to the free vibration decay response to obtain the equivalent viscous damping in the fundamental mode.

$$\xi = \frac{\ln(X_0 / X_n)/n}{\sqrt{4\pi^2 + [\ln(X_0 / X_n)/n]^2}} \qquad (2.1)$$

The steering assembly was rapped in all three directions by impact from a light hammer to induce free vibrations. The vibrations were recorded in the respective directions. The resulting logarithmic signal was filtered for suspension fundamental modes. The filtered signals logarithmic decay curves are shown in figure 2.6 (a), (b) and (c). In higher modes damping was assumed to be the same as that in the fundamental mode.

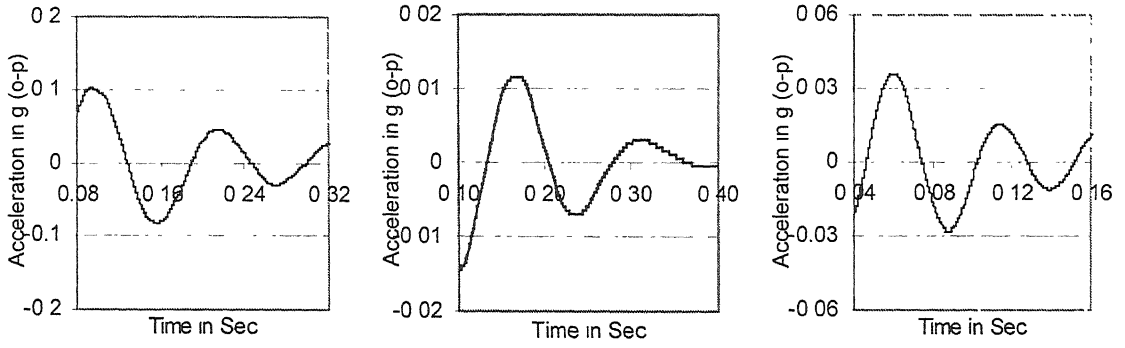

(a) : **X - X dirn rap - response** (b) : **Y - Y dirn rap – response** (c) : **Z - Z dirn rap - response**

FIGURE 2.6 - **Suspension decay curves**

Half power method was also employed to estimate equivalent viscous damping. The suspension was subjected to harmonic forcing and the response was recorded at various excitation frequencies. Typical Frequency Response Function curve is shown in Fig. 2.7. Damping was computed using [12],

$$\xi = (\varpi_2 - \varpi_1)/(\varpi_2 + \varpi_1) \qquad (2.2)$$

TABLE 2.8 - **Suspension characteristics under free vibration test**

Direction	Damping ratio, ξ
X	0.125
Y	0.214
Z	0.143

TABLE 2.9 - **Steering assembly characteristics under harmonic excitation**

Direction	Peak acceleration in g	Engine speed in r. p. m	Damping ratio, ξ
X	1.22	4100	0.132
Y	0.65	3460	0.243
Z	0.62	3125	0.171

As can be seen from the results damping has different values in the three directions, X, Y and Z. It can also be seen that values obtained from the two methods are comparable for a specific direction. For ease of computation in the FEM model-damping values in all three directions is assumed to be identical and a constant single value 0.15.

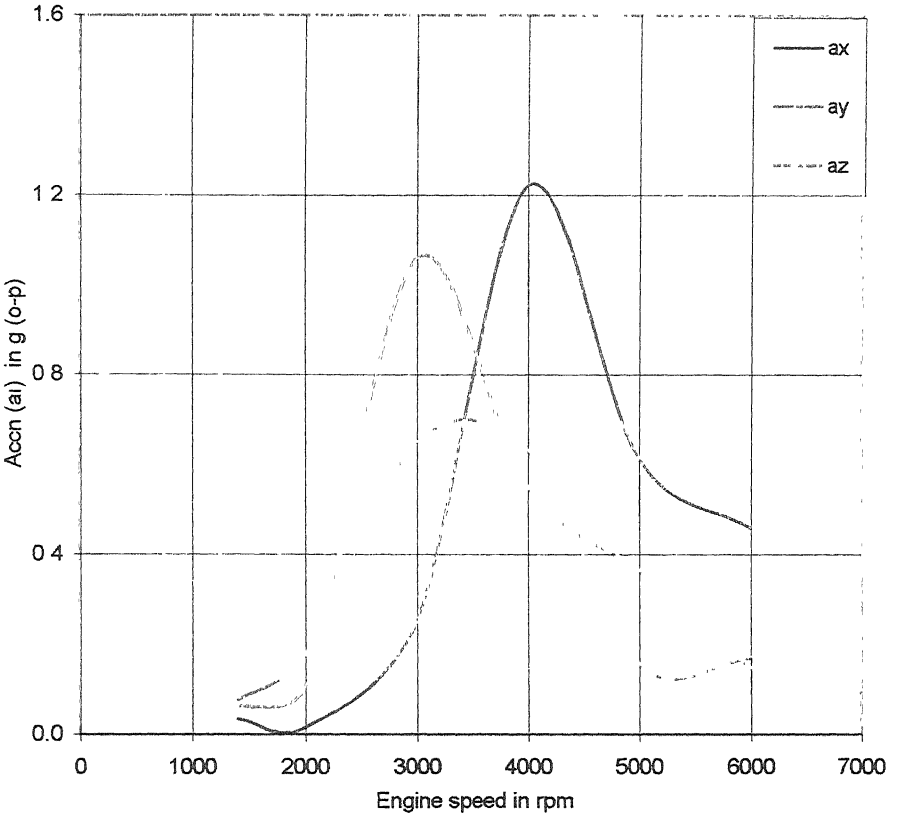

FIGURE 2.7 – **FRF curve of steering bar assembly**

2.8 Dynamic Load Computation

The analysis in the present study concerns engine forces. The engine force is made up of six components. They are:

(i) Force resulting from combustion

(ii) The external load from the clutch

(iii) Inertia load due to rotating and reciprocating parts

(iv) Frictional load due friction between the moving and stationary units

(v) Load generated due to pumping the oil and actuation of the valve train

(vi) Due to misalignment and clearances in rotating and reciprocating components

Figure 2.8 shows the simplified representation of the study engine. The reciprocating and rotating masses are shown as lumped masses at respective locations with force acting on the system.

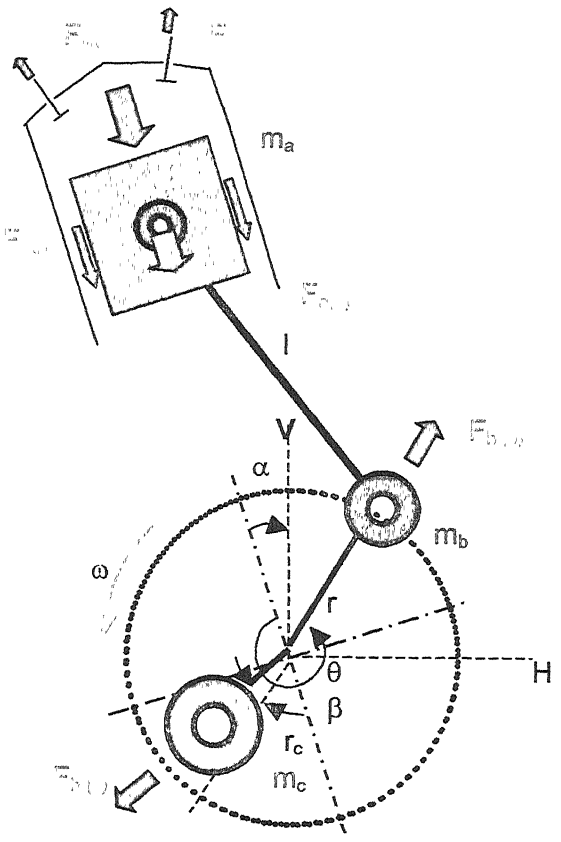

FIGURE 2.8 - **Arrangement of study engine**

The excitation force on the crankshaft is the vector sum of all the above. The torque balance at the crankshaft is [16],

$$T_{combustion} - T_{drive\ train} - T_{mass\ inertia} - T_{friction} - T_{valves,\ pump\ \&\ magneto} - T_{alignment\ \&\ clearance} = 0 \quad (2.3)$$

For no load (idle running) condition, one gets

$$T_{drive\ train} = 0 \quad (2.4)$$

The resultant force acting on the crankshaft bearing is periodic with the engine running frequency and gets transmitted to the entire structure. Of the six forces listed above the first three are computed in the present study. They constitute the predominant components.

(I) Combustion Load Estimation

The pressure - crank angle (p - θ) diagram is used in estimating the combustion force spectrum. This exercise was carried out experimentally. The AVL indicator test rig was used for this experiment. The engine was excited over a full speed range, from 2500 to 6000 rpm under minimum part load and full load. The pressure - crank angle diagrams were recorded at engine speeds of 2500, 3000, 4000, 5000 and 6000 rpm, using an Indicator Machine. The indicated mean effective pressure (imep) for full range was computed by calculating the net effective area of indicator ($p - v$) cards using Pro/Engineer. The brake mean effective pressure (bmep) for different speeds is calculated using the measured brake power for different engine speeds. The frictional mean effective pressure (fmep) is computed knowing the indicated and brake mean effective pressures. For no load condition fmep is equivalent to imep. From these data the p - θ diagrams the combustion force on the piston was computed over full crank angle. The indicated pressure attains peak, at the end of compression, occurs at half of the running frequency. The combustion force on crank pin can be calculated as [16]

$$F_{(\theta)} = (p_{i(\theta)} - p_a)A_p \qquad (2.5)$$

The results obtained for the study engine are shown in Fig. 2.9. for no load condition.

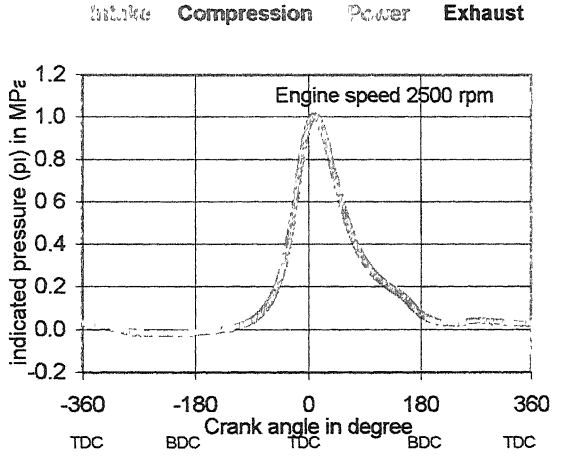

(a) : **p - θ diagram**

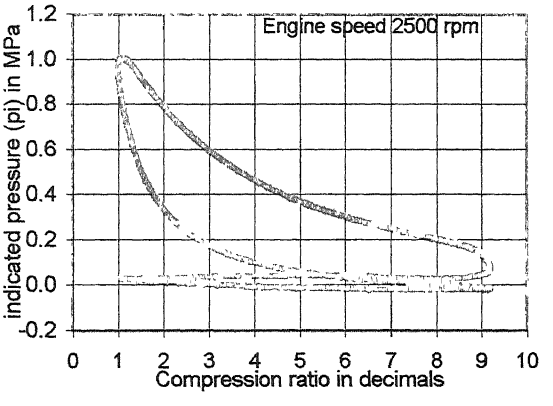

(b) : **p - v diagram**

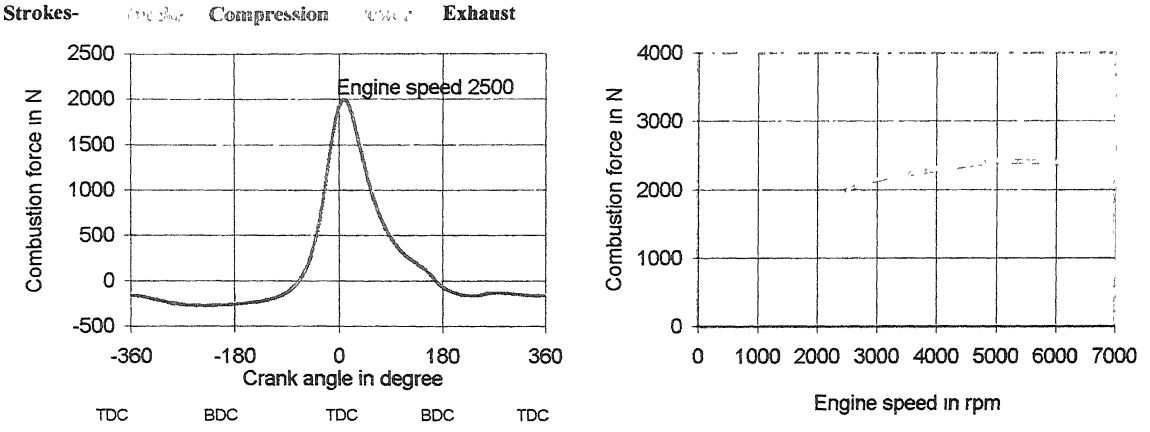

(c) : **Combustion force - crank angle diagram** (d) : **Peak combustion force - spectrum at 11° aTDC**

FIGURE 2.9 - **Engine indicator diagrams**

For the study engine the peak indicated pressure is around 5.3 MPa with imep 1.416 MPa at steady 6000 engine rpm under full load condition and for motoring this reaches 0.5MPa. For no load condition (minimum part load) the peak gets raised up to 1.0 Mpa. The net gas load during idling is 2174.64 N in the direction of slider. This load is employed as the amplitude of the harmonic loading applied to the finite element model. The frequency range varies from zero to 6000 rpm.

(II) Inertia Force Estimation

The inertia force on the engine bearings is the vector sum of rotating and reciprocating inertia forces at engine speed. Since the single cylinder engine cannot be completely balanced, unbalance force always exists. This force grows parabolically with engine speed. This inertia force continuously changes its magnitude and direction. This force can be computed using [17]

$$R_x = m_a r\varpi^2 \sin(\theta+\alpha) + m_c r_c \varpi^2 \sin(\theta+\alpha+180^\circ+\beta) \tag{2.6}$$

$$R_y = m_a r\varpi^2 \cos(\theta+\alpha) + m_b r\varpi^2[\cos(\theta+\alpha) + (r/l)\cos(2(\theta+\alpha))] + m_c r_c \varpi^2 \sin(\theta+\alpha+180^\circ+\beta) \tag{2.7}$$

The inertia force of a normal engine is, as expected is like a cardioidal, where the peak inertia force has occurred (Fig. 2.10 a) at an angle 256 degree from the slider axis. In the present case, typically, the magnitude of the peak inertia force of the engine is found to be 1178.11 N, for a steady engine speed of 6000 rpm. This load is applied to the finite element model as a ramp (linear) load over the entire frequency range engine. The peak loads for various engine speeds are plotted in Fig. 2.10 (b).

These loads are fed as input to the finite element program for forced vibration calculations. In order to simplify computation, the parabolically growing load is ramped linearly up to the maximum engine rpm. The responses are computed individually for the various loads discussed above and then superimposed to obtain the overall response of the vehicle.

2.9 Vibration Response Locations

For the purpose of comparison of the overall vibration characteristics five different locations were selected on the motorcycles. Two of these locations were on engine, (cylinder head and engine mounting); while the other three points were located on the vehicle structure (footrest tip, seat mounting and steering bar). The Table 2.10 gives the response location co-ordinates.

TABLE 2.10 – **Vibration response locations**

SL. No	Location	Co-ordinate		
		X	Y	Z
1	Cylinder head	0.00	52.73	-201.95
2	Engine mounting	0.00	-19.00	-348.50
3	Foot rest	190.00	-70.50	-94.10
4	Seat mounting	0.00	326.50	96.30
5	Steering bar	192.98	598.89	-369.86

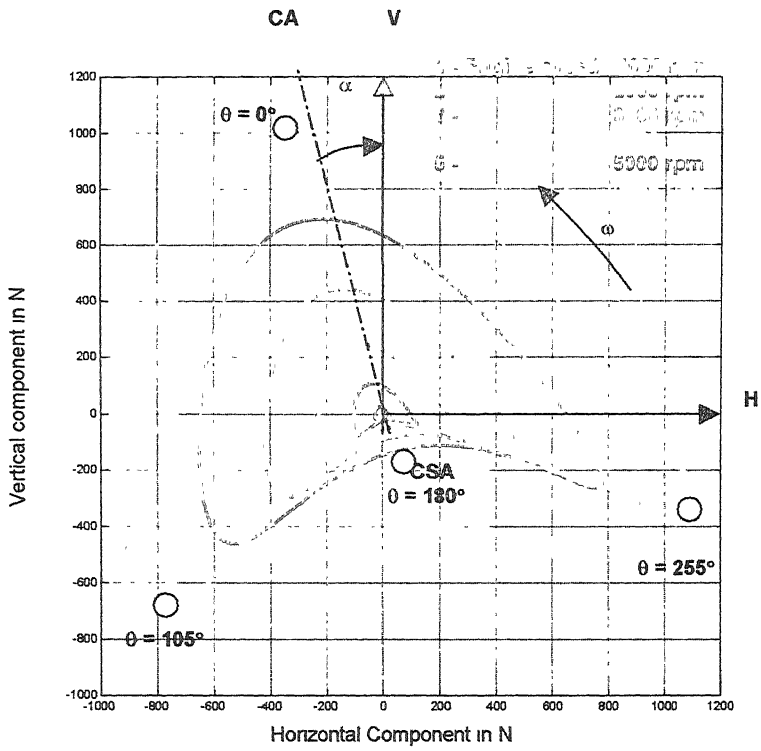

(a) : **Polar diagram of inertia force**

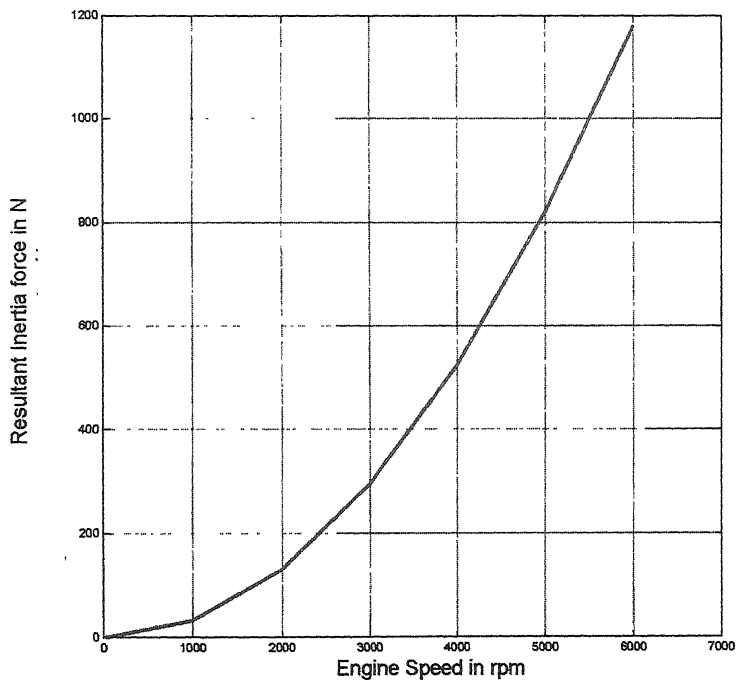

(b) : **Peak inertia force spectrum**

(at 256 degree from cylinder axis in the direction of rotation)

FIGURE 2.10 - **Engine inertia diagrams**

2.10 Forced Vibration Response

The displacement and von-Mises stress contours have been plotted for the entire vehicle structure within the engine running speed range of 0-6000 rpm at intervals of 1200 rpm, Figs 2.11 (a - j) show the vibration response under combustion loading and Figs. 2.12 (a - j) show the vehicle response under inertial loading.

As can be seen from all the plots the locations undergoing maximum stress are

(i) Backside of the engine mountings brackets

(ii) Central beam

(iii) Seat support beams.

The maximum stresses range from 40 MPa to 150 MPa. The force amplitude was earlier computed to be of the order of 2 kN.

The maximum displacements take place on

(i) Steering bar and

(ii) Foot rest.

The maximum displacement magnitudes range between 200 μm to 400 μm.

As can be seen from the plots the stress and displacement magnitudes vary significantly with the operating speed of the engine (consequently, the vehicle speed). The acceleration levels, which also incorporate frequency of operation, range up to a maximum of 1.5 g. (under combined loading). The combined response due to both combustion and inertia loadings is given in the form of FRF curves in Figs. 2.13 (a - f). The plots are to be understood in conjunction with the Campbell plot of Fig. 2.5. The Campbell plot predicts the vehicle has 3500 rpm and 5260 rpm as critical speeds causing excessive vibrations in the vertical (Y) direction. In X-direction (transverse axis) the critical speeds are 2260 rpm and 4800 rpm, while in the longitudinal direction (Z-axis) the critical speeds are 3340 rpm, 3470 rpm are the critical speeds. Noting that the engine excitation is in vertical plane, the Y-direction vibrations are most severe.

The following observations can be made on the basis of the FRF plots -Figure 2.13, under combined combustion and inertia loading.

(i) The cylinder head exhibits the maximum vibrations, of the order of 1.3 g, in Y direction, 0.4 g in Z direction and 0.1 g in X directions at 3600 rpm which is equivalent to a vehicle speed of 38 kmph.

(ii) The engine mounting undergoes maximum vibrations, of the order of, 0.7 g in Y direction, 0.6 g in Z direction and 0.2 g in X directions at 3600 rpm which is equivalent vehicle speed 38 kmph.

(iii) The foot rest has shown the maximum vibrations 2.3 g in Y direction, 1.4 g in Z direction and 0.3 g in X directions at 3600 rpm with equivalent vehicle speed 38 kmph.

(iv) The seat mounting has shown the maximum vibrations 2.4 g in Y direction, 1.2 g in Z direction at 3600 rpm with equivalent vehicle speed 38 kmph. and 0.4 g in X directions at 5200 rpm with equivalent vehicle speed 60 kmph.

(v) The steering bar has shown the maximum vibrations 2.2 g in Y direction, 2.2 g in Z direction at 3600 rpm with equivalent vehicle speed 38 kmph. and 0.6 g in X directions at 5200 rpm with equivalent vehicle speed 60 kmph.

Figure 2.14 shows the vector sum of individual displacements, velocities and accelerations of the study vehicle for selected locations. The wheel reactions are also compared under combustion loading for engine excitation from 1200 to 6000 rpm. On the basis of these plots the various components of the motorcycle can be arranged in the following order of susceptibility to vibrations (Seat Mounting Bracket being most susceptible, with resonant acceleration levels going up to 3.9 g, while those for the engine mounting being 1.1 g):

(i) Seat mounting bracket

(ii) Steering arm

(iii) Foot rest

(iv) Cylinder head

(v) Engine mounting

Stage I : Engine Speed 1200 rpm

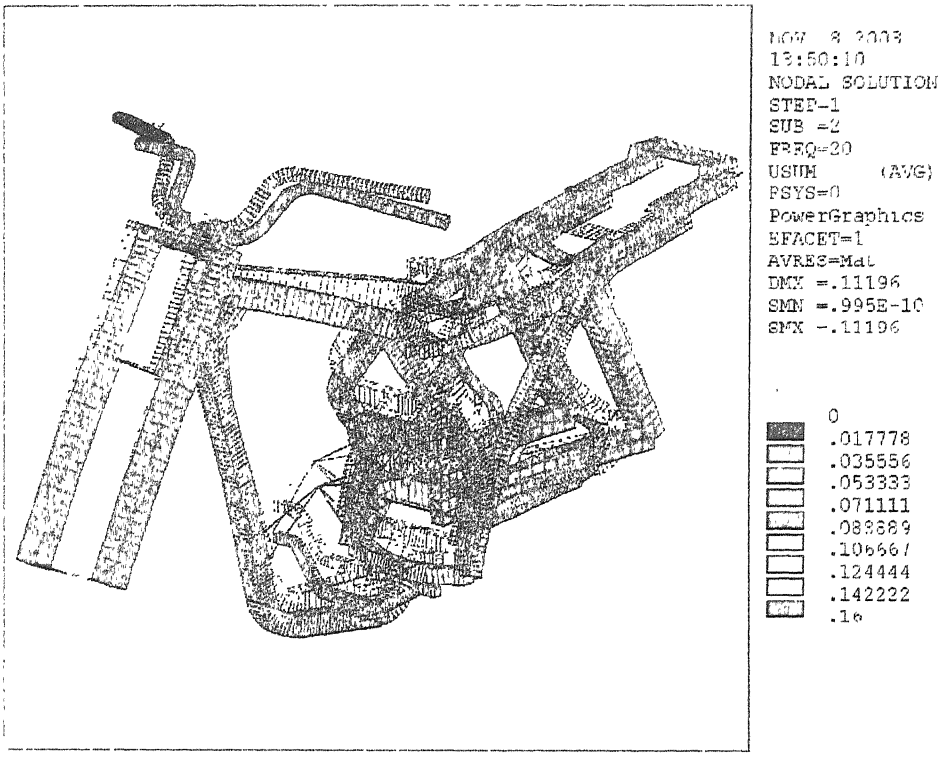

(a) : **Displacement contour**

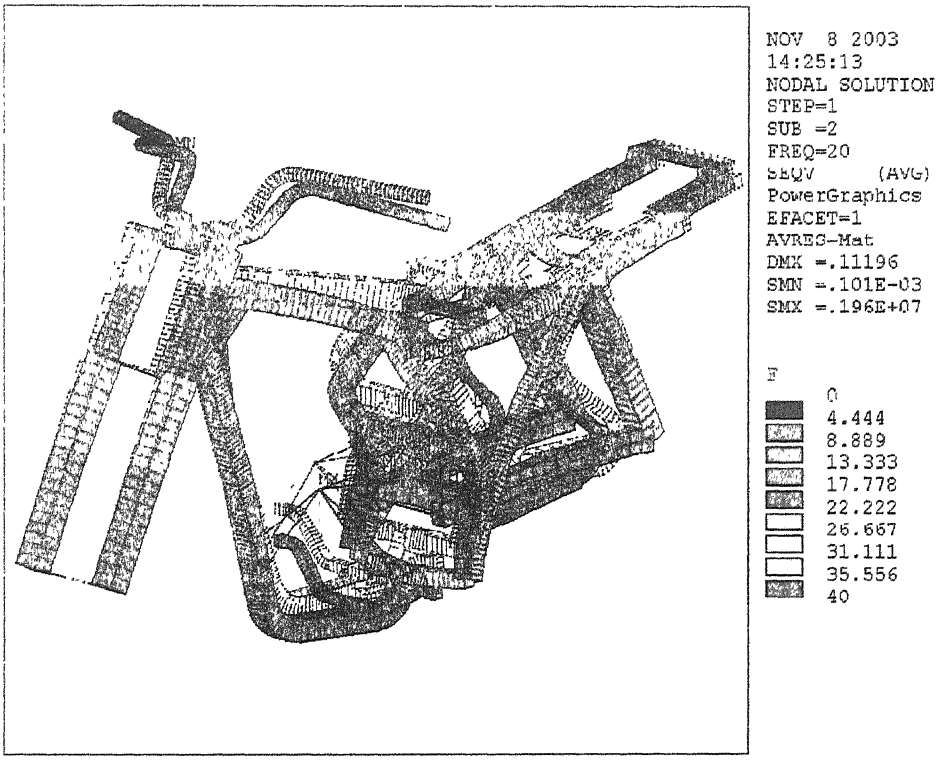

(b) : **Stress contour**

FUGURE 2.11 (a & b) – **Forced vibration response under combustion loading**

Stage II : Engine Speed 2400 rpm

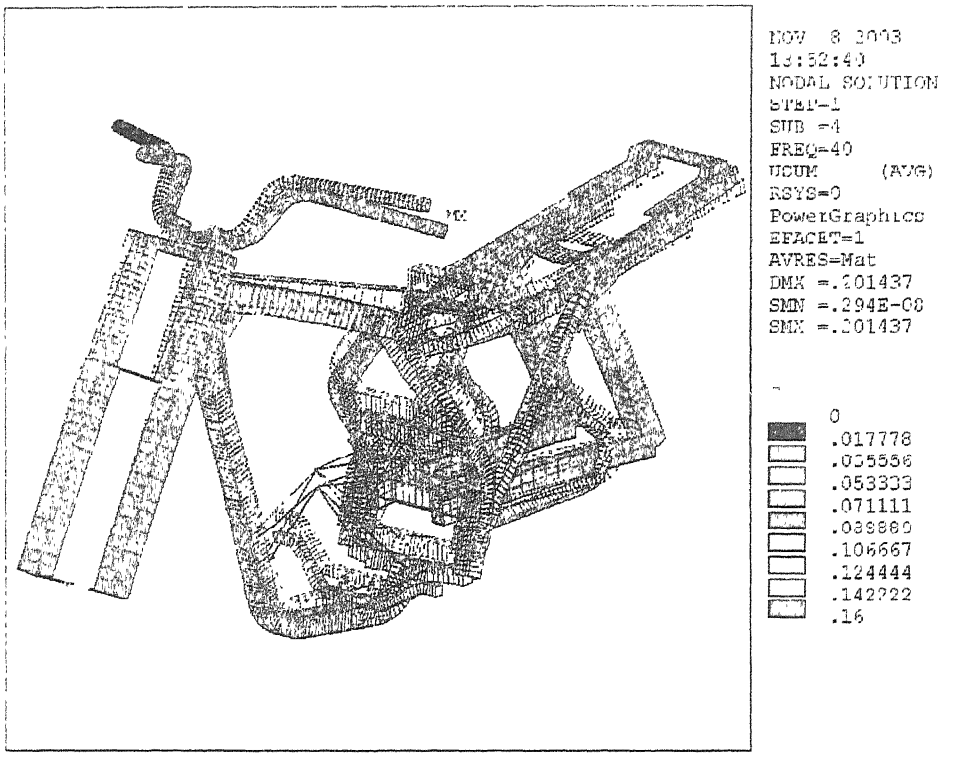

(c) : **Displacement contour**

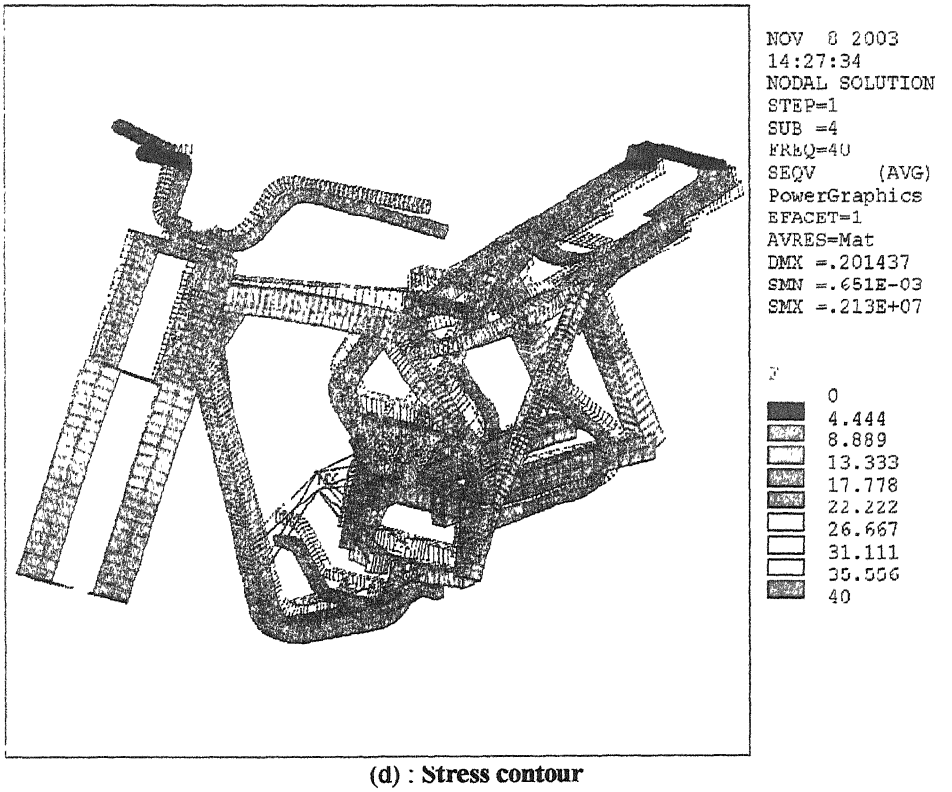

(d) : **Stress contour**

FUGURE 2.11 (c & d) – **Forced vibration response under combustion loading**

Stage III : Engine Speed 3600 rpm

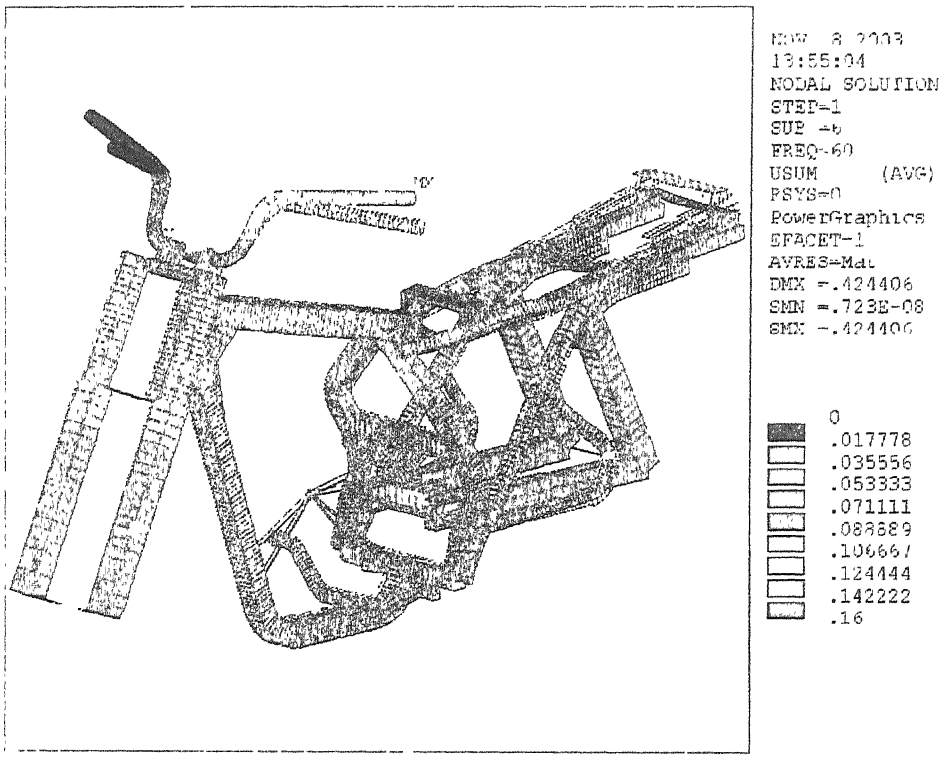

(e) :- **Displacement contour**

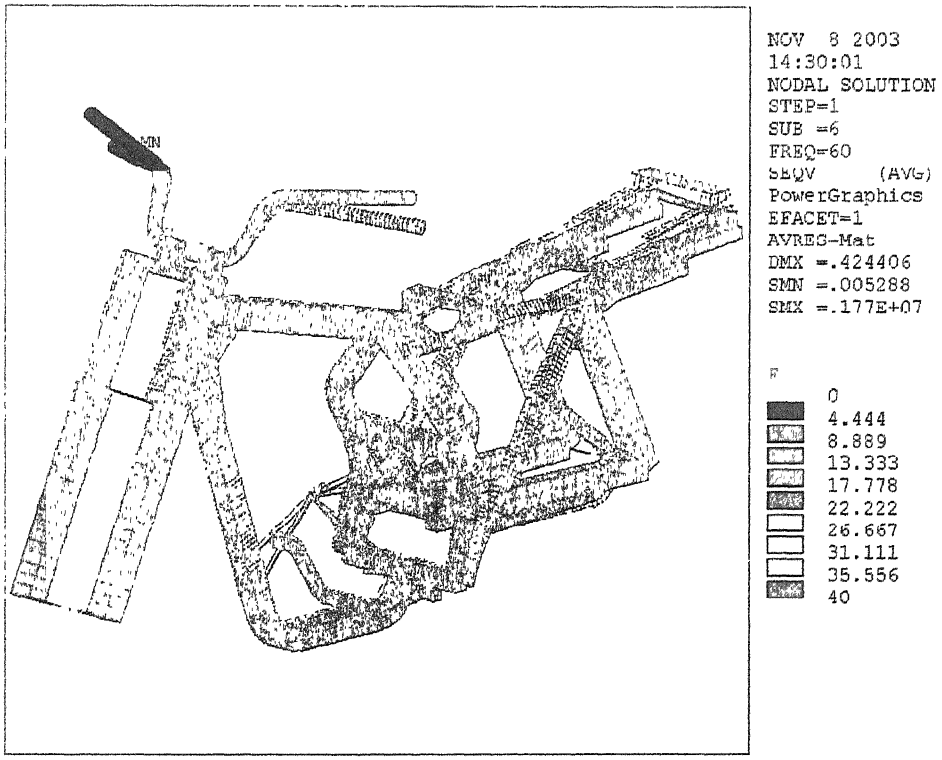

(f) : **Stress contour**

FUGURE 2.11 (e & f) – **Forced vibration response under combustion loading**

Stage IV : Engine Speed 4800 rpm

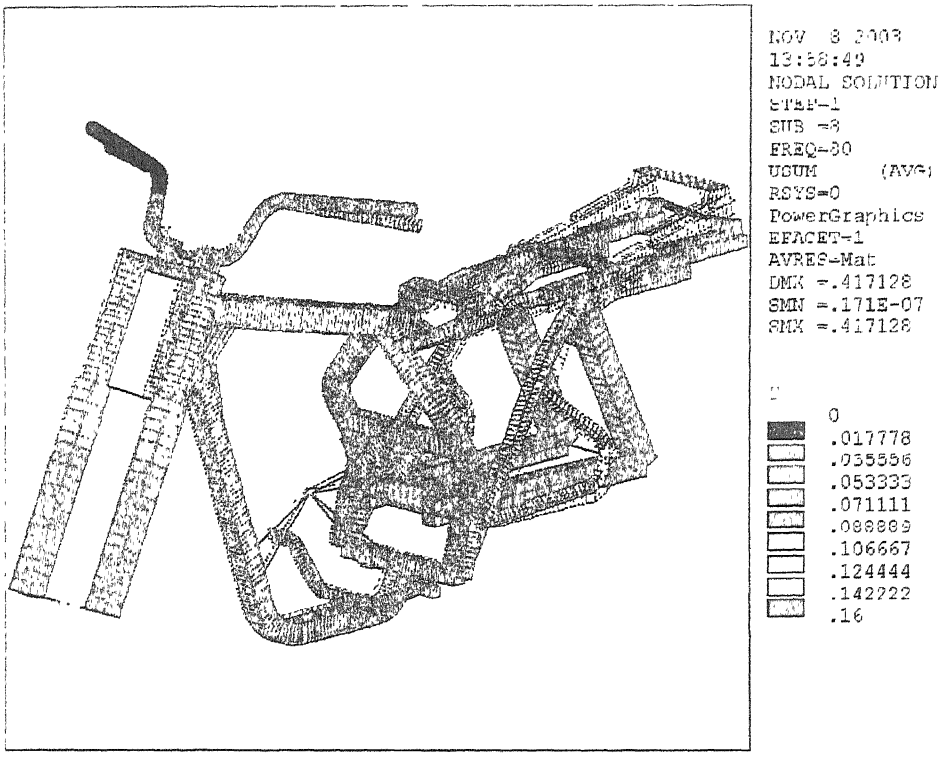

(g) : **Displacement contour**

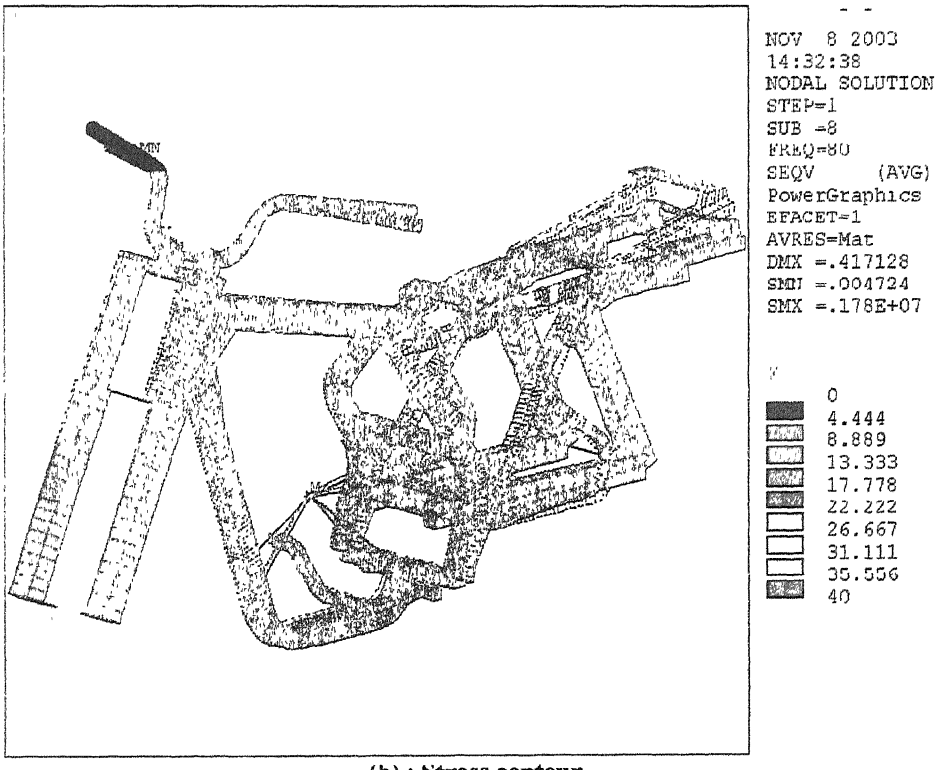

(h) : **Stress contour**

FUGURE 2.11 (g & h) – **Forced vibration response under combustion loading**

Stage IV : Engine Speed 6000 rpm

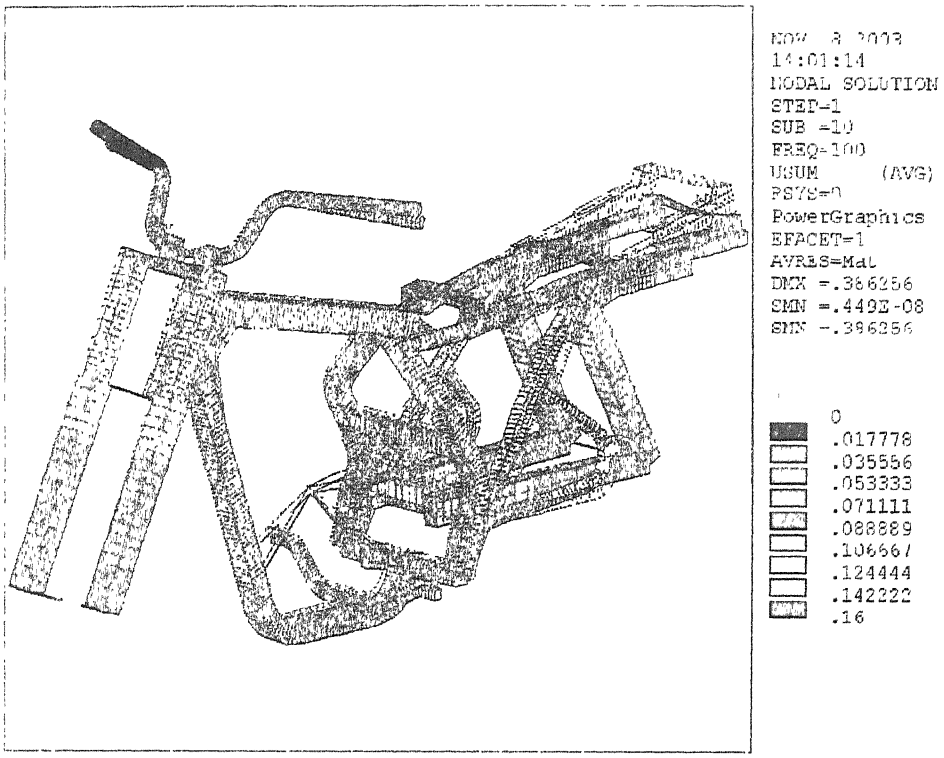

(i) : **Displacement contour**

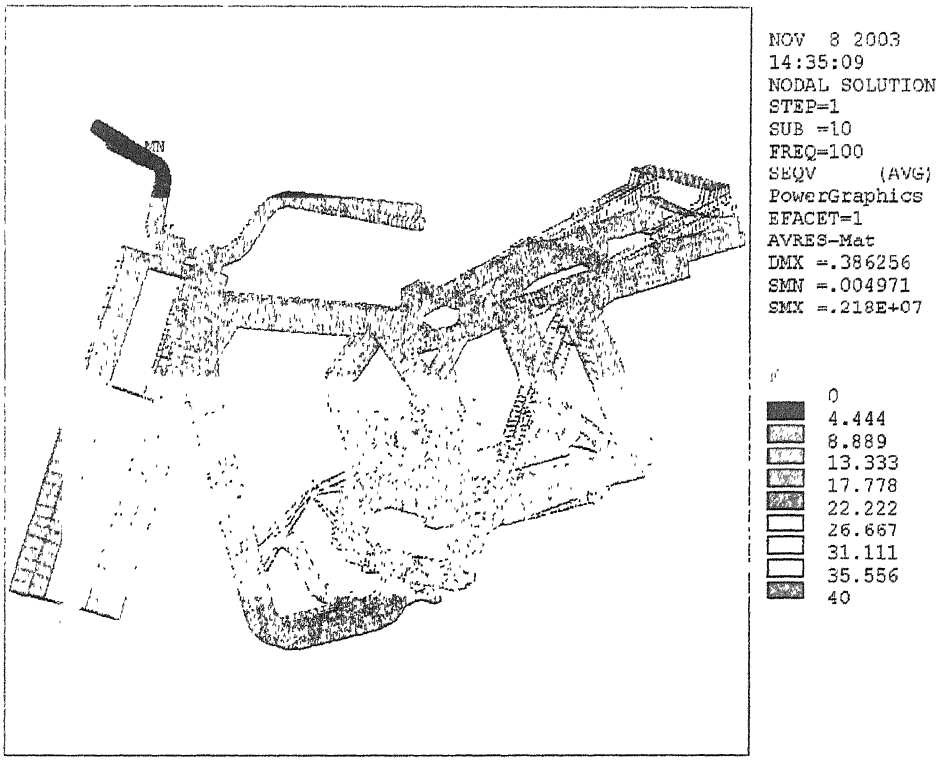

(j) : **Stress contour**

FUGURE 2.11 – **Forced vibration response under combustion loading**

Stage I : Engine Speed 1200 rpm

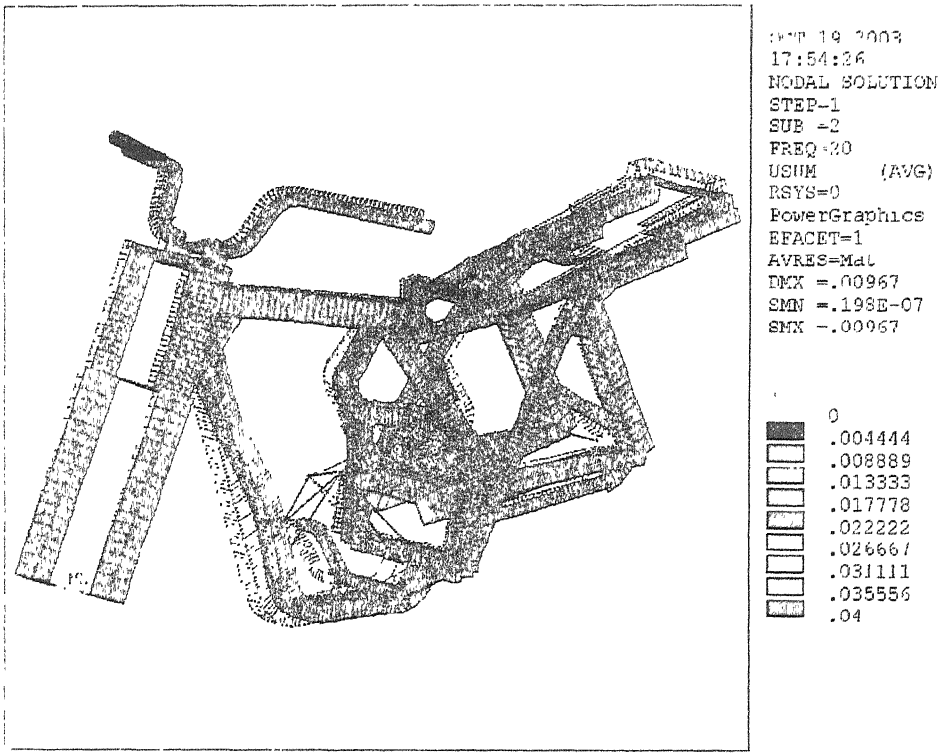

(a) : **Displacement contour**

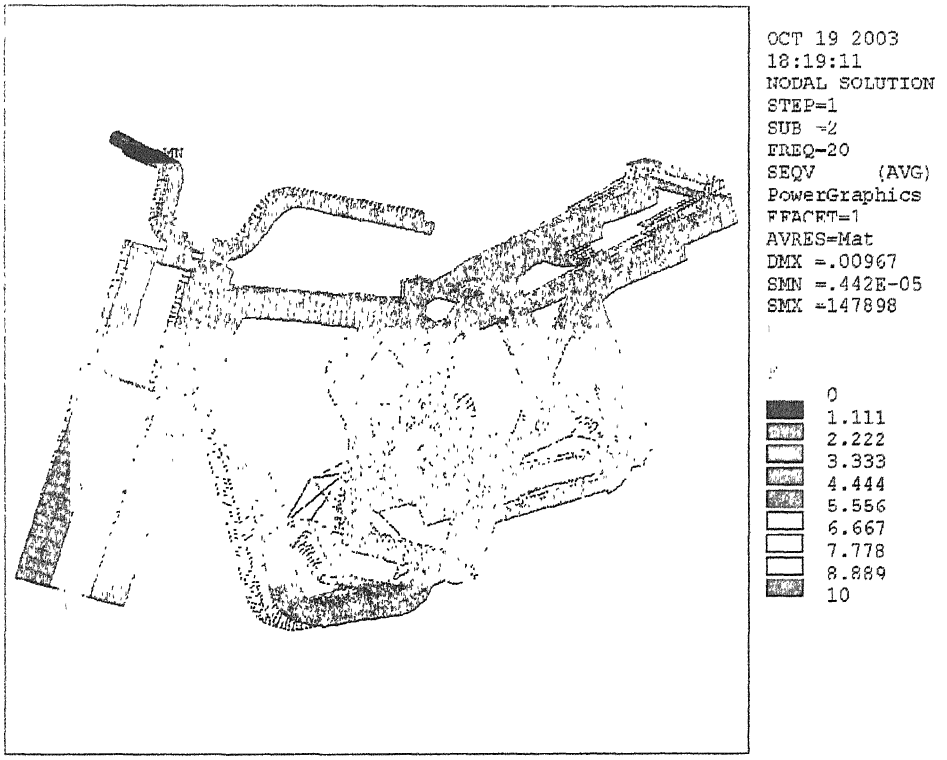

(b) : **Stress contour**

FUGURE 2.12 (a & b) – **Forced vibration response under inertia loading**

Stage II : Engine Speed 2400 rpm

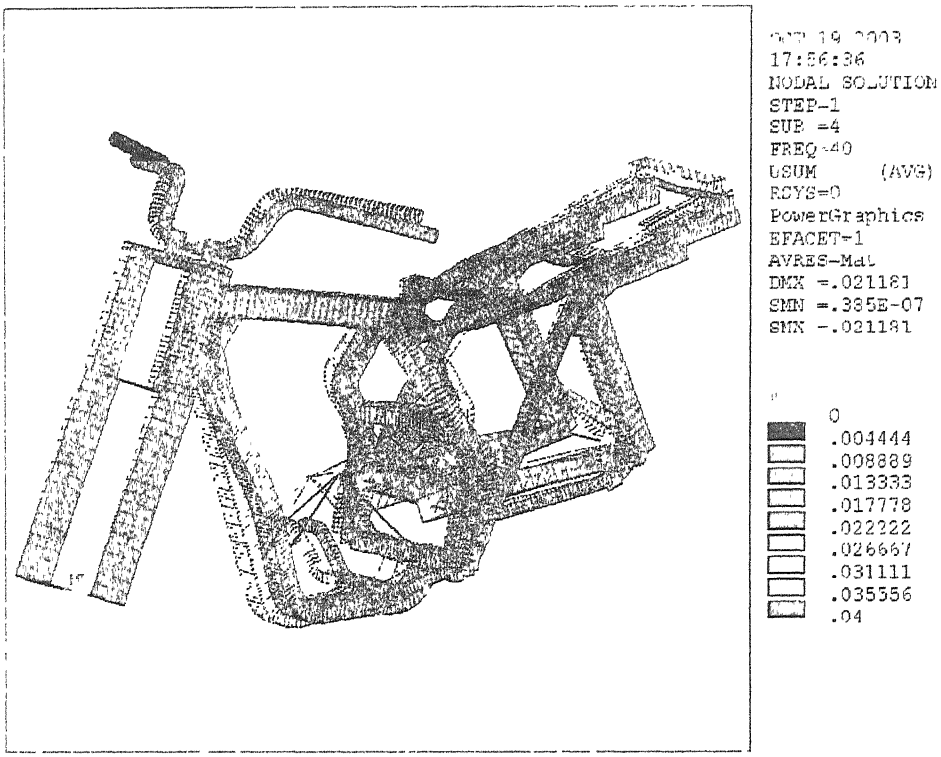

(c) : **Displacement contour**

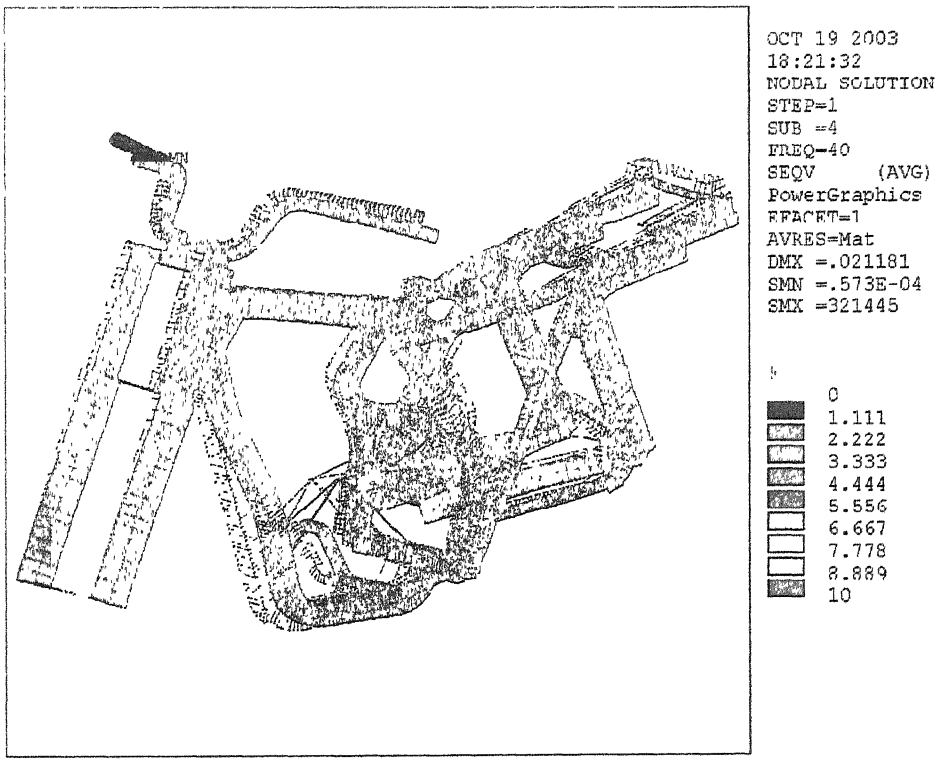

(d) : **Stress contour**

FUGURE 2.12 (c & d) – **Forced vibration response under inertia loading**

Stage III : Engine Speed 3600 rpm

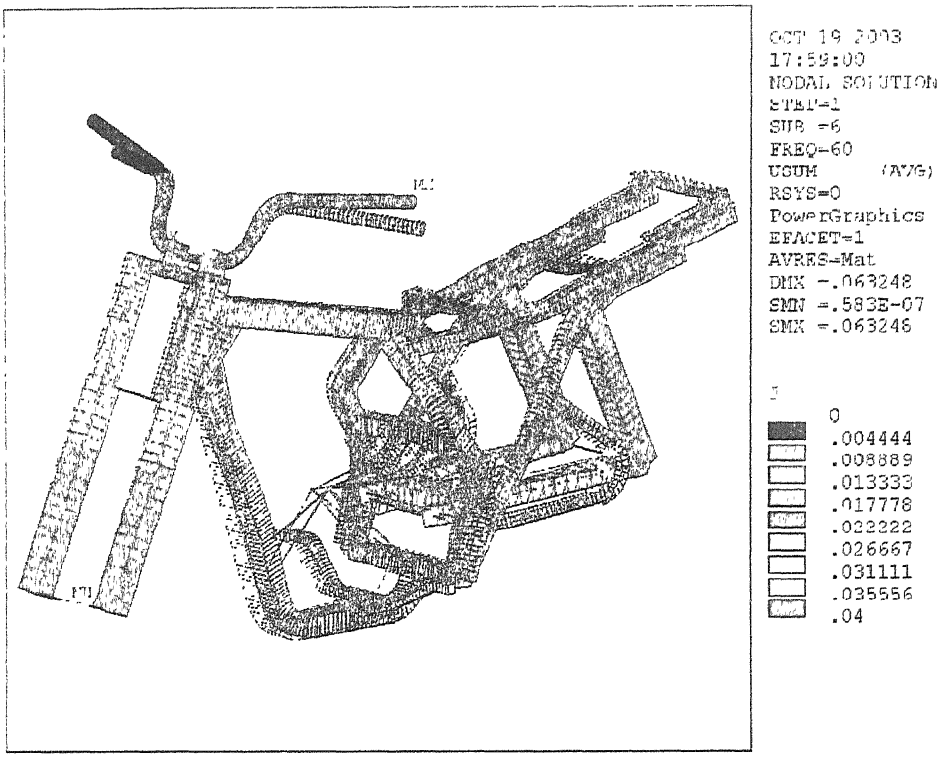

(e) : **Displacement contour**

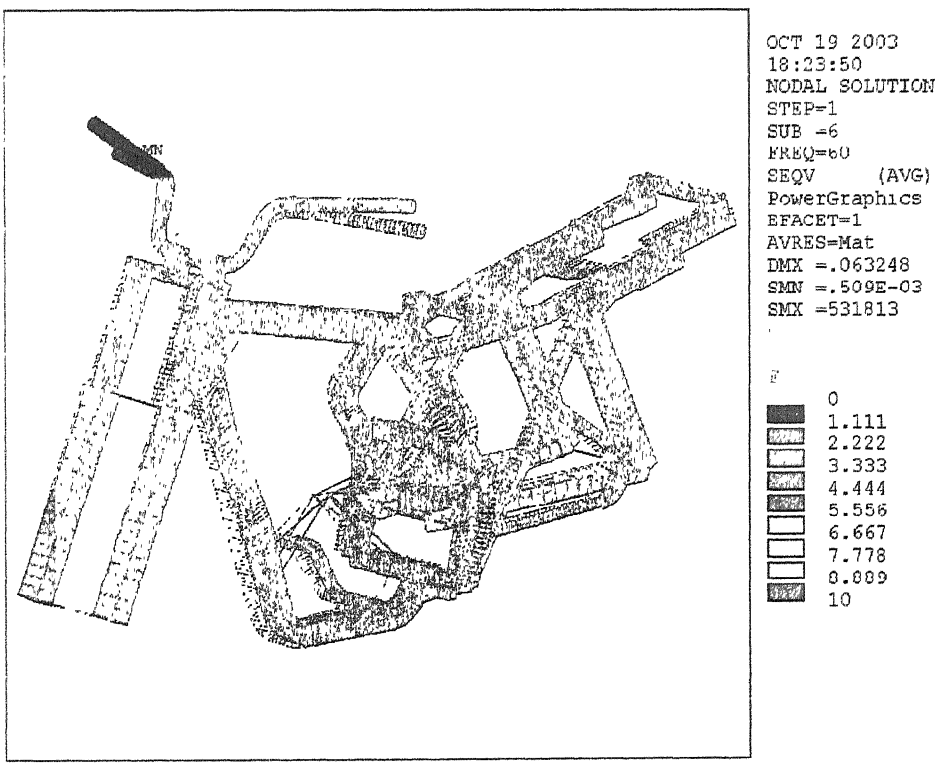

(f) : **Stress contour**

FUGURE 2.12 (e & f) - **Forced vibration response under inertia loading**

Stage IV : Engine Speed 4800 rpm

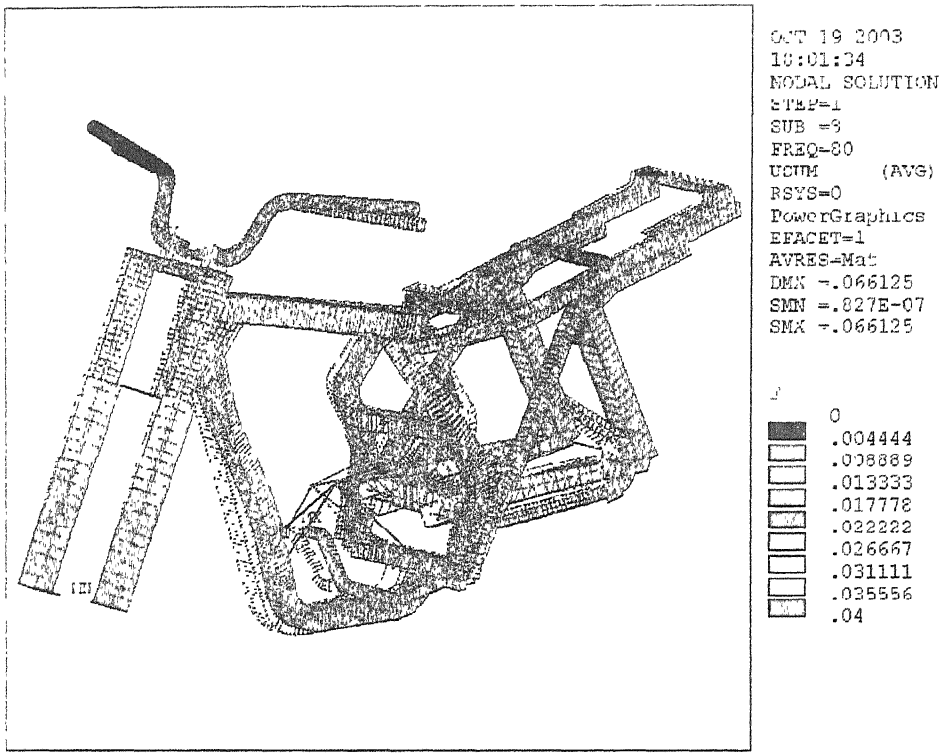

(g) : **Displacement contour**

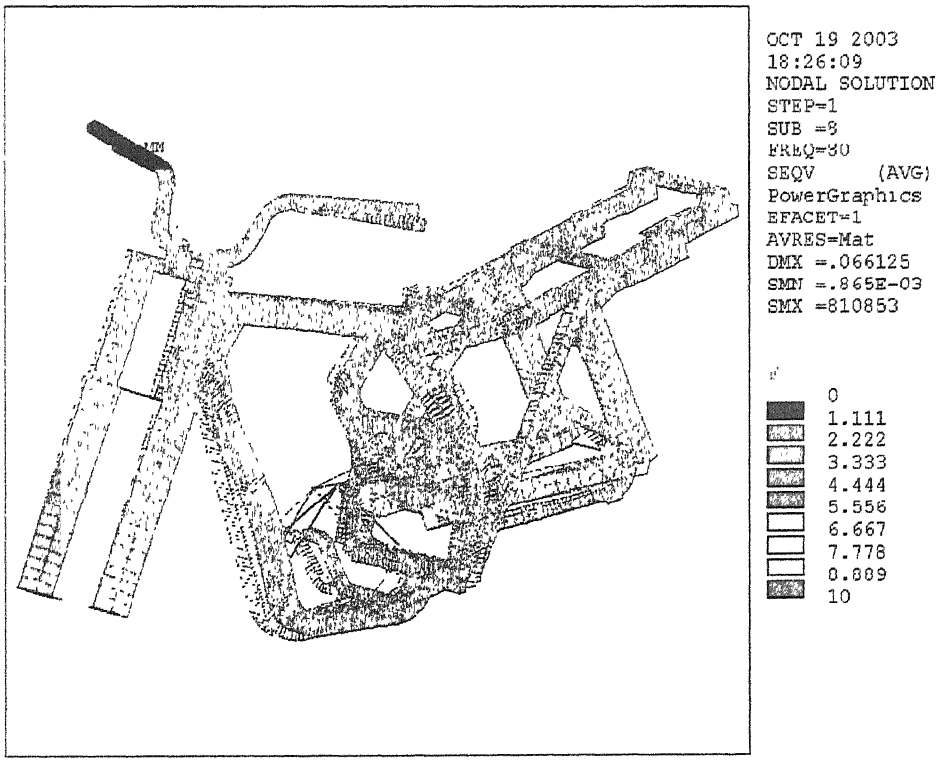

(h) : **Stress contour**

FUGURE 2.12 (g & h) – **Forced vibration response under inertia loading**

Stage V : Engine Speed 6000 rpm

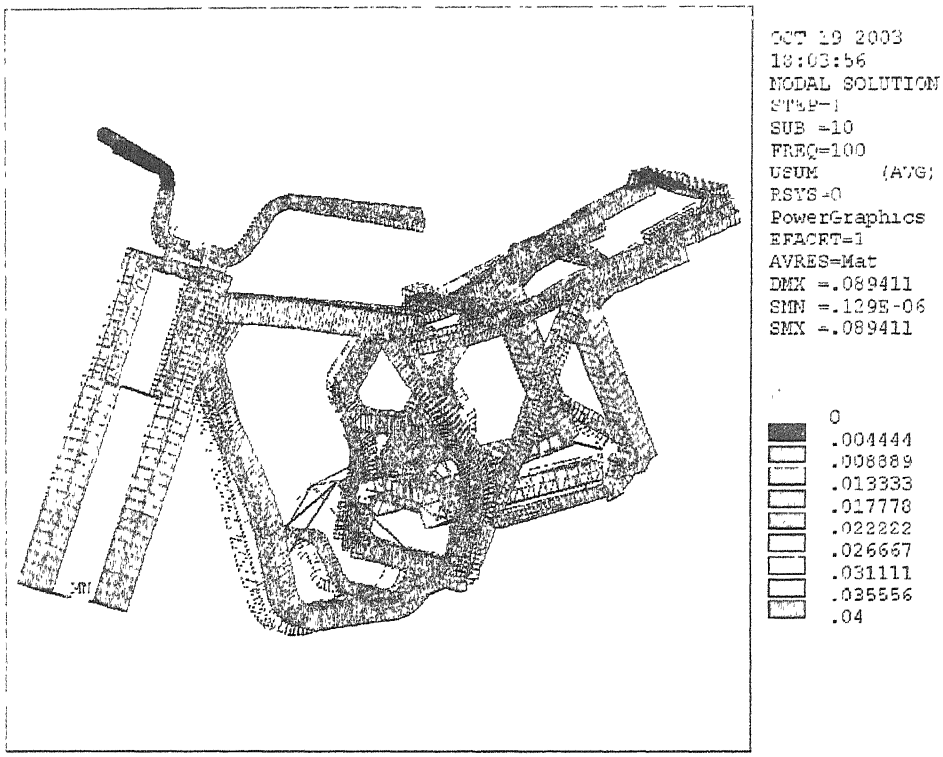

(i) : **Displacement contour**

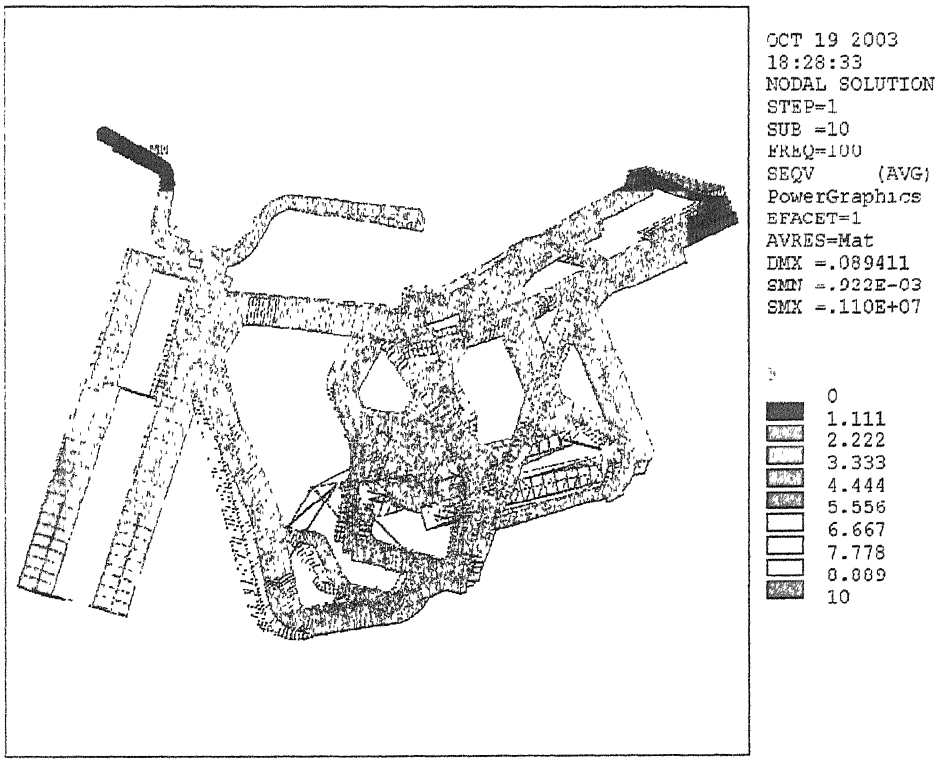

(j) : **Stress counter**

FUGURE 2.12 – **Forced vibration response under inertia loading**

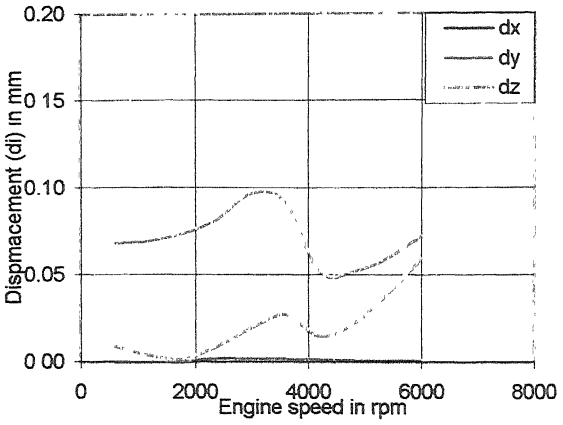

(a) : **Cylinder head displacement**

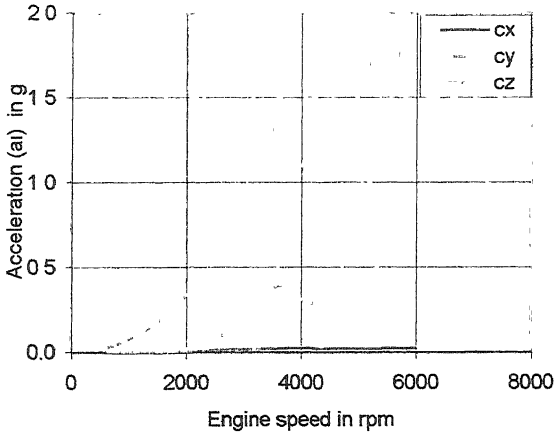

(b) : **Cylinder head accelerations**

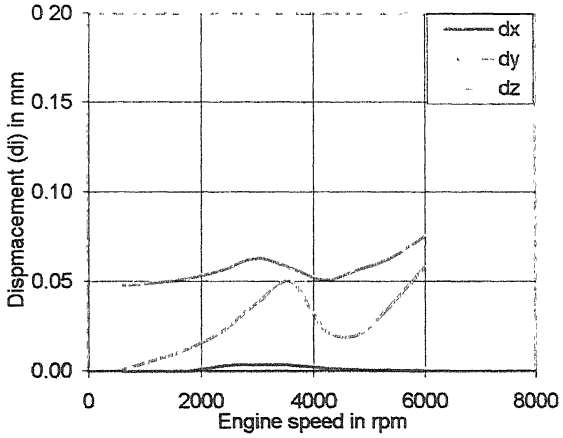

(c) : **Engine mounting displacement**

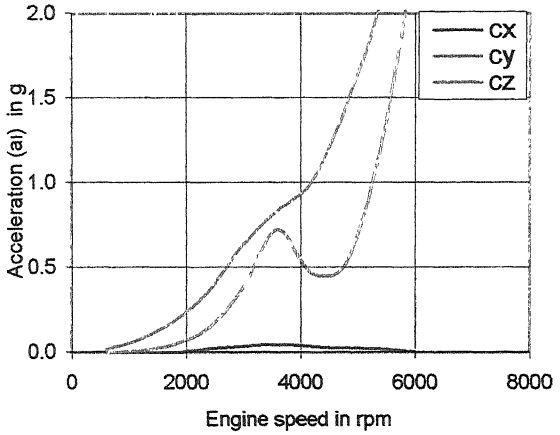

(d) : **Engine mounting acceleration**

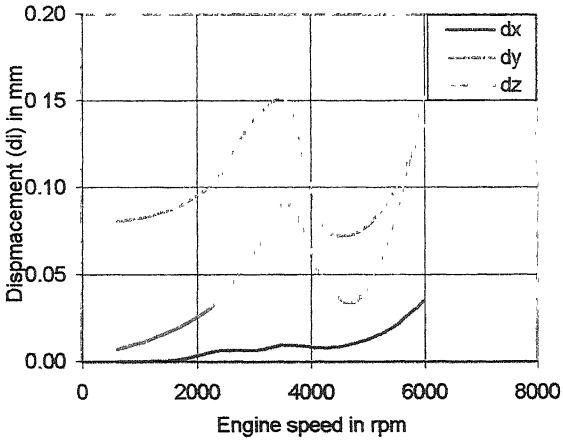

(e) : **Foot rest displacement**

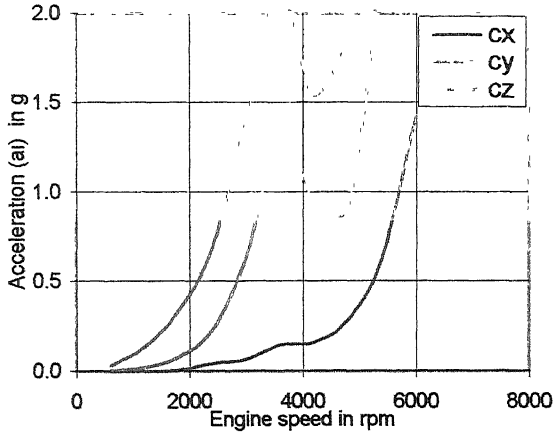

(f) : **Foot rest acceleration**

FUGURE 2.13 (a-f) - **FRF plots under combined combustion and inertia loading**

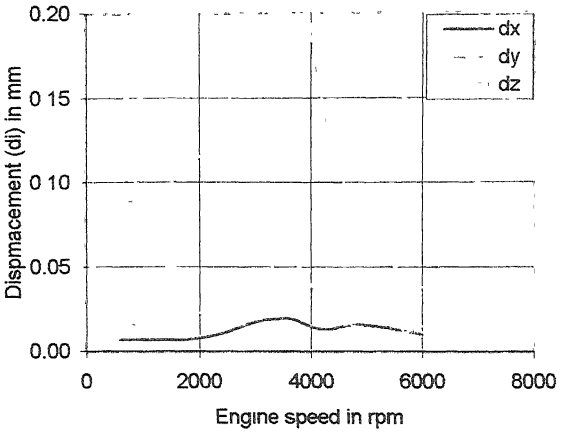

(g) : **Seat mounting displacement**

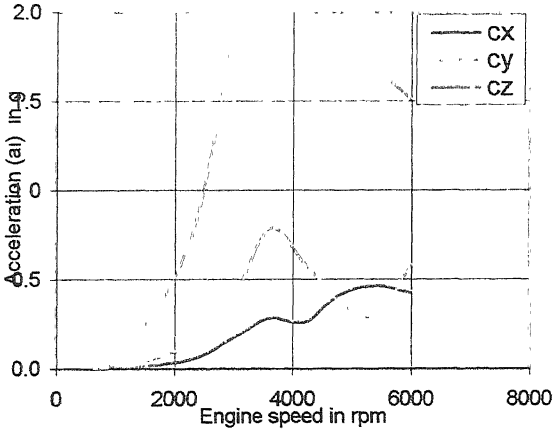

(h) : **Seat mounting acceleration**

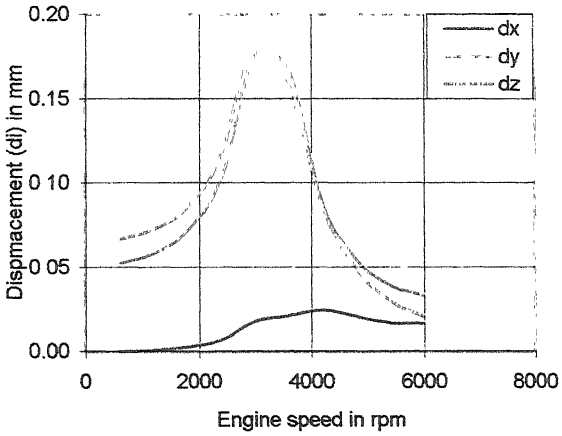

(i) : **Steering bar displacement**

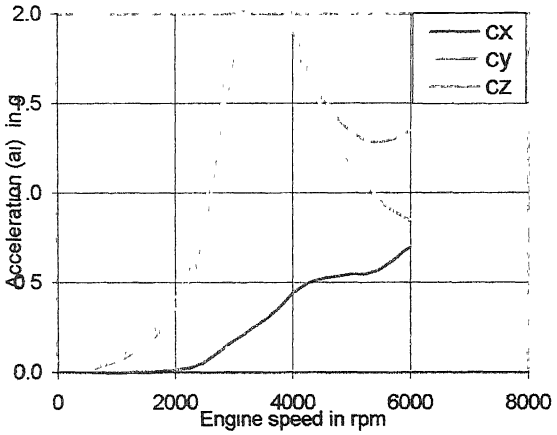

(j) : **Steering bar acceleration**

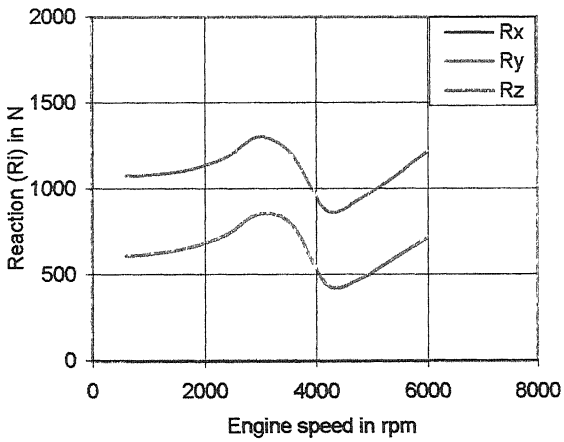

(k) : **Front wheel reaction**

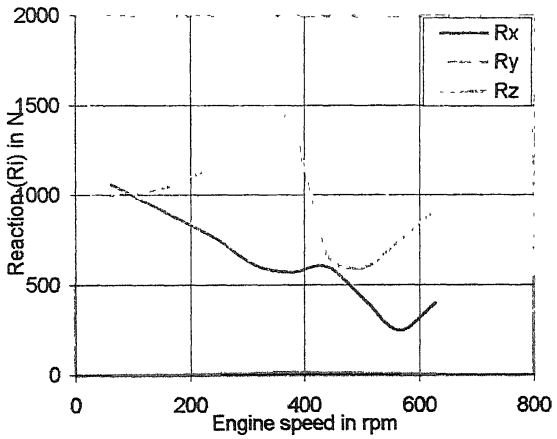

(l) : **Rear wheel reaction**

FUGURE 2.13 – **FRF plots under combined combustion and inertia loading**

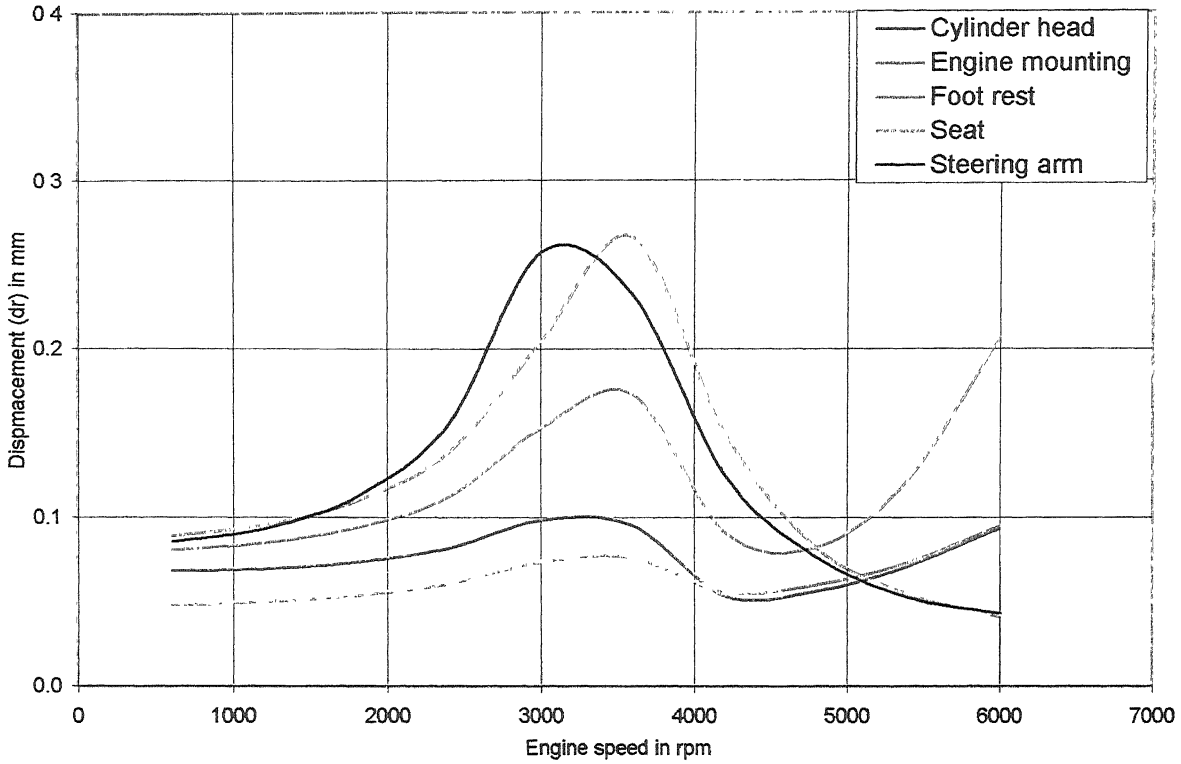

(a) : **Resultant displacements**

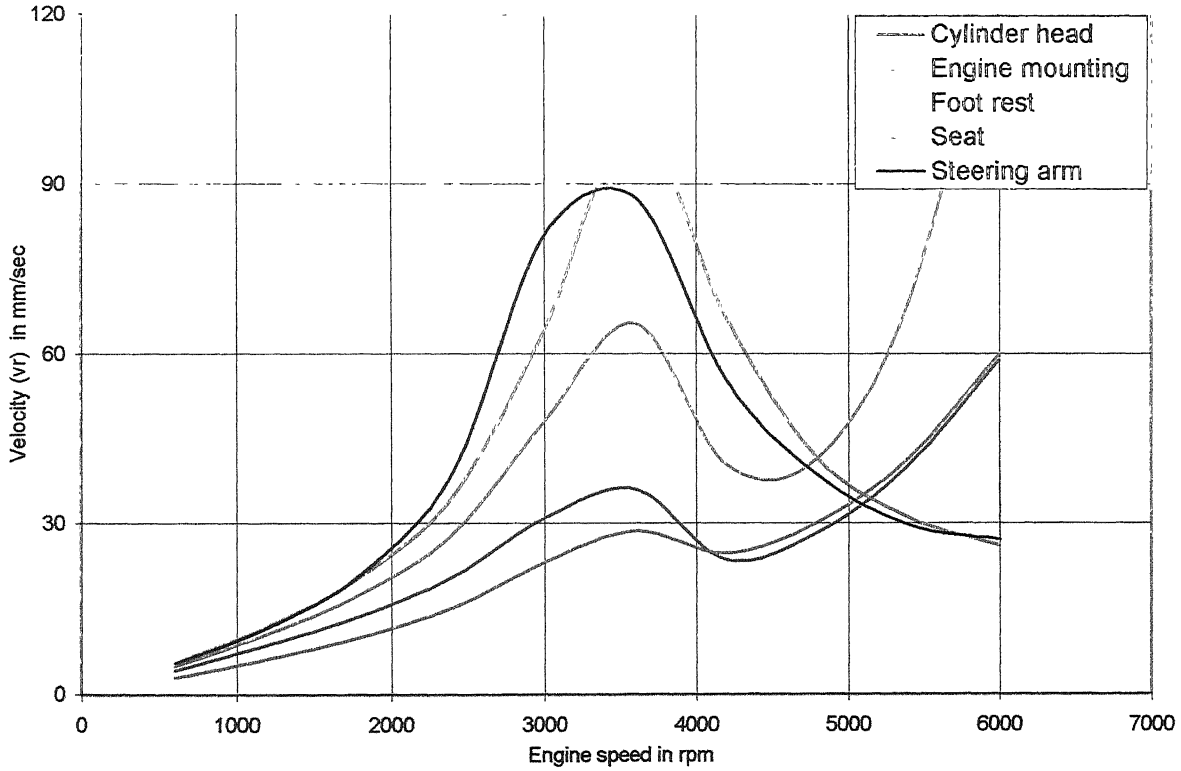

(b) : **Resultant velocities**

FUGURE 2.14 **(a-b)–Overall vibrations of vehicle under combined combustion and inertia loading**

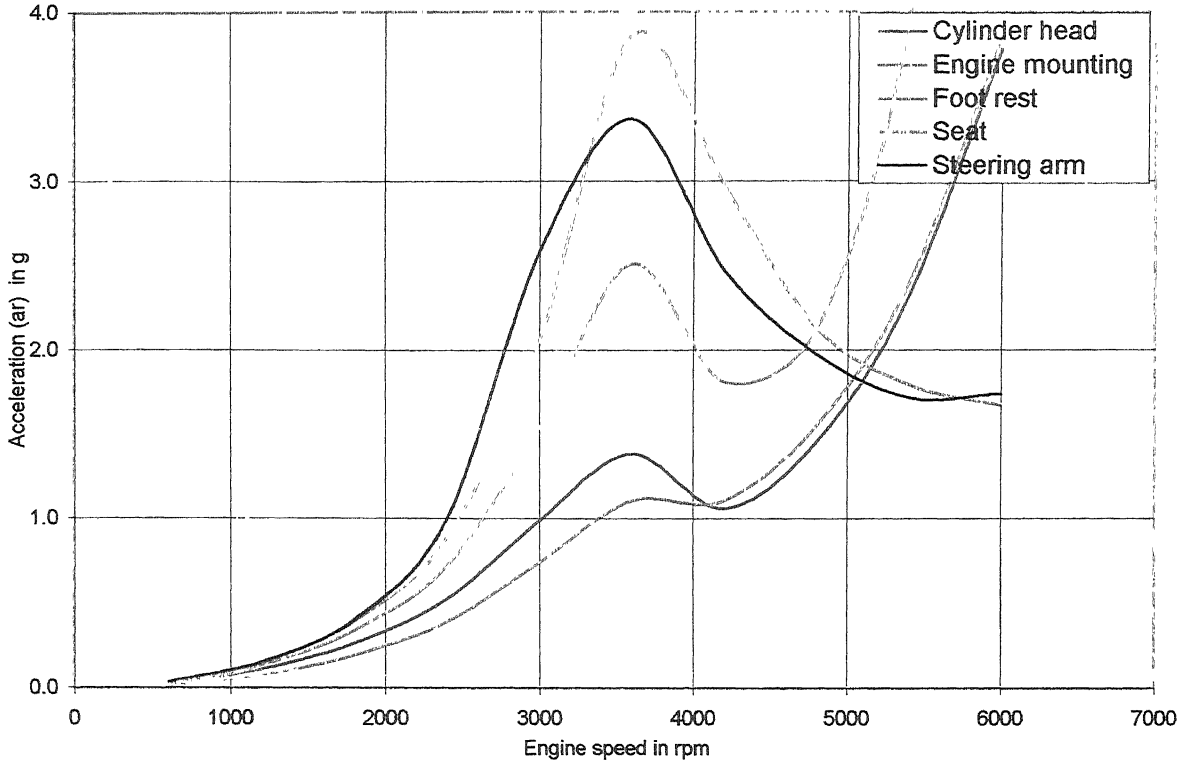

(c) : **Resultant acceleration**

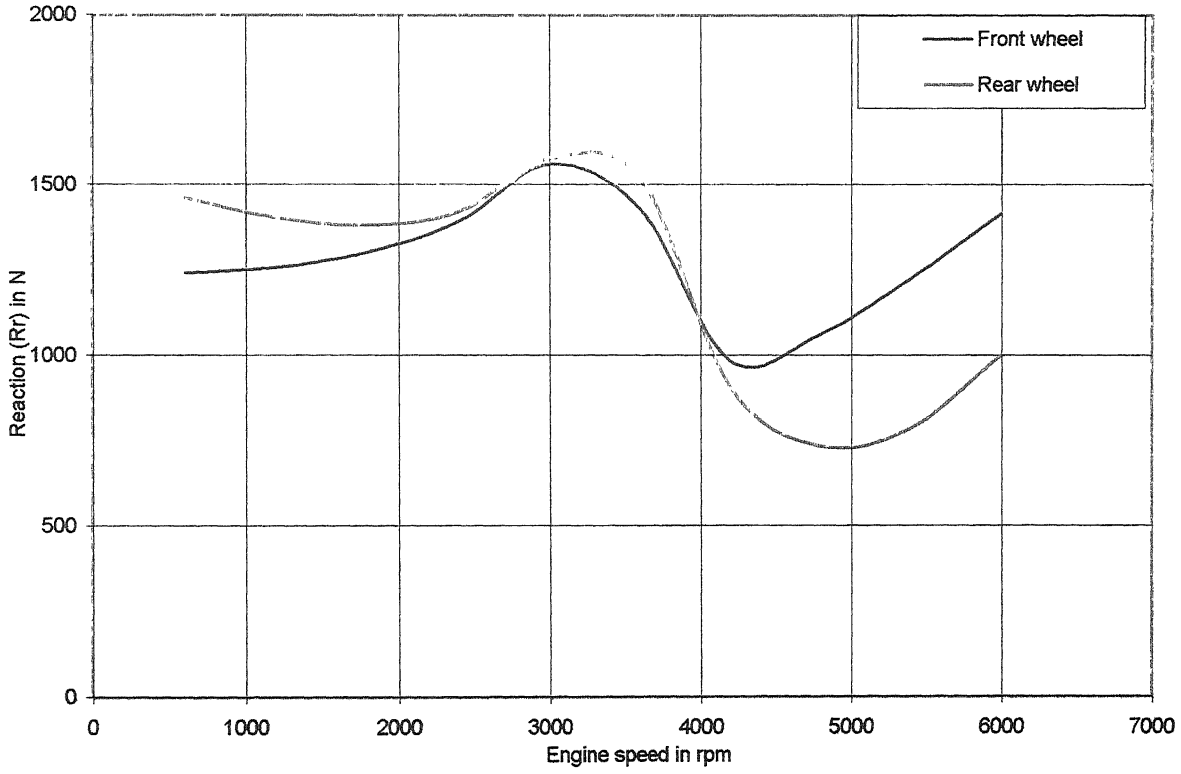

(d) : **Resultant reactions**

FUGURE 2.14 – **Overall vibrations of vehicle under combined combustion and inertia loading**

2.11 Remarks

On the basis of the modeling and simulation described above it was decided to further investigate the free and forced vibration response of motorcycles through specifically designed controlled experiments. It was also decided carry out these experiments on vehicles of different makes and brands for a comparative assessment of rider comfort parameters.

Chapter - 3

EXPERIMENTAL INVESTIGATIONS

Investigations have been carried out on motorcycles of different makes and brands to make a comparative assessment of their vibration characteristics, in addition to validating the Finite Element Model developed, as described in the earlier chapter. The brand names have not been revealed in the thesis, since the exercise is purely academic. The vehicles belong to the identical swept volume and identified by numbers.

Vehicle structure quality is generally evaluated on the basis of the stiffness recorded in drop, fatigue and crash tests. Evaluation of engine performance, on the other hand is based on gas and oil pressure, temperature, power available at wheel, maximum speed, acceleration and retardation tests. Most of these tests are destructive in nature and result in partial or full damage to the vehicle. They also consume a lot of time and gives scant information on ride comfort levels and machine health condition.

Vibration based tests are primarily non-destructive in nature and are known to be useful indicators of machine dynamic characteristics. In addition to being good diagnostic tools for determination of machine health, tests also help in determining the dynamic properties and correct boundary conditions to be employed in analytical and computational models.

3.1 Vibration Signal Processing and Characteristics

The vibration signal contains discrete frequencies, associated harmonics, natural frequencies and various types of noise. In order to assess the mechanical behaviour of machinery, it is necessary to convert the signal in to discrete form. Then, filtering the frequency of interest for study or increasing the sampling rate and/or transforming the domain of interest are the various techniques used for such a study. This is accomplished by using the features available in a typical FFT analyser.

Time Domain Analysis

The time domain is the representation of actual sequence of events occurring on the machine. This gives amplitude versus time plot and provides information on the variation in the process. The relative strength of each harmonics cannot be determined in this analysis. This can be too complex for analysis if excessive noise, signal modification or several frequencies are present.

Frequency Domain Analysis

This gives the information about the amplitude and phase content at various frequencies. This frequency spectrum can be related to direct excitation frequencies or their orders, natural frequencies, sidebands and sub-harmonics. These multiple orders are due to variety of faults that are present in the machinery. The exact fault can be predicted by comparing with good test data and the quality of a machine can be determined by comparing the vibratory signal of different machine for the same excitation frequencies.

Orbit Analysis

Signals obtained from orthogonal probes mounted across the shaft, when plotted give the actual trace of the shaft rotation. The trace makes a closed loop, which is called orbit. The orbital analysis gives the information about pre-loading, torque reaction, pressure angle and direction of rotation.

3.2 Test Rig Development

The test rig is a desktop vehicle model, which consists of a vehicle (Figure 3.1 and 3.2), a portable FFT analyser, engine speed adjustable tachometer, test bed, engine cooling blower, and an exhaust gas ventilation system.

3.3 Instrumentation

In the present study, two sensors were used to pickup the vibration signals at the following locations (Figure 3.1 and 3.2).

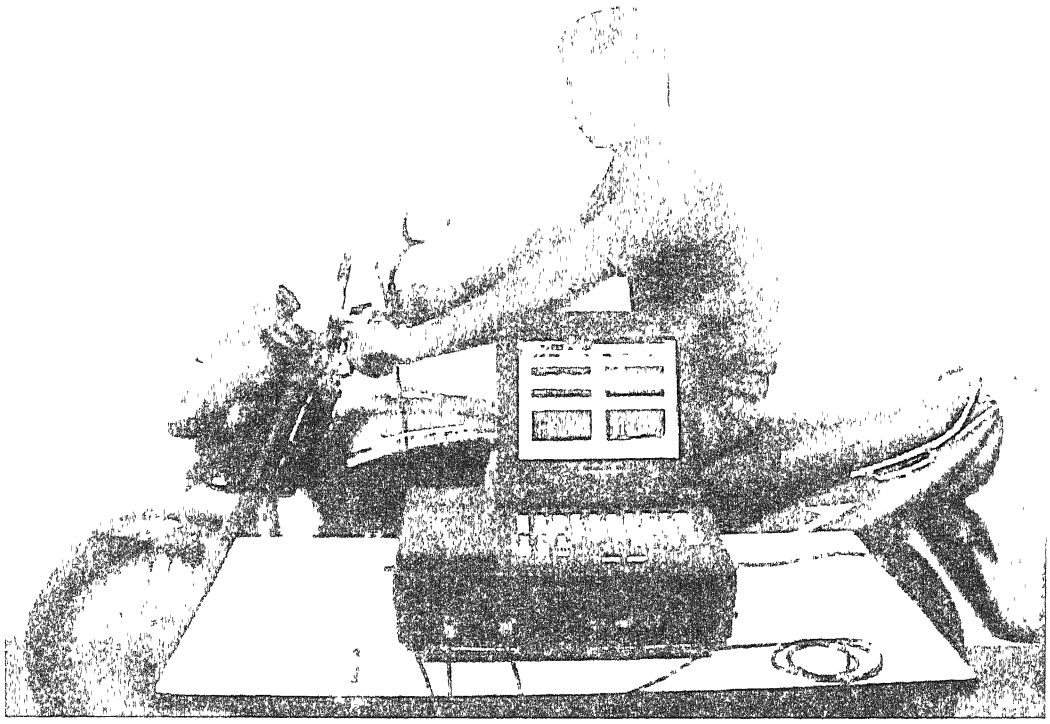

Figure 3.1 - **Photograph of the experimental configuration**

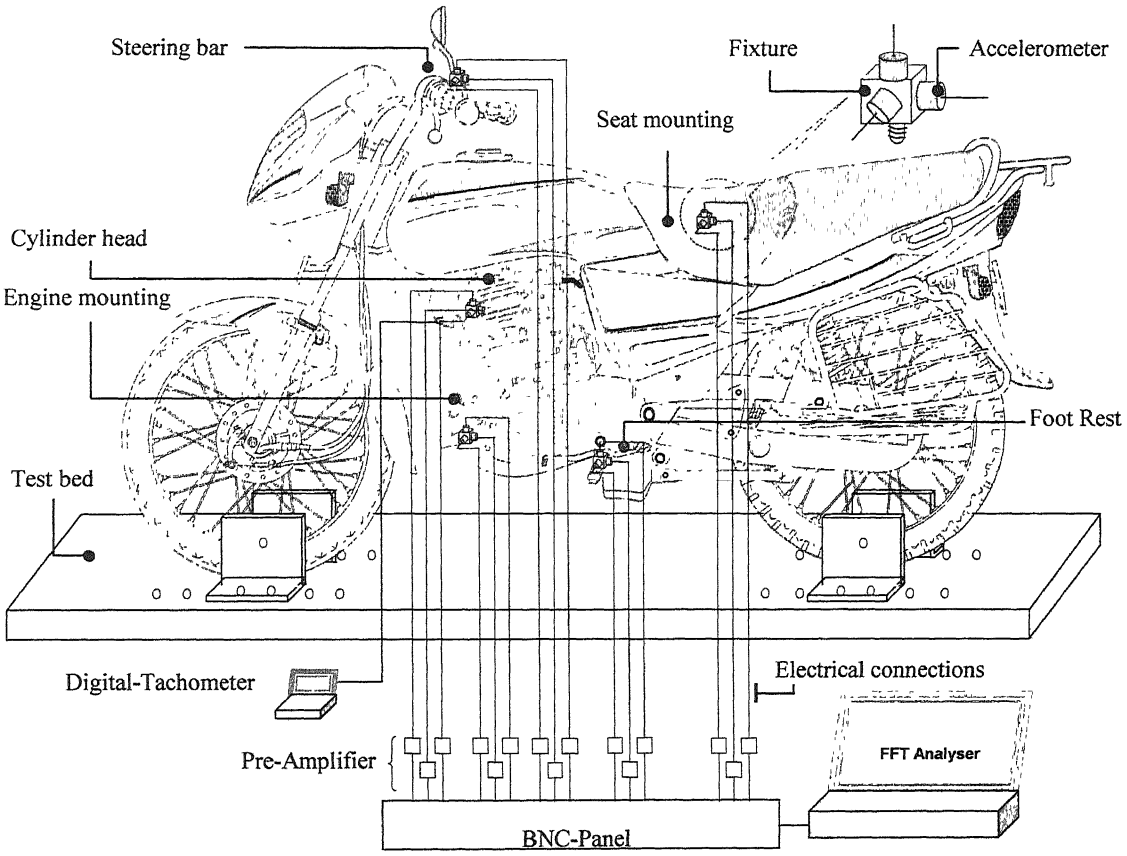

FIGURE 3.2 - **Schematic diagram of experimental configuration**

3.4 Testing Procedure Development

पुरुषोत्तम कार्तीनाथ केलकर पुस्तकालय
भारतीय प्रौद्योगिकी संस्थान, कानपुर
अवाप्ति सं. 168432

The procedure followed for the vibration measurement has various steps such as test-conditions specification, selection of accelerometer positions, setting of transducers mounting fixtures, vehicle preparation engine-operation specification and data logging.

Test Conditions

The vehicle testing was performed in the laboratory in order to exercise better control on configurations and test conditions. The focus was to comparatively evaluate the vibrations of different vehicles. Road condition is not a parameter under consideration, during the study. The test location was selected based on the minimum ground vibrations. The vehicle was put on a test bed with the rider sitting over the seat at driver position and vehicle resting on both wheels (Figure 3.1 and 3.2). The engine was positioned for gear in neutral and with clutch engaged.

Transducers Mounting Fixtures

The vibrations were measured with a uni-axial ONO SOKKI NP-3331 pre-amplifier acceleration transducer. The fixtures were designed to mount this accelerometer, which provides for a short threaded portion for tightening the base structure mounting and three orthogonal surfaces for measuring the acceleration pickup.

Accelerometer Positions

The measurements were taken at two locations on the engine and three different points on the vehicle. In the engine, one point on lateral side of the cylinder head (Figure 3.3, a), and another on the lower front engine mounting were chosen (Figure 3.3, b). On the vehicle structure, one point on the tip of the foot-rest (Figure 3.3 (c)), another on the plate on seat frame - just below the rider seat position (Figure 3.3 (d)) and one more location on the steering bar mirror mounting location (Figure 3.3 (e)) - were chosen.

At each location accelerations were measured taken in three directions - axial direction, vertical direction and transverse direction.

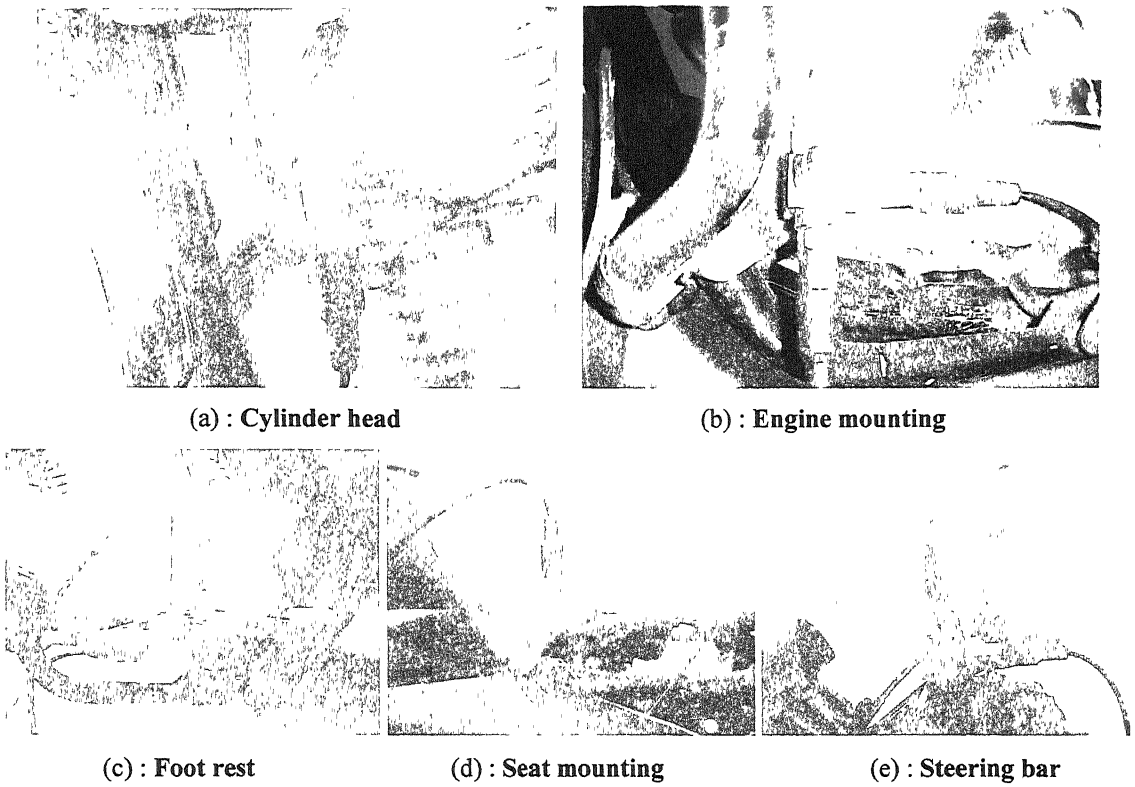

(a) : **Cylinder head** (b) : **Engine mounting**

(c) : **Foot rest** (d) : **Seat mounting** (e) : **Steering bar**

FIGURE 3.3 - **Sensor locations**

Engine Operating Conditions

The engine was accelerated continuously from 1400 rpm to 6000 rpm in six stages. 1400 rpm is the engine idling speed of all engines and 6000 rpm is considered a safe upper limit value. Data is collected at average engine speeds of 1400, 2000, 3000, 4000, 5000 and 6000rpm. The engine is allowed to run for five minutes at each average angular speed stage so as to reach the steady state. The engine was continuously cooled by a high capacity blower and before each higher stage measurements the engine was brought to its normal temperature. The exhaust gas of the running engine was pumped out using exhaust ventilation system.

Input Parameters

The data is collected at a sampling frequency of 1280 Hz for duration of 3.2 seconds (4096 samples). The average speed of the engine was adjusted with the help of an Engine Tachometer DET-610 with an accuracy of ± 10 rpm. The Fourier Transforms were obtained by averaging sixty-four spectra through a Hanning window. The test is repeated three times for repeatability. The visual frame of 500 Hz was selected in the FFT Analyser to see up to the first eight engine order excitations and 212 crankshaft revolutions, which are equivalent to 106 thermodynamic cycles of the engine for an average angular speed of 4000rpm.

Results and Analysis

Data acquisition and signal processing were carried out using CF-3200 portable FFT analyser from ONO SOKKI. The various malfunctions involved in the engine (cylinder head and engine mounting) and their effect on the vehicle – human interface locations (steering bar tip, foot rest and seat mounting) on vehicle were monitored and the resulting vibration signals were transformed to the frequency domain by application of a fast Fourier transform. This was done to assess the comfort levels of the ride, quality of the engine and the structure. The running frequency peak-amplitude was filtered from the frequency spectrum at each stage and the frequency response curve was generated with this data. The response curves of the vehicles were put together for comparison. The damping ratios of the curves were calculated using standard vibration techniques.

3.5 Vehicle Selection and Configuration

Experiments were performed with four different vehicles of different make in the range and a vehicle rejected in the field for vibration. The vehicles selected are from executive and premium segment, two from executive and three from premium segment based on their sale. The vehicles are numbered from 1to 4 based on the displacement and power. The specifications of the vehicles are given in Table 3.1.

TABLE 3.1 (a) : **Engine details**

Parameter	**Vehicle No. 1**	**Vehicle No. 2**	**Vehicle No. 3**	**Vehicle No. 4**
Type	Single cylinder, 4-stroke, air cooled	Single cylinder, 4-stroke, air cooled	Single cylinder, 4-stroke, air cooled	Single cylinder, 4-stroke, air cooled
Valve Train	2 valve, ohc	2 valve, ohc	2 valve, ohc	2 valve, ohc
Displacement	143.9cc	133cc	109.15cc	109.2cc
Bore x Stroke	57mm x 56.4mm	58.5mm x 49.5mm	53mm x 49.5mm	51mm x 53.5mm
Comp Ratio	9.5:1	9.5:1	9.0:1	9.3:1
Max Power	11.83bhp@8500rpm	11bhp@8000rpm	8.5bhp@7750rpm	8.1bhp@7250rpm
Max Torque	11.68Nm@6500rpm	10.5Nm@4500rpm	10.5Nm@4500rpm	8.15Nm@5500rpm
Power to Weight	88.27bhp/ton	84.51 bhp/ton	75.89 bhp/ton	76.11 bhp/ton
Ignition	Digital CDI	microprocessor	CDI electronic	Electronic digital

TABLE 3.1 (b) : **Gearbox details**

Parameter	**Vehicle No. 1**	**Vehicle No. 2**	**Vehicle No. 3**	**Vehicle No. 4**
Clutch	Wet multi plate	Wet multi plate	Wet multi plate	Wet multi plate
Primary Reduction	3.47 Gear Drive	4.055 Gear Drive	3.579 Gear Drive	3.52 Gear Drive
Final Reduction	2.8 Roller Chain	2.174 Chain Drive	2.859 Chain Drive	3.3 Chain Drive
Gear Box	5-speed constant mesh	5-speed constant mesh	4-speed constant mesh	4-speed constant mesh
Gear Ratio	2.85, 1.87, 1.32, 1.000, 0.898	2.769, 1.688, 1.200, 1.000, 0.839	3083, 1.882 1.318, 1.041	2.833, 1.600, 1.143, 0.917

TABLE 3.1 (c) : **Chassis details**

Parameter	**Vehicle No. 1**	**Vehicle No. 2**	**Vehicle No. 3**	**Vehicle No. 4**
Type	Tubular double cradle	Tubular single cradle	Tubular single cradle	Tubular single cradle
Fr. Suspension	Telescopic Forks	Telescopic forks	Telescopic forks	Telescopic forks
Rear Suspension	Adjustable Swing arm	Adjustable Swing arm	Adjustable Swing arm	Adjustable Swing arm
Wheel size F/R	1.6 X 18 / 1.82 X 18	1.6 X 18 / 1.6 X 18	1.6 X 18 / 1.6 X 18	1.6 X 18 / 1.6 X 18
Tyres F/R	2.75 X 18 / 3.00 X 18	2.75 X 18 / 3.00 X 18	2.75 X 18 / 3.00 X 18	2.5 X 18 / 2.75 X 18

TABLE 3.1 (d) : **General data**

Parameter	**Vehicle No. 1**	**Vehicle No. 2**	**Vehicle No. 3**	**Vehicle No. 4**
Kerb Weight	133kg	126.5kg	112kg	105.5kg
Max Payload	130kg	130kg	130kg	130kg
Wheelbase	1265mm	1285mm	1230mm	1200mm
Length	1960mm	2030mm	2010mm	1975mm
Width	790mm	760mm		
Height	1065mm	1100mm	1080mm	1015mm
Gr. Clearance	155mm	150mm	NA	NA
Min Turning Radius	2010mm	1950mm	NA	NA
Fuel Tank Capacity	18liters	12.5liters	12.2liters	11liters

3.6 Vibration Characteristics of Vehicles

3.6.1 Time Domain Signals

Fig 3 4 shows the typical time domain cylinder head accelerations signals at 4000 engine rpm

Location 1 : Cylinder Head **Engine speed 4000 rpm (66.67 Hz)**

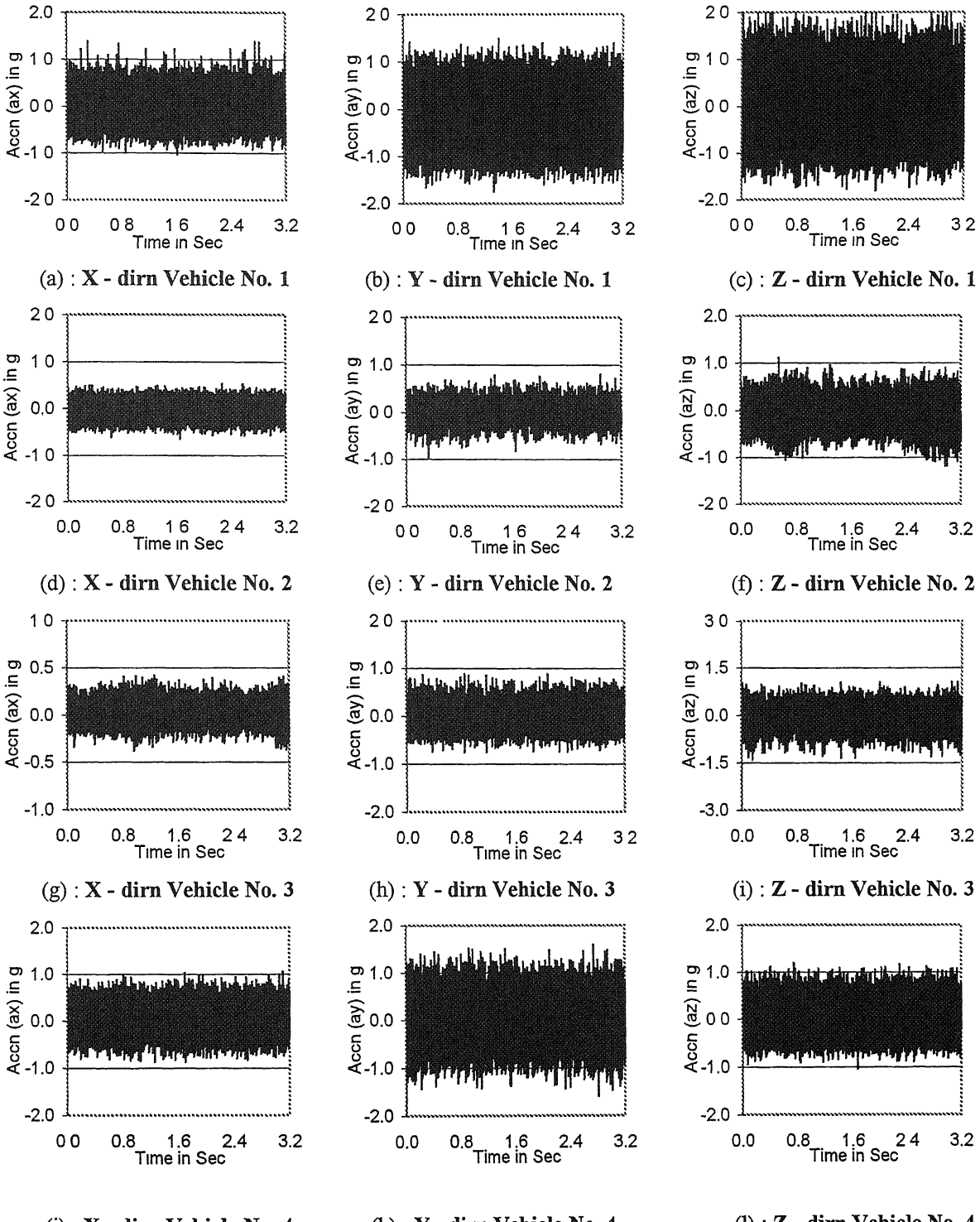

(a) : **X - dirn Vehicle No. 1** (b) : **Y - dirn Vehicle No. 1** (c) : **Z - dirn Vehicle No. 1**

(d) : **X - dirn Vehicle No. 2** (e) : **Y - dirn Vehicle No. 2** (f) : **Z - dirn Vehicle No. 2**

(g) : **X - dirn Vehicle No. 3** (h) : **Y - dirn Vehicle No. 3** (i) : **Z - dirn Vehicle No. 3**

(j) : **X - dirn Vehicle No. 4** (k) : **Y - dirn Vehicle No. 4** (l) : **Z - dirn Vehicle No. 4**

FIGURE 3.4 – Time domain signals of cylinder heads

3.6.2 Frequency Domain Signals

Fourier Transform is carried out for the time domain data of Fig. 3.4. The FFT spectra from the cylinder head are shown in Figures 3.5 to 3.9. These plots give a picture of the engine operating conditions. The plots should ideally contain only the fundamental harmonic of the operating frequency.

It can be seen that for Vehicle Number 1 in Figure 3.5, the second harmonic in most instances is as prominent as the first one. This shows that the harmonicity of engine forces is less in this vehicle in comparison to others and consequently the operation is jerkier. Similarly Vehicle Number 4 shows higher amplitudes at higher harmonics, which again indicates that the engine operation is jerky. It may also be an indication of improper assembly or loose mechanical components in the assembly. Vehicle Numbers 2 and 4 have their gradually decreasing response harmonics, which can be considered as indicators of smoother operation.

Similar observations can be made from the FFTs of engine mounting vibrations (Figure 3.6). Here the amplitude levels are approximately half of those on the engine head. Vehicle number 4 is seen to exhibit lower vibration amplitudes in the x-direction, while for y directions the performance of Vehicle Number 3 appears to be better.

As far as vibrations on the footrest are concerned (Figure 3.7) Vehicle Number 3 exhibits good properties in y-direction, but not so good performance in the z direction. Vehicle number 1 contains a predominant second harmonic, while vehicle number 4 is also found to vibrate more, with a large number of frequencies getting excited in the x direction.

Seat vibration FFTs are shown in Figure 3.8, Y-direction vibrations are found to be high for Vehicle Number 3. Vehicle Number 2 has very low levels of vibrations, indicating good seat fixtures. Vehicle Number 1, again has abnormally high second harmonic of seat vibration also. It has high vibrations in the z-direction too.

Location No. 1 : Cylinder Head **Engine speed 4000 rpm (66.67 Hz)**

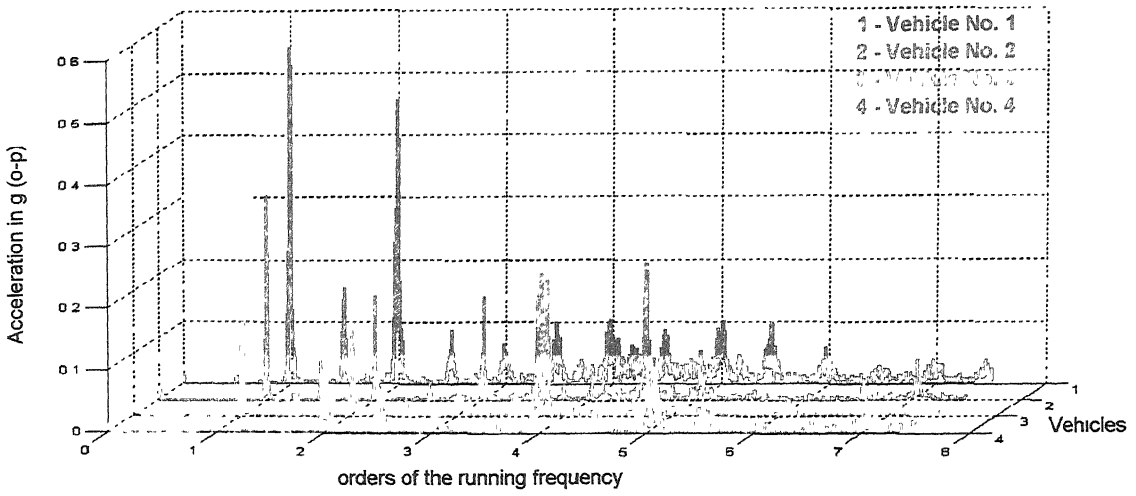

(a) : **X - Direction**

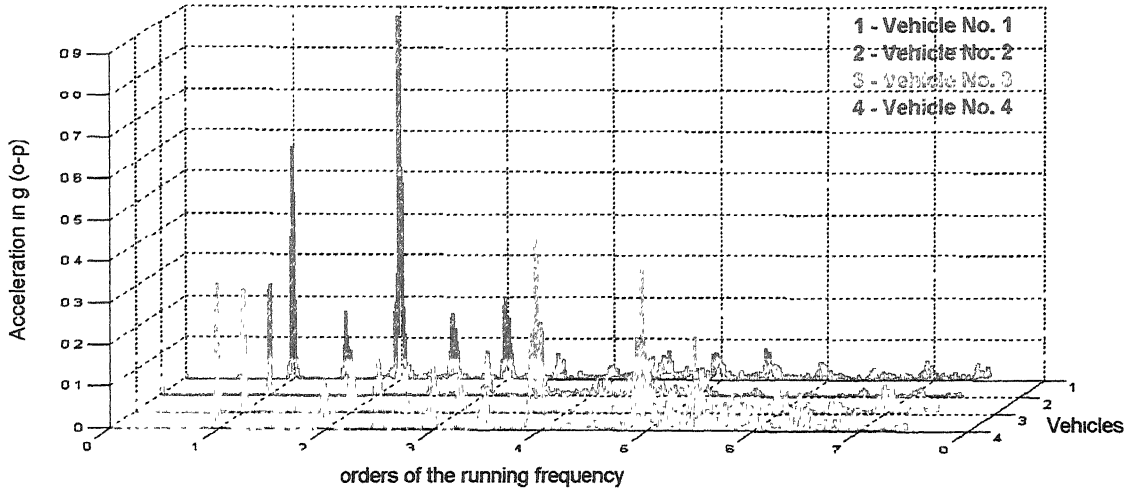

(b) : **Y - Direction**

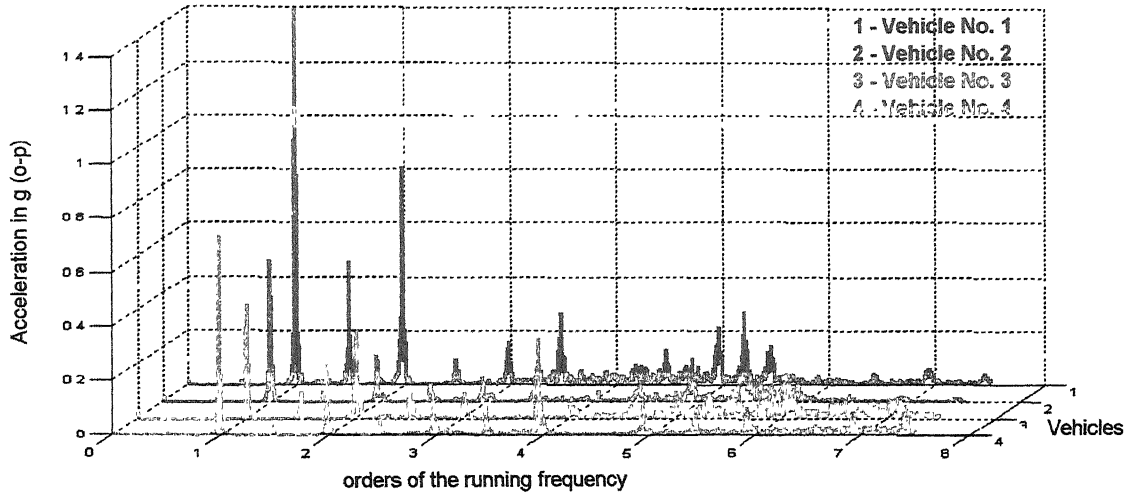

(c) : **Z - Direction**

FIGURE 3.5 - **Comparison of FFT spectrum of cylinder heads**

Location No. 2 : Engine Mounting **Engine speed 4000 rpm (66.67 Hz)**

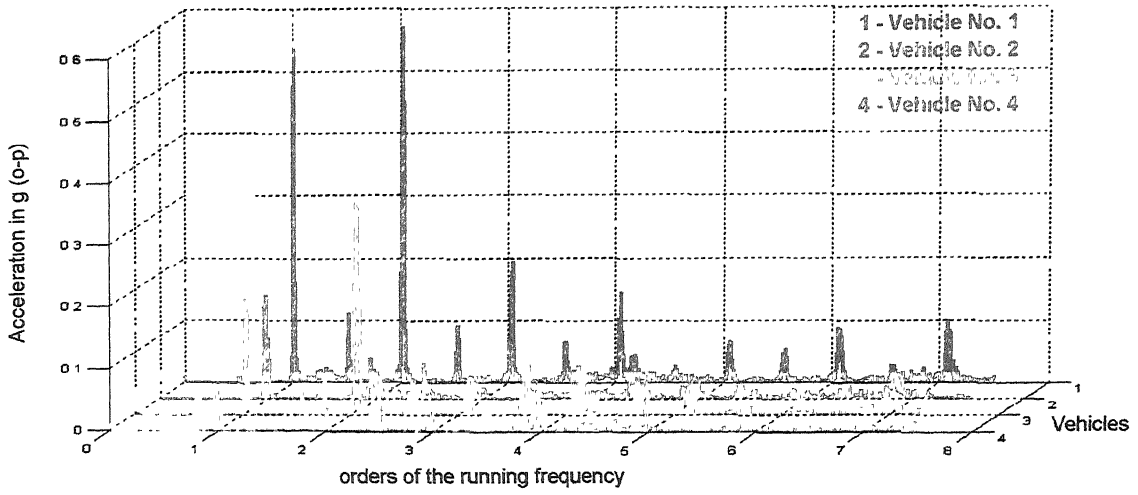

(a) : **X - Direction**

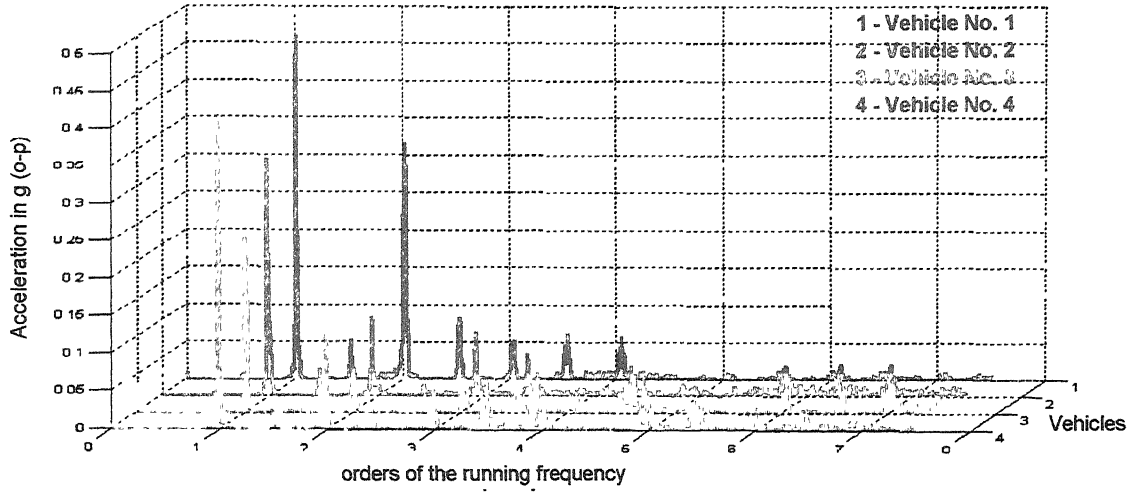

(b) : **Y - Direction**

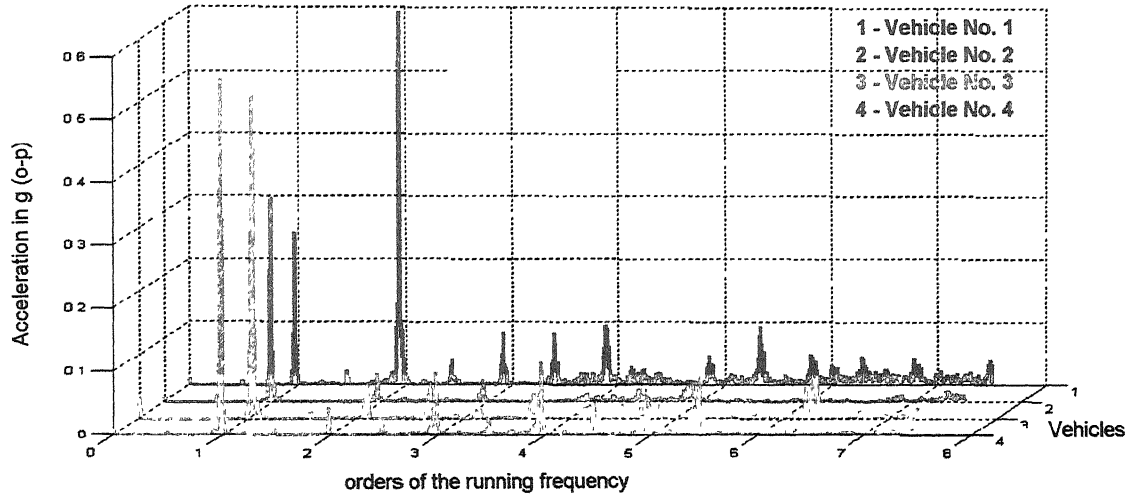

(c) : **Z - Direction**

FIGURE 3.6 - **Comparison of FFT spectrum of engine mountings**

Location No. 4 : Seat Mounting **Engine speed 4000 rpm (66.67 Hz)**

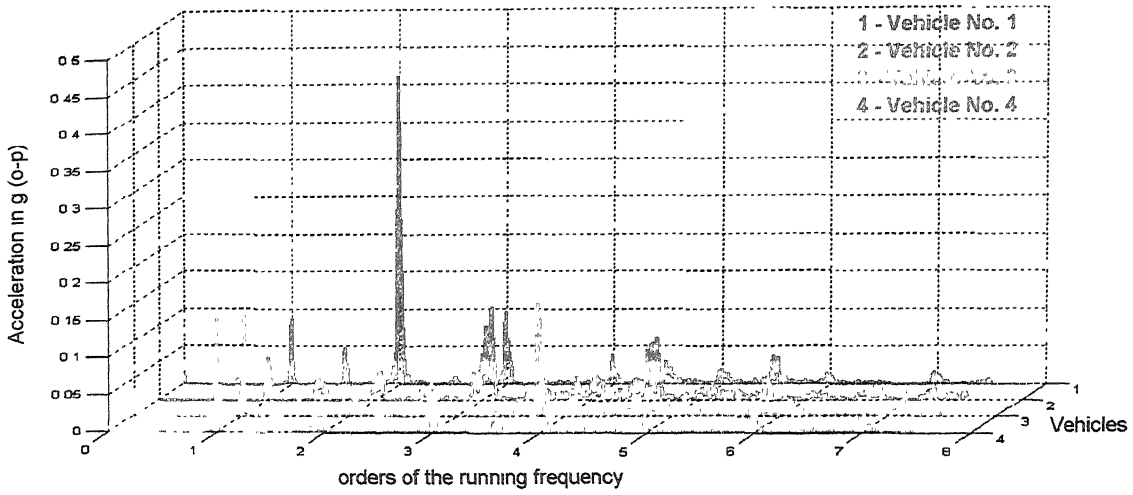

(a) : **X - Direction**

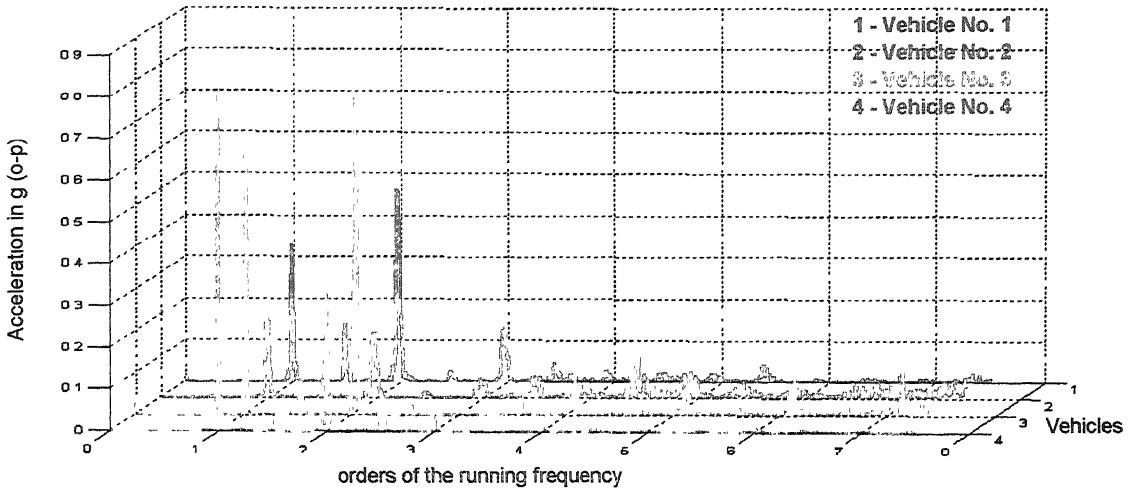

(b) : **Y - Direction**

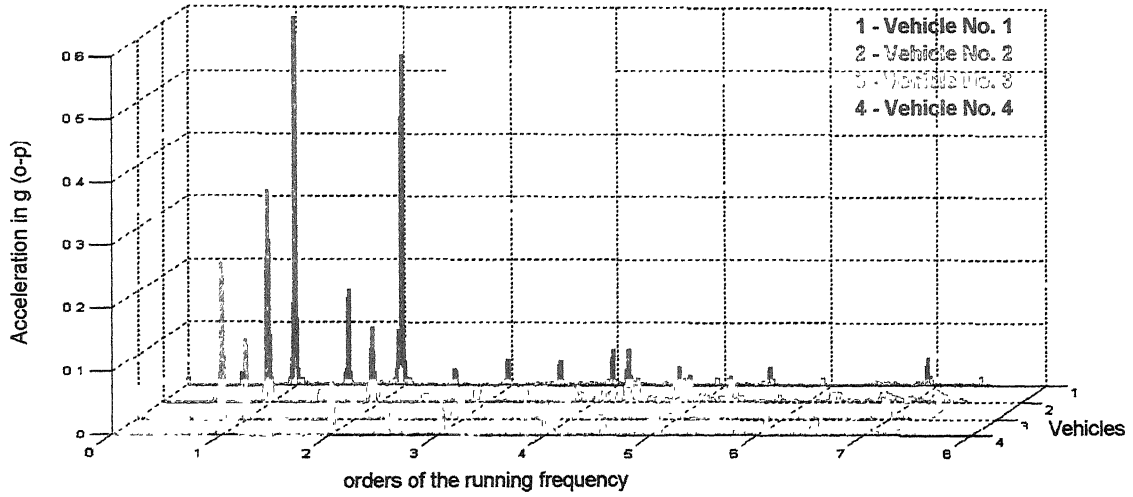

(c) : **Z - Direction**

FIGURE 3.8 - **Comparison of FFT spectrum of seat mountings**

Location No. 5 : Steering Bar **Engine speed 4000 rpm (66.67 Hz)**

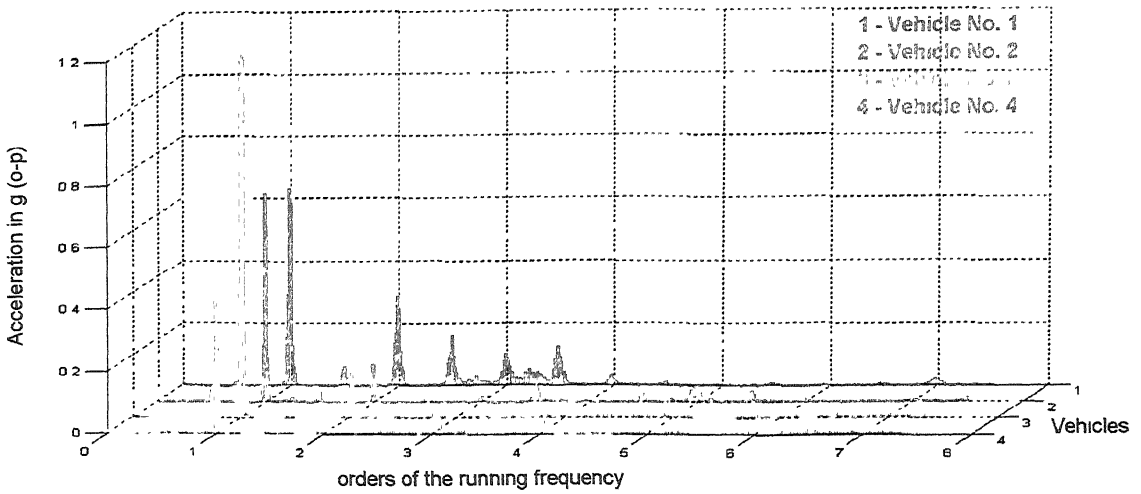

(a) : **X - Direction**

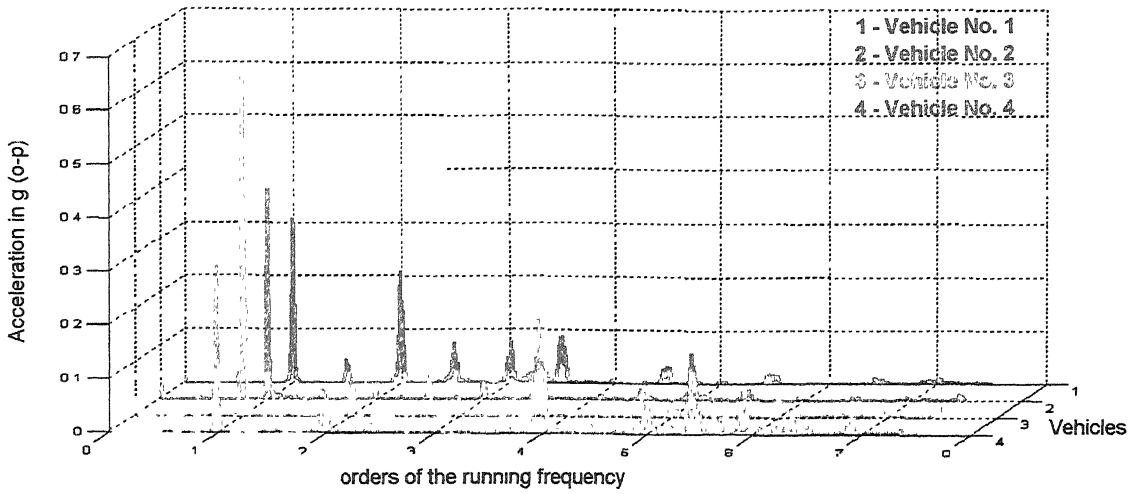

(b) : **Y - Direction**

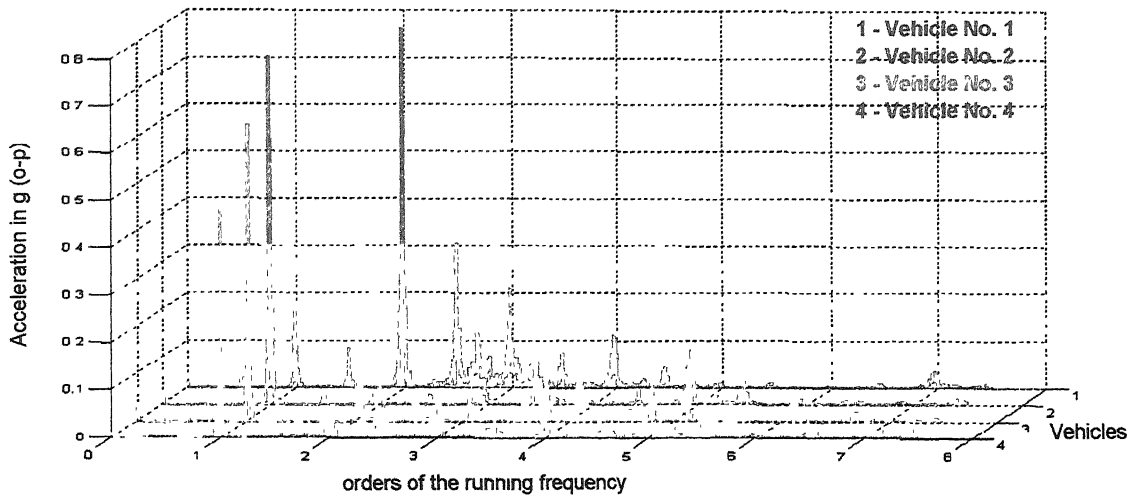

(c) : **Z - Direction**

FIGURE 3.9 - **Comparison of FFT spectrum of steering bars**

Steering bar FFT signals are shown in Figure 3.9, Vehicle number 4 is seen to exhibit the best performance by keeping its vibration at lowest levels. Vehicle number 3 display high amplitudes of steering- bar vibrations. Higher order harmonics are most predominant, in case of steering - bar vibrations, with higher order harmonic amplitudes being negligible in comparison.

3.6.3 Frequency Response Functions

Frequency Response Function Plots (Figure 3.10 to 3.13) are obtained by plotting the first harmonic amplitude versus the running speed of the engines. These plots have been obtained for all the vehicles under consideration and for all the measurement locations. At each of these locations the FRF is plotted for all three-measurement directions. These plots show that the operating range (0-7200 rpm engine speed) of the vehicles would incorporate two major critical speeds. These critical speeds are cantered out 3500 rpm and 5500 rpm (40 kmph and 65 kmph, respectively), though the particular resonances vary marginally from vehicle to vehicle.

Overall frequency response Functions have been computed from by vectorial addition of the FRFs x, y and z directions. These overall FRFs have been obtained for all measurement locations and plotted in Figure 3.14 (b to f). A comparative picture is obtained by drawing the FRF curve at a specific location, for all the vehicles on the same plot. Figure 3.14 a gives the associated top gear chart for the vehicles.

It can be seen in the speed chart that Vehicle Number 1 have low overall speed reduction, which gives the high vehicle speed for same engine speed in comparison to other vehicles.

It can be seen that cylinder head vibrations of Vehicle Number 1 and 3 grow towards high values at critical speed, while those in 2 and 4 remain controlled. Similar observations can be made for engine mounting (Figure 3.14 (c)), with vibration control being observed to be best in Vehicle Number 4. However, Vehicle Number 4 does not

exhibit good control on footrest vibrations (Figure 3.14 (d)). Here the performance of Vehicle Number 1 is found to be better than others.

Seat mounting vibrations (Figure 3.14 (e)) are seen to be lowest in case of Vehicle Number 4. Large vibrations are seen in the case of Vehicle Number 3. Vehicle 1 and 2 show trends similar to Vehicle Number 3.

In the case of steering bar vibrations (Figure 3.14 (f)), Vehicle Number 4 again exhibits the best performance, while Vehicle Number 1, shows an increasing trend towards the second critical. Vehicle Number 2 and 3 show similar trends, with two critical within engine speed of 6000 rpm, and vibration levels significantly higher than Vehicle Number. 4.

3.7 Comparison with Computational Results

It is to be noted that the finite element modelling has been carried out for Vehicle Number 3. The directional FRF values from experiments and FEM are shown together, for various measurement locations in Figure 3.15 (a to j). Figure 3.15 (b, d, f, h and j) pertains to the overall FRF values. While very good correlation can be observed between experimental and computed FRFs, for the case of steering-bar vibrations, it can be said to be comparable for other measurement locations – with critical speeds correlating well in quite a few cases and the order of FRF amplitude levels correlating well in most cases.

The point to be noted that, the computed combustion and inertia force spectrum are assumed to be sufficient in comparison of FEM and experimental FRF curves.

Keeping in mind the complicated structural design of the motorcycle and the limitations in incorporating all their features, the above results suggest that the finite element modelling exercise has been appropriate.

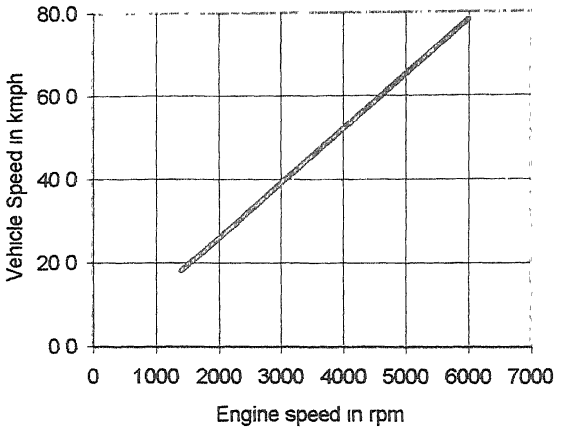

(a) : **Engine - Vehicle speed chart**

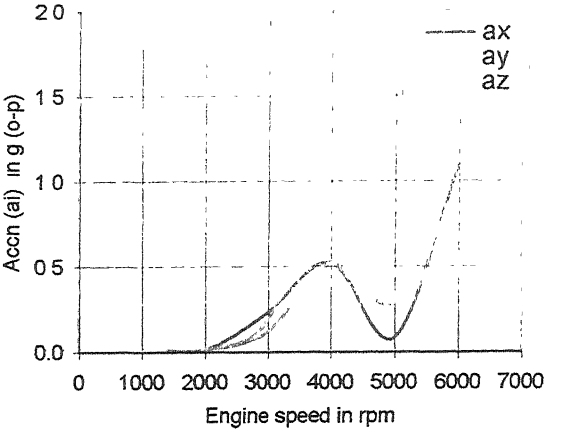

(b) : **Cylinder head**

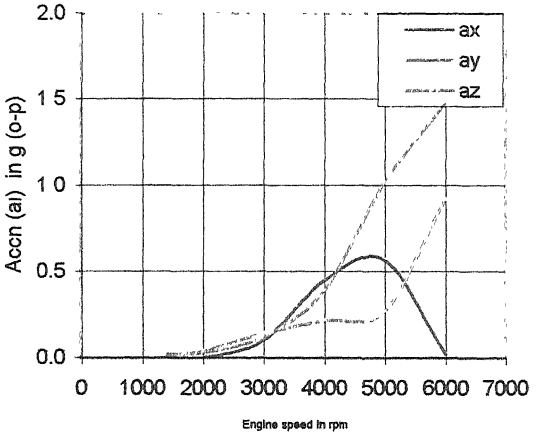

(c) : **Engine mounting**

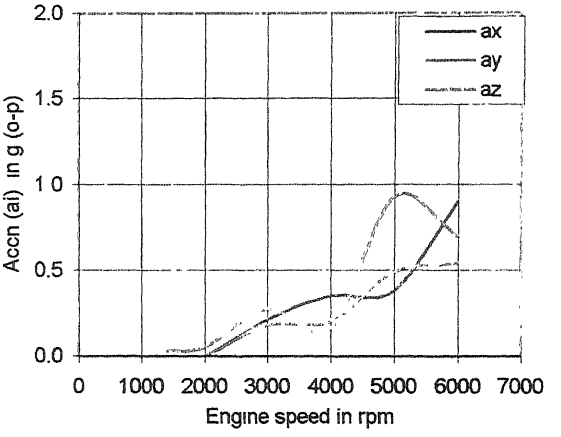

(d) : **Foot rest**

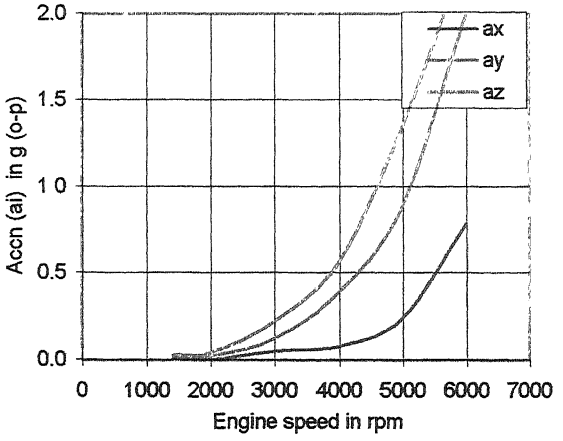

(d) : **Seat mounting**

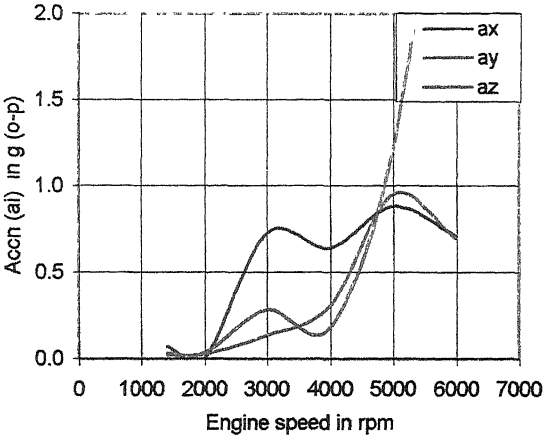

(e) : **Steering bar**

FIGURE 3.10 – **Speed and frequency response plots : Vehicle No. 1**

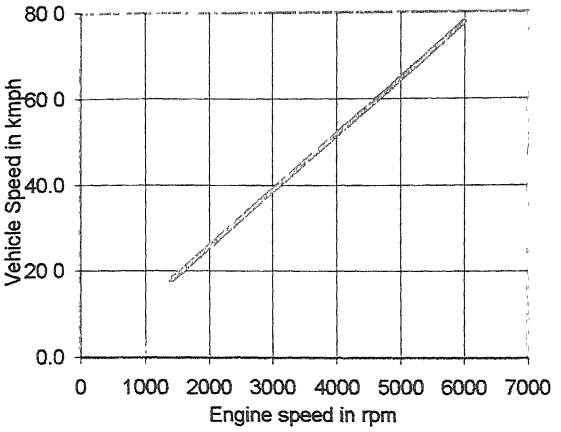

(a) : **Engine - Vehicle speed chart**

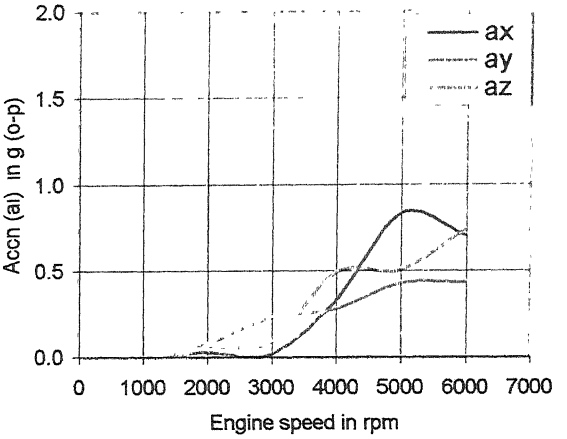

(b) : **Cylinder head**

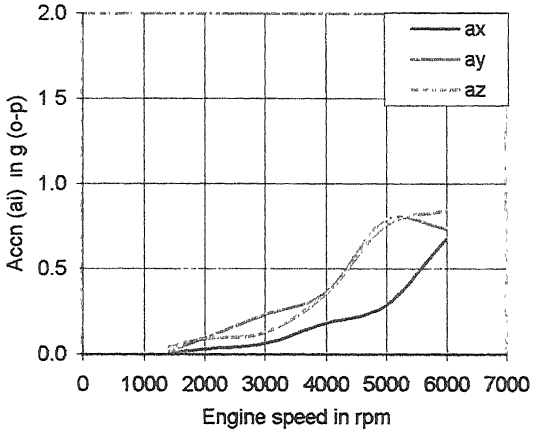

(c) : **Engine mounting**

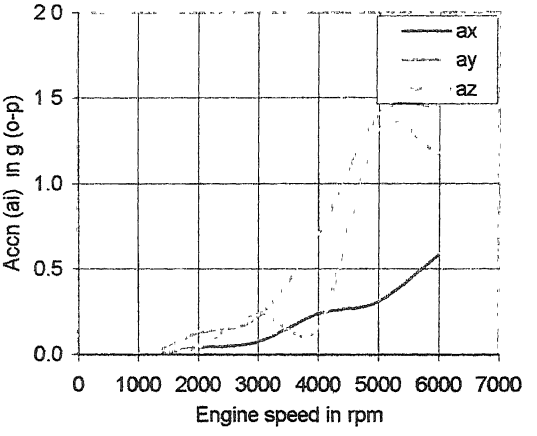

(d) : **Foot rest**

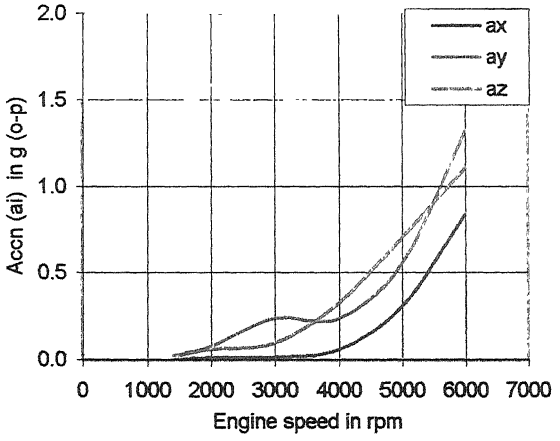

(d) : **Seat mounting**

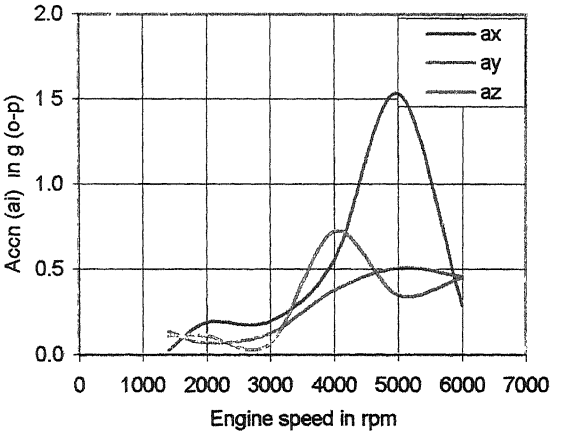

(e) : **Steering bar**

FIGURE 3.11 – **Speed and frequency response plots : Vehicle No. 2**

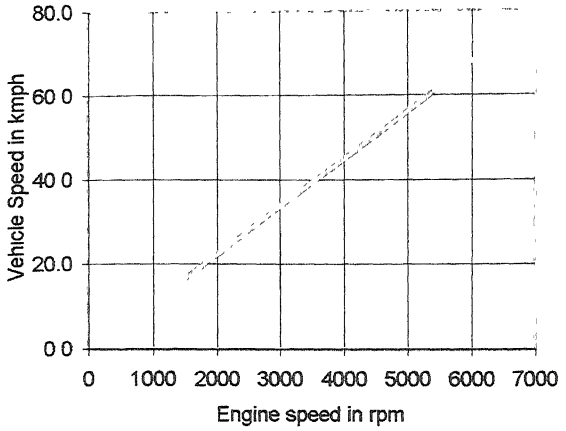

(a) : **Engine - Vehicle speed chart**

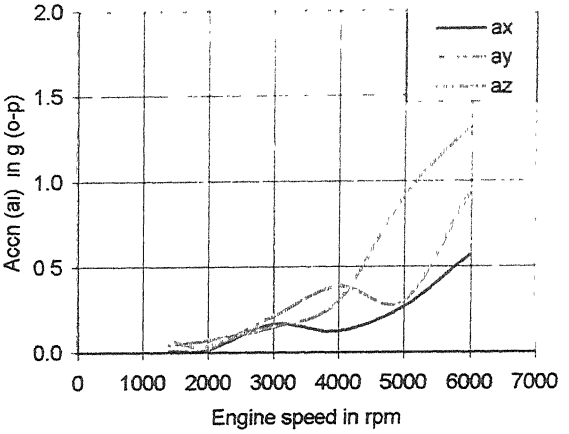

(b) : **Cylinder head**

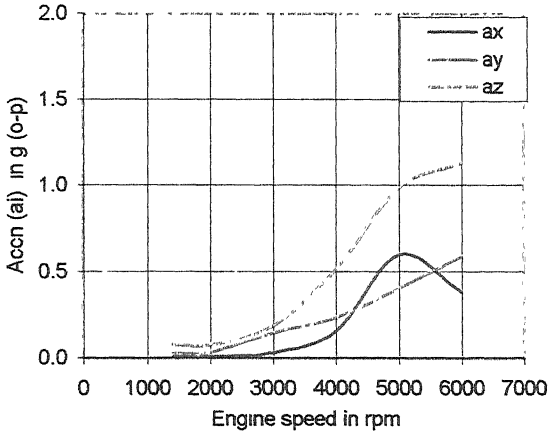

(c) : **Engine mounting**

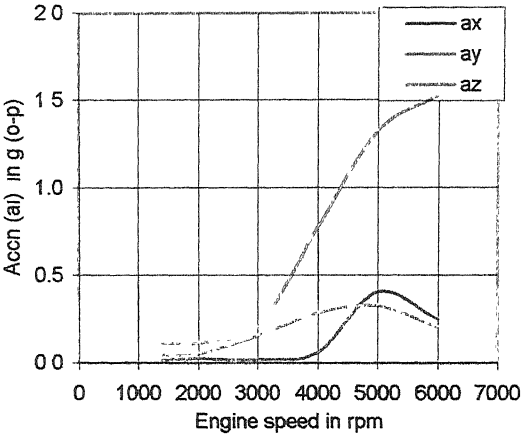

(d) : **Foot rest**

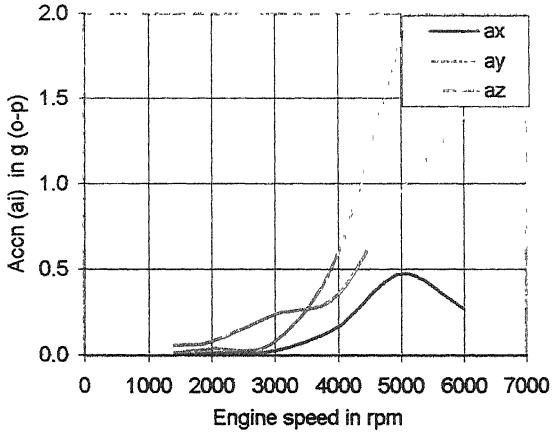

(d) : **Seat mounting**

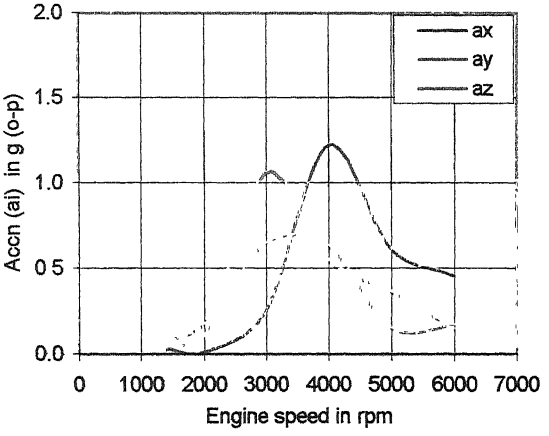

(e) : **Steering bar**

FIGURE 3.12 – **Speed and frequency response plots : Vehicle No. 3**

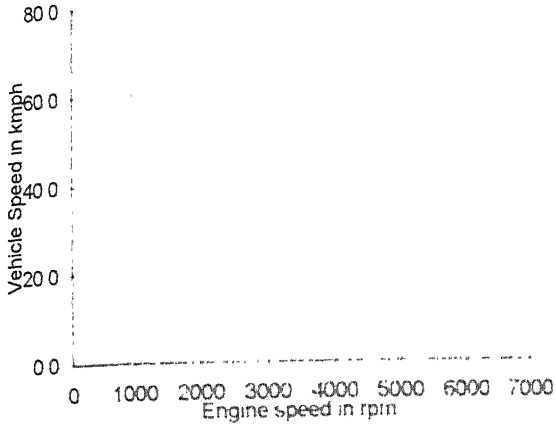

(a) : **Engine - Vehicle speed chart**

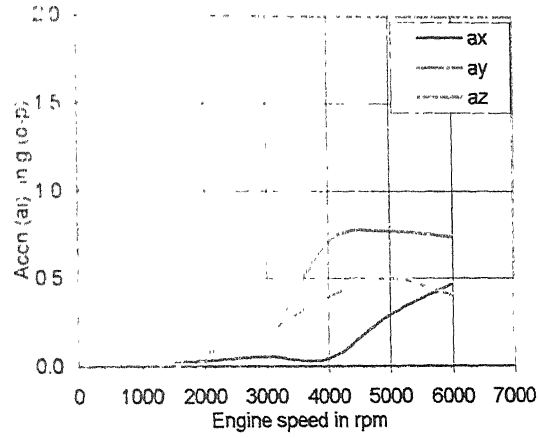

(b) : **Cylinder head**

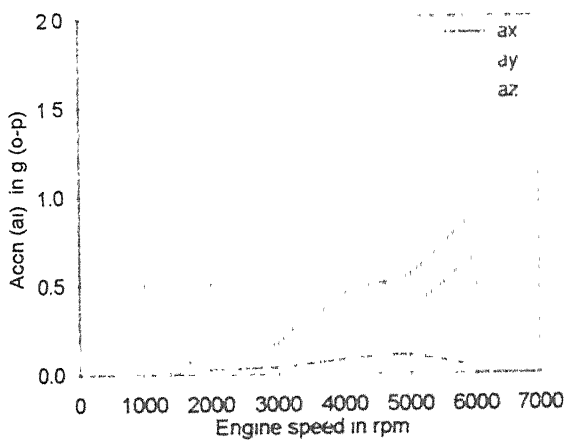

(c) : **Engine mounting**

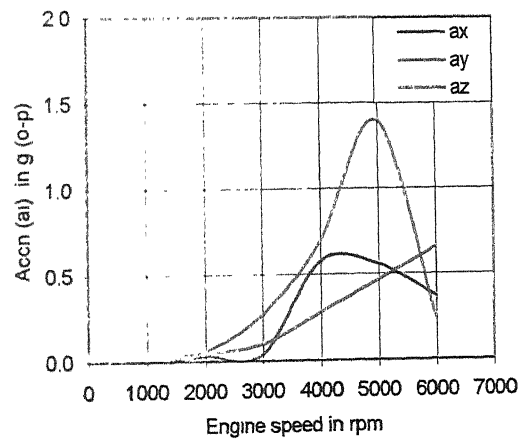

(d) : **Foot rest**

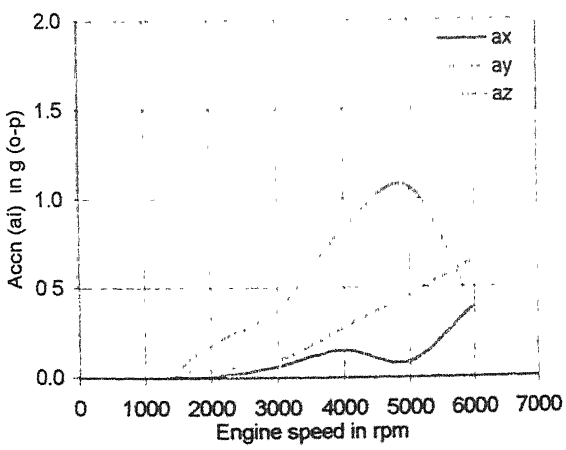

(d) : **Seat mounting**

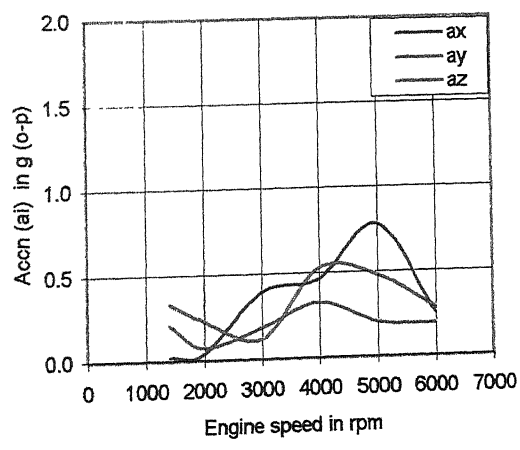

(e) : **Steering bar**

FIGURE 3.13 – **Speed and frequency response plots : Vehicle No. 4**

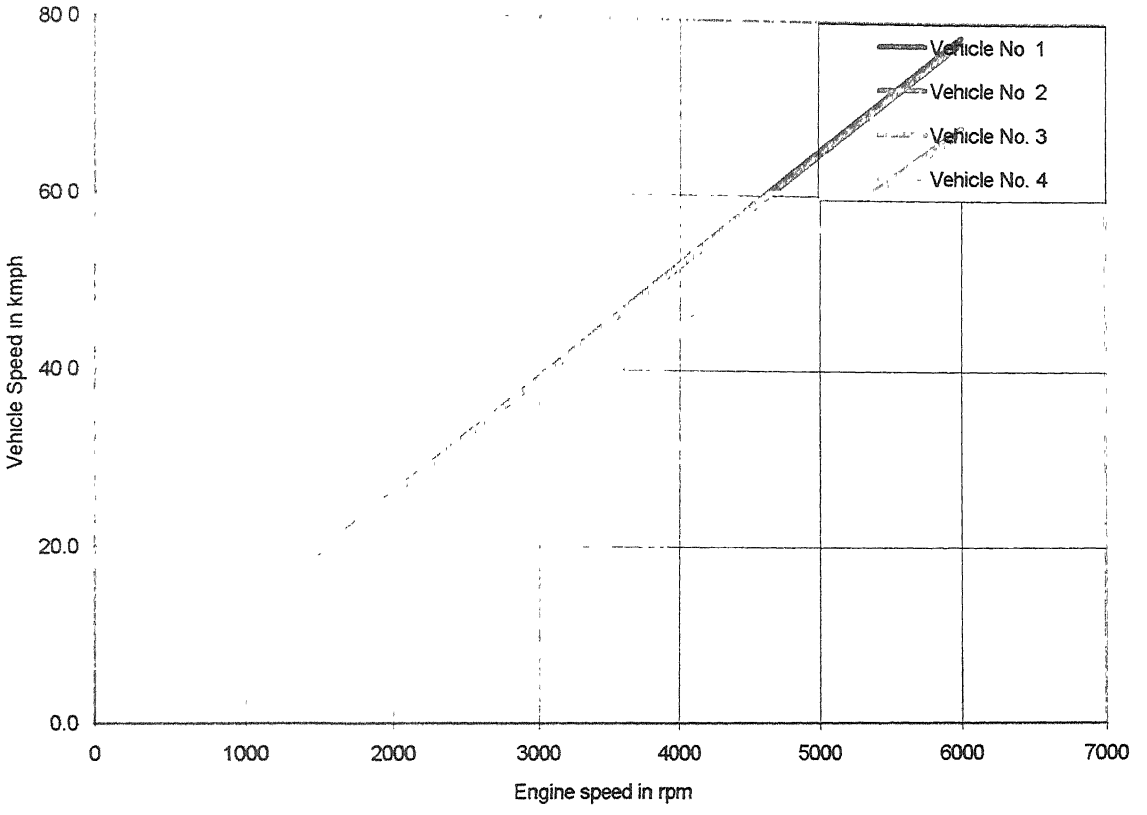

(a) : **Engine - Vehicle speed chart**

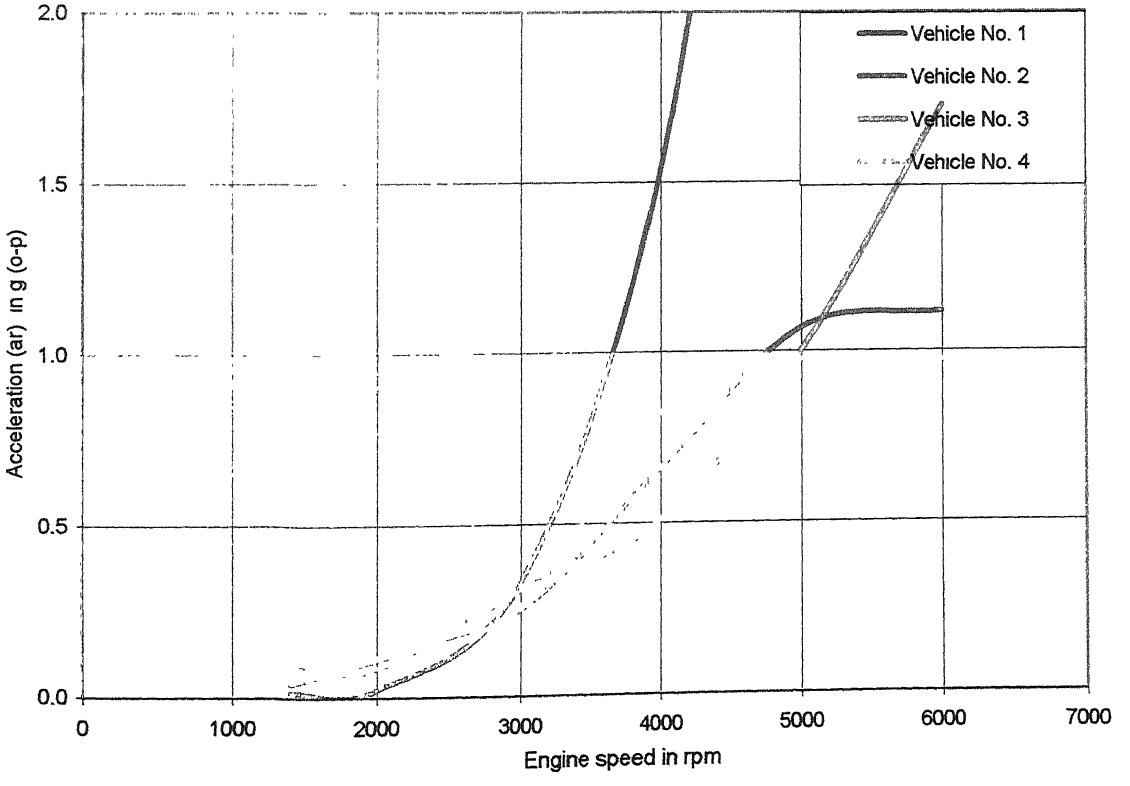

(b) : **Cylinder head**

FIGURE 3.14 (a & b) – **Speed and comprasion of overall vibrations of all vehicles**

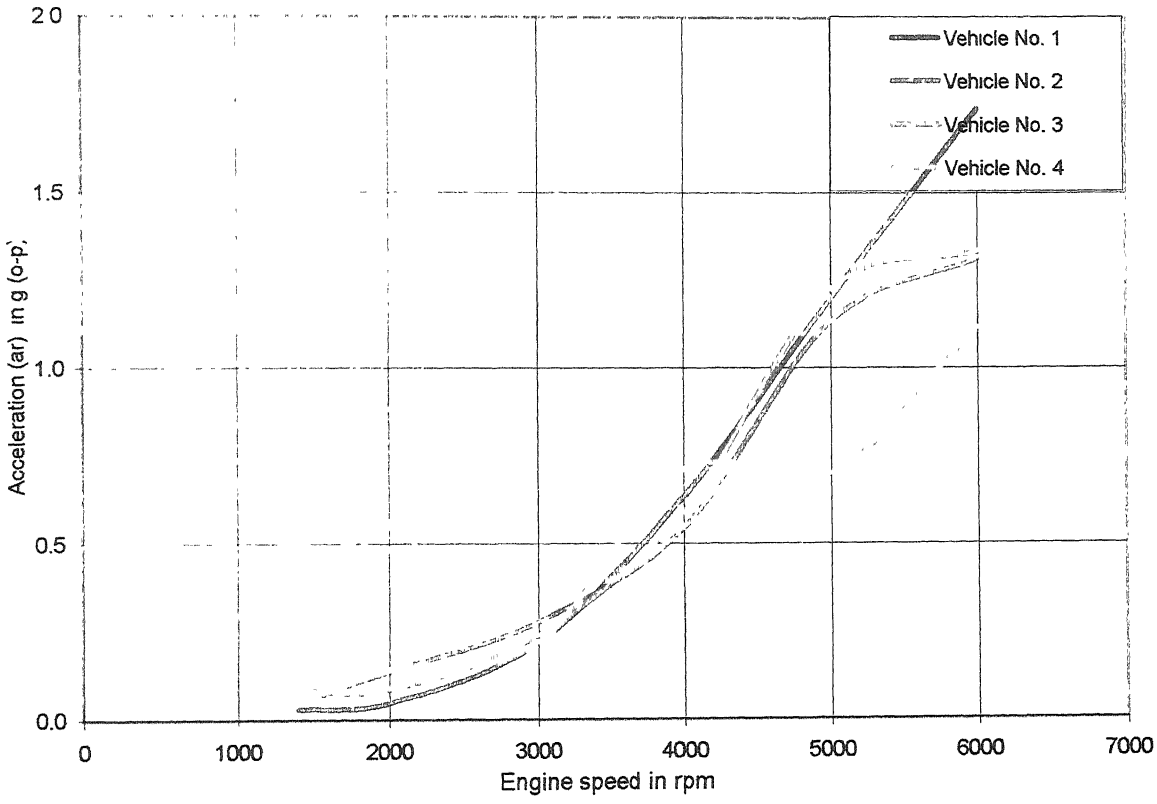

(c) : **Engine mounting**

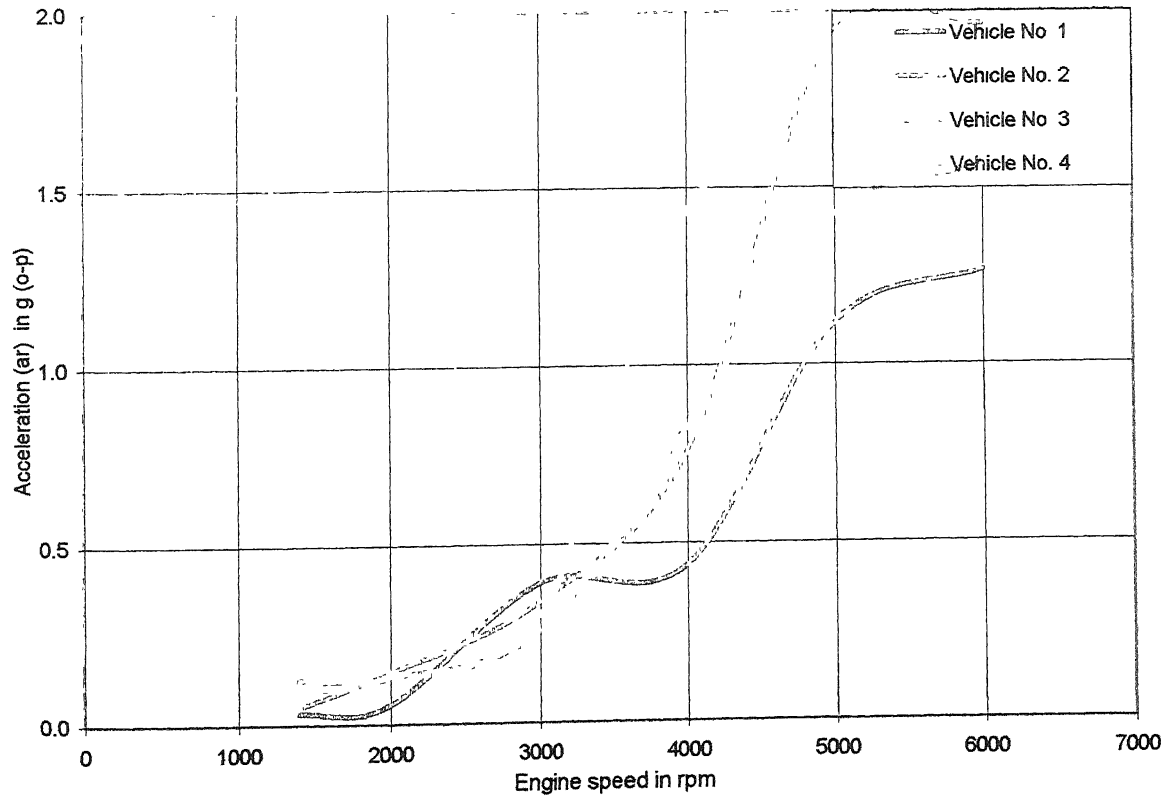

(d) : **Foot rest**

FIGURE 3.14 (c & d) – **Speed and comprasion of overall vibrations of all vehicles**

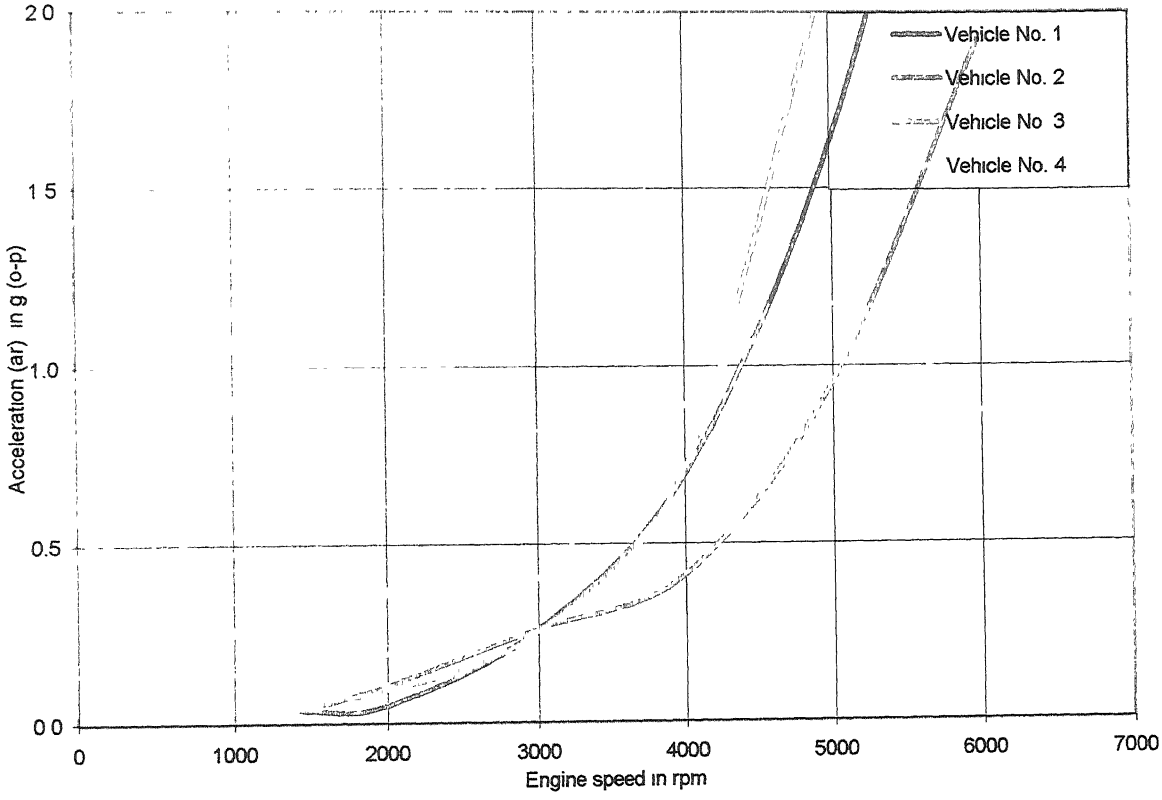

(e) : **Seat mounting**

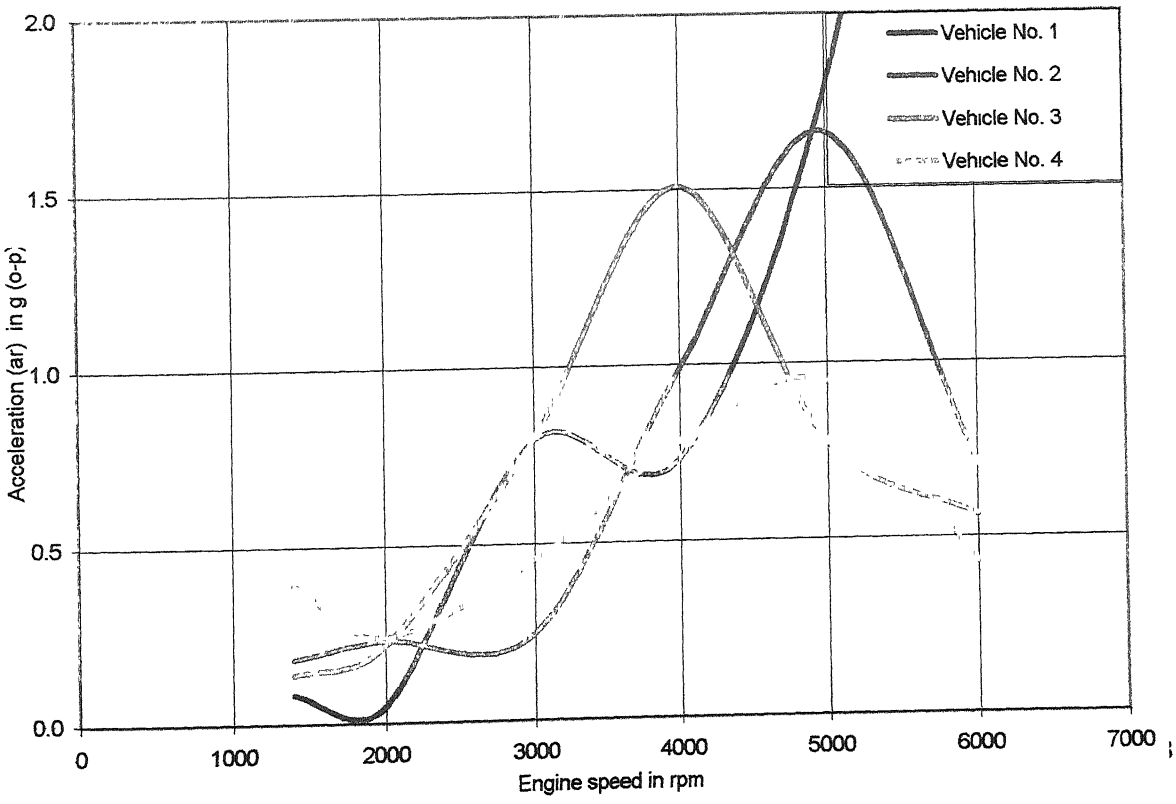

(f) : **Steering bar**

FIGURE 3.14 – **Speed and comprasion of overall vibrations of all vehicles**

Location No. 1 : Cylinder Head

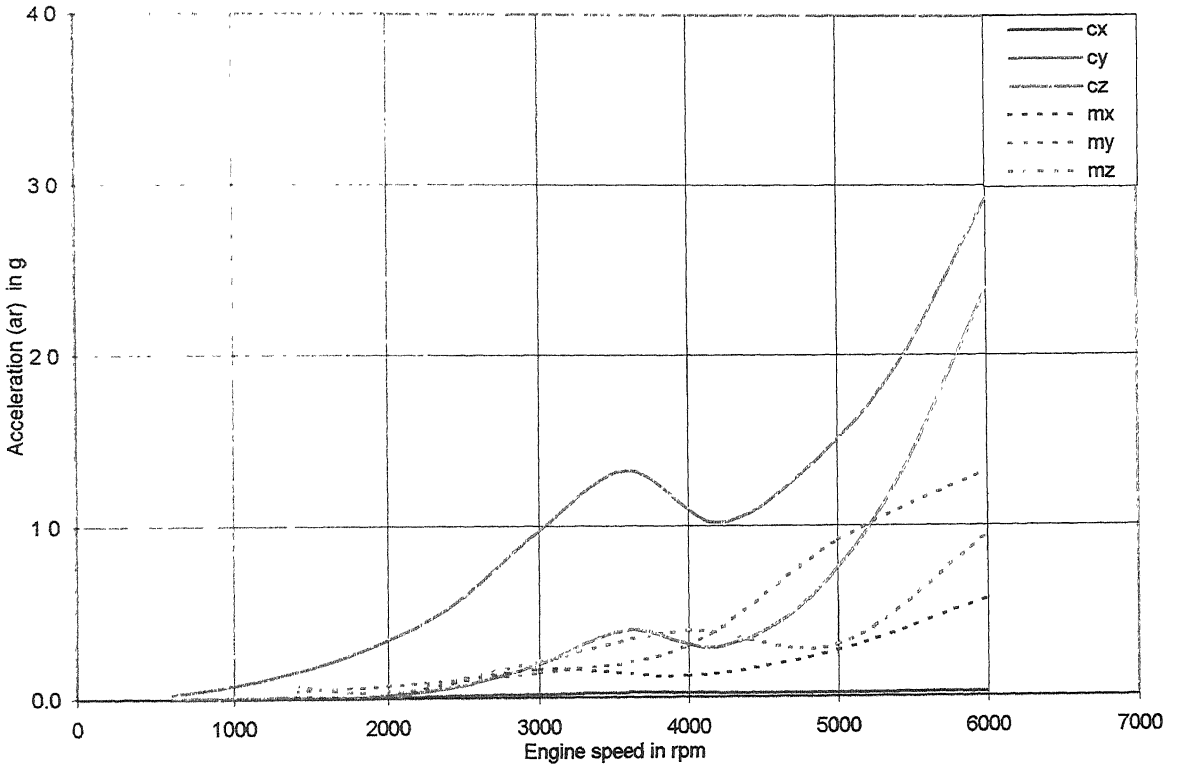

(a) : **Component accelerations**

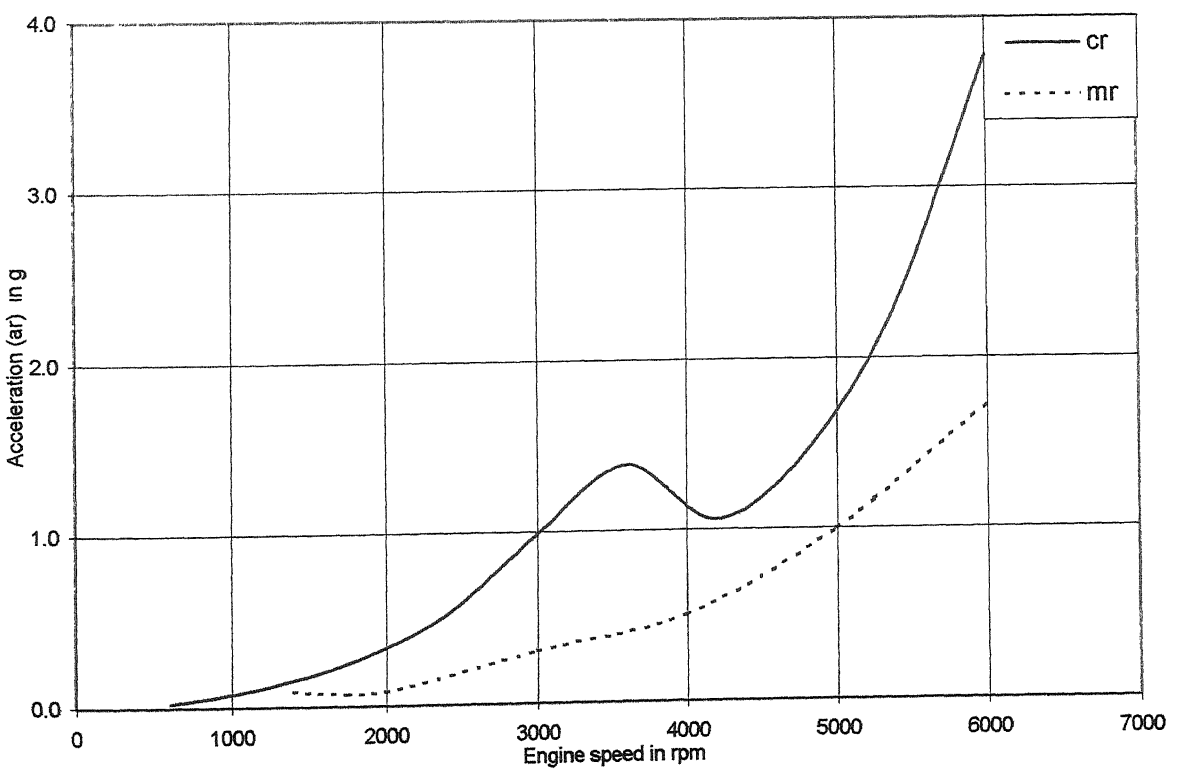

(b) : **Resultant accelerations**

FIGURE 3.15 (a & b) – **Comparison with computational results**

Location No. 2 : Engine Mounting

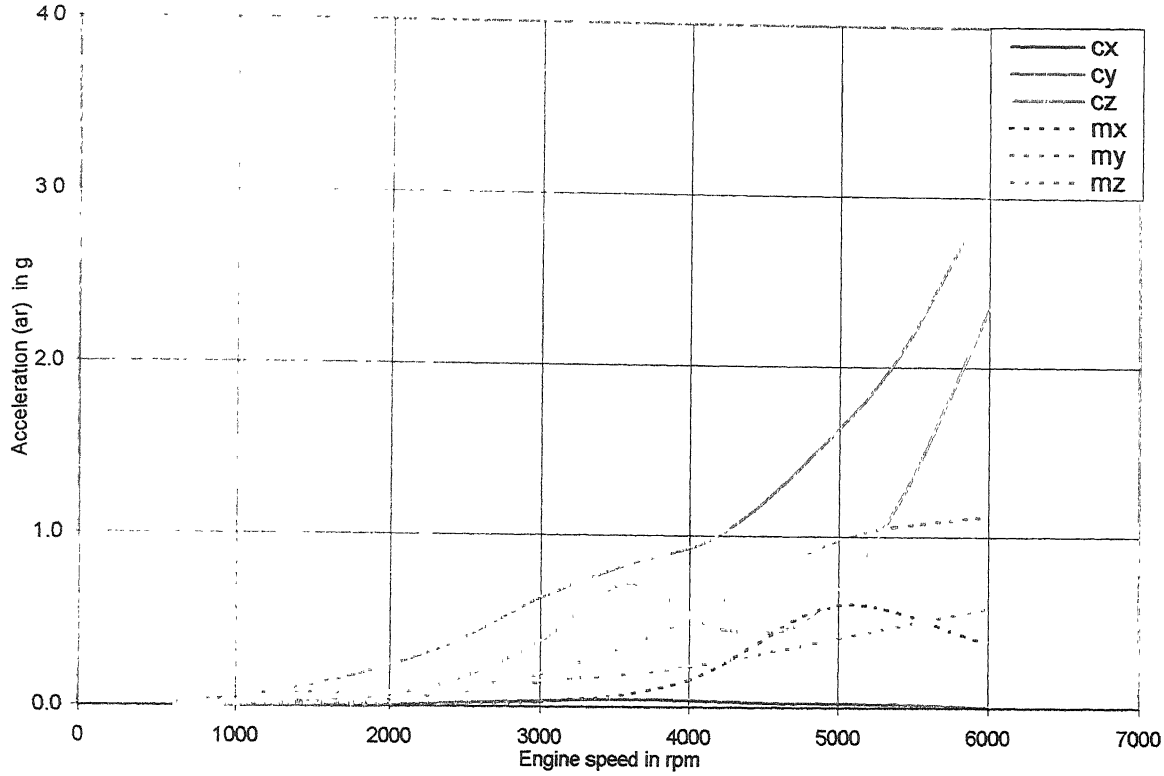

(c) : **Component accelerations**

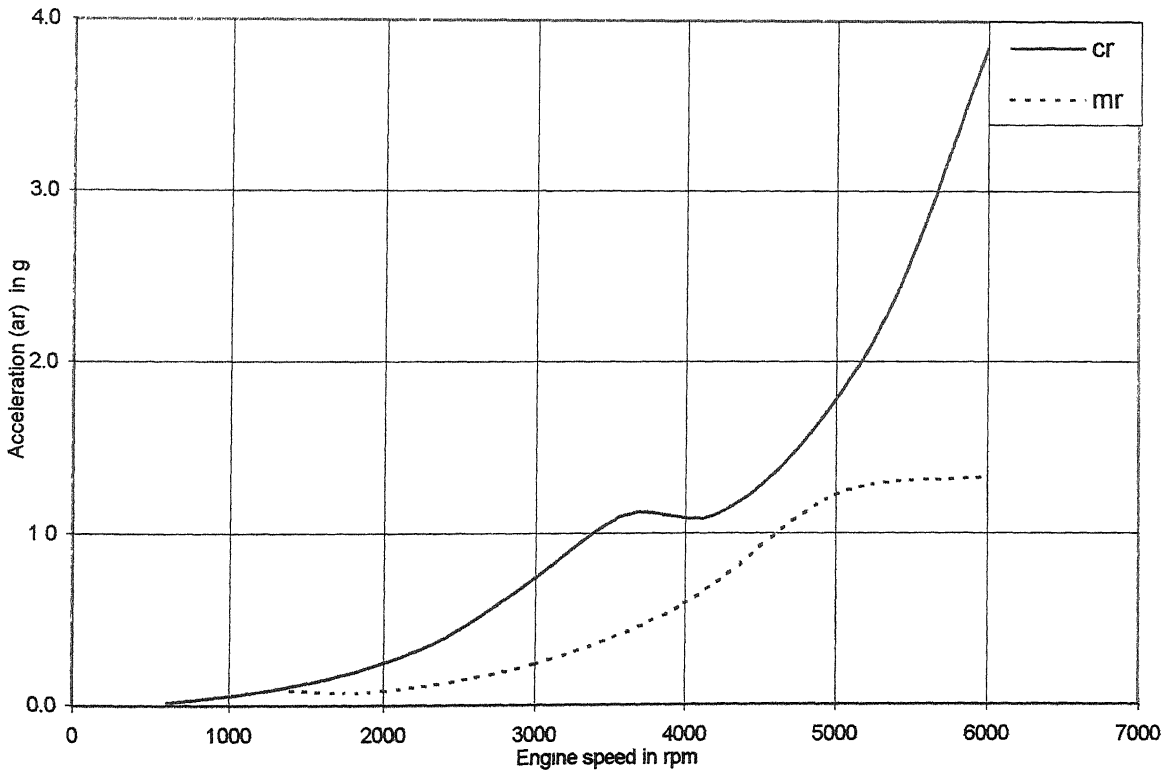

(d) : **Resultant accelerations**

FIGURE 3.15 (c & d) – **Comparison with computational results**

Location No. 3 : Foot Rest

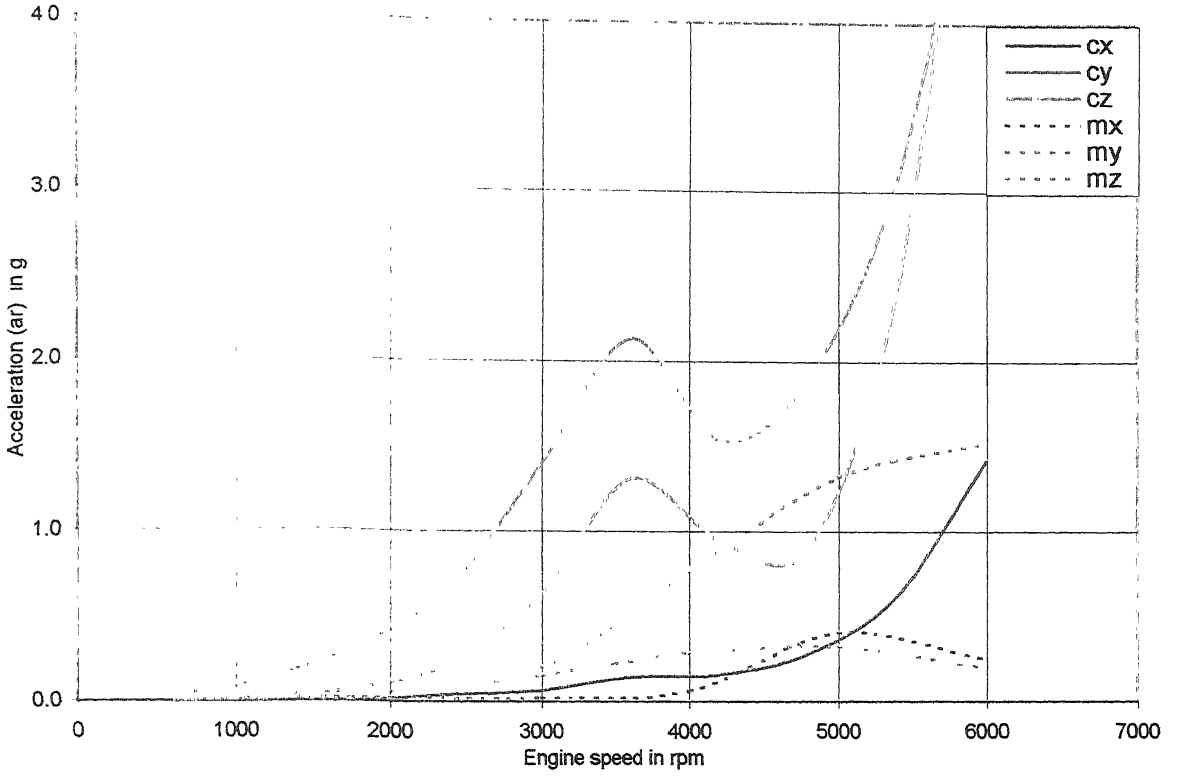

(e) : Component accelerations

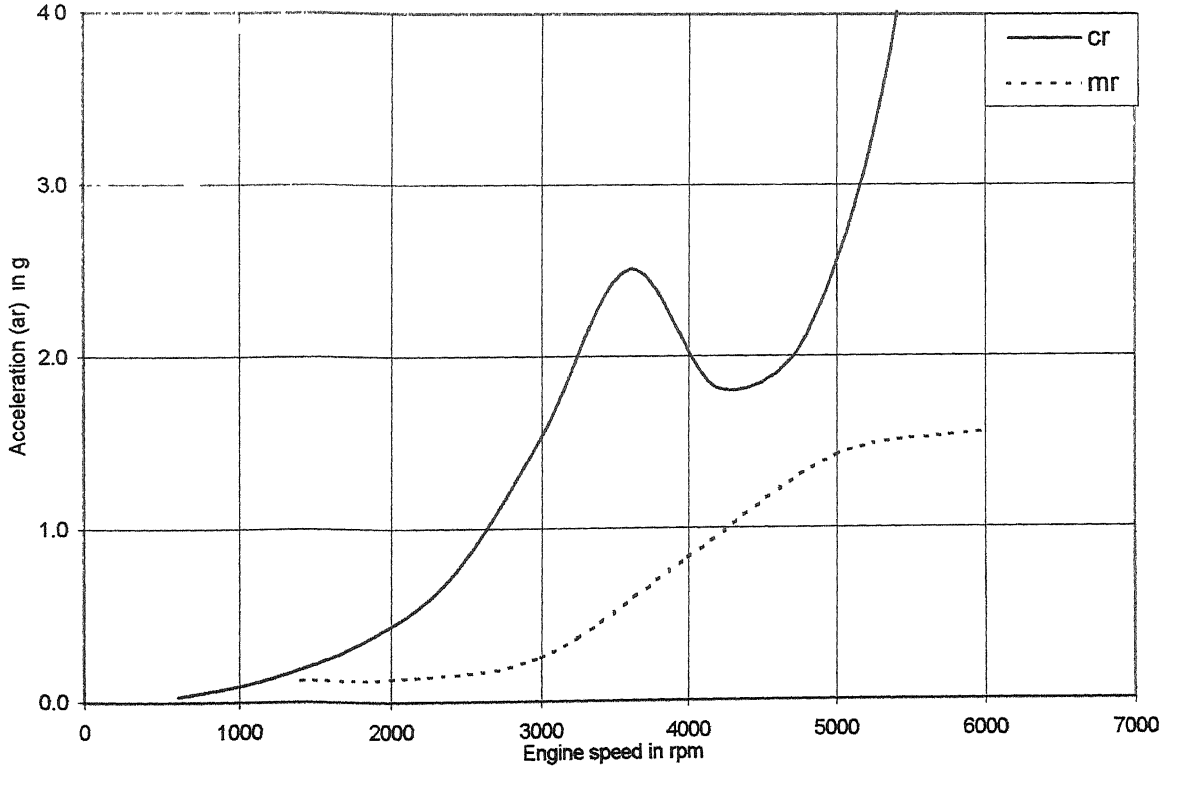

(f) : Resultant accelerations

FIGURE 3.15 (e & f) – **Comparison with computational results**

Location No. 4 : Seat Mounting

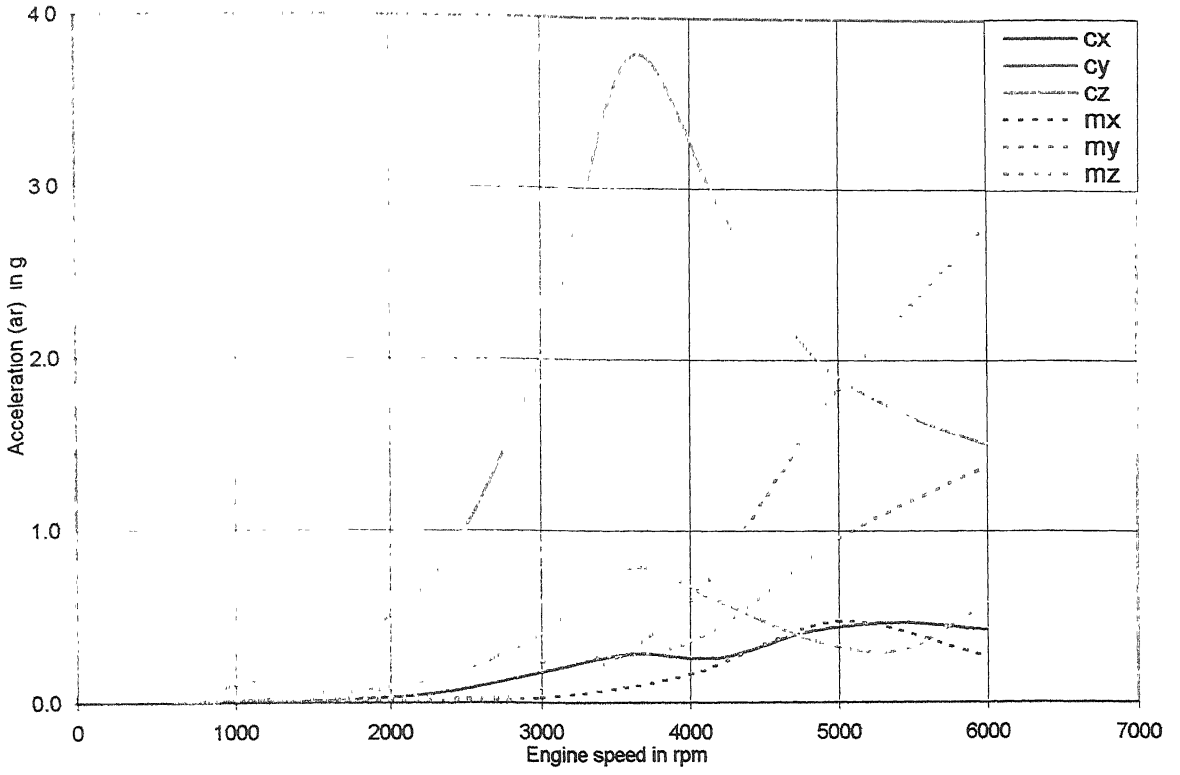

(g) : **Component accelerations**

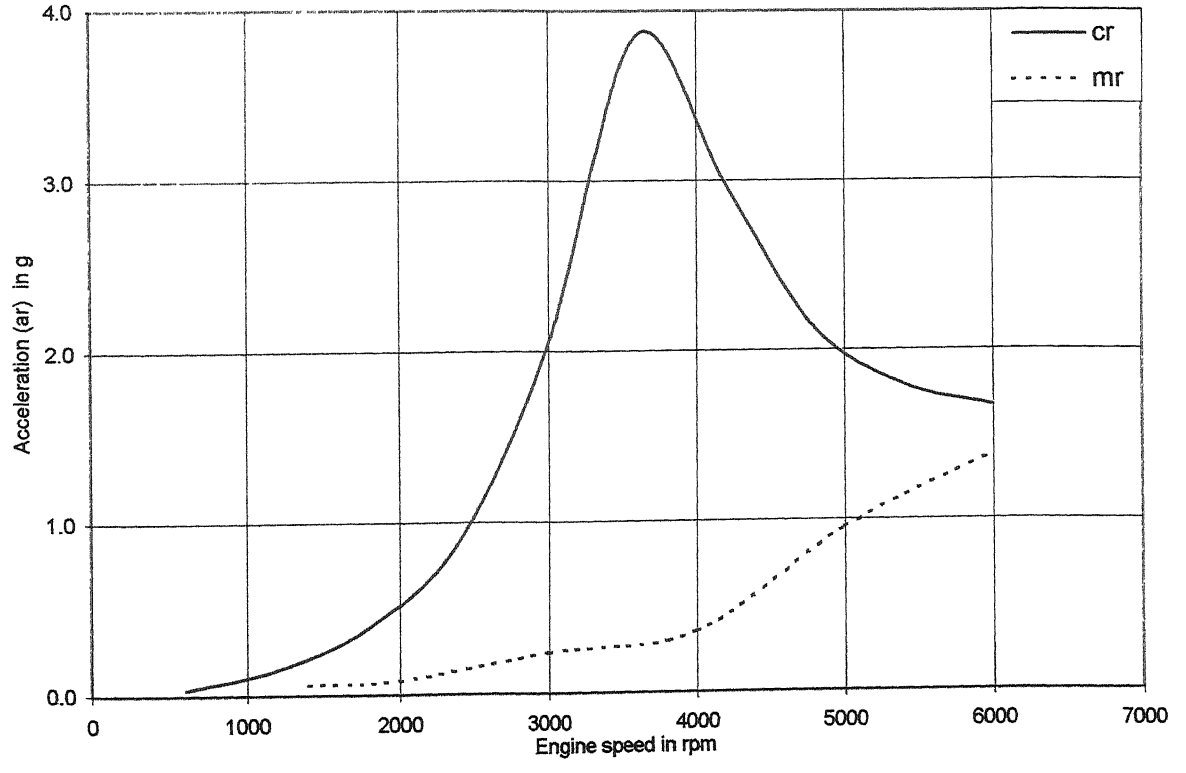

(h) : **Resultant accelerations**

FIGURE 3.15 (g & h) – **Comparison with computational results**

Location No. 5 : Steering Bar

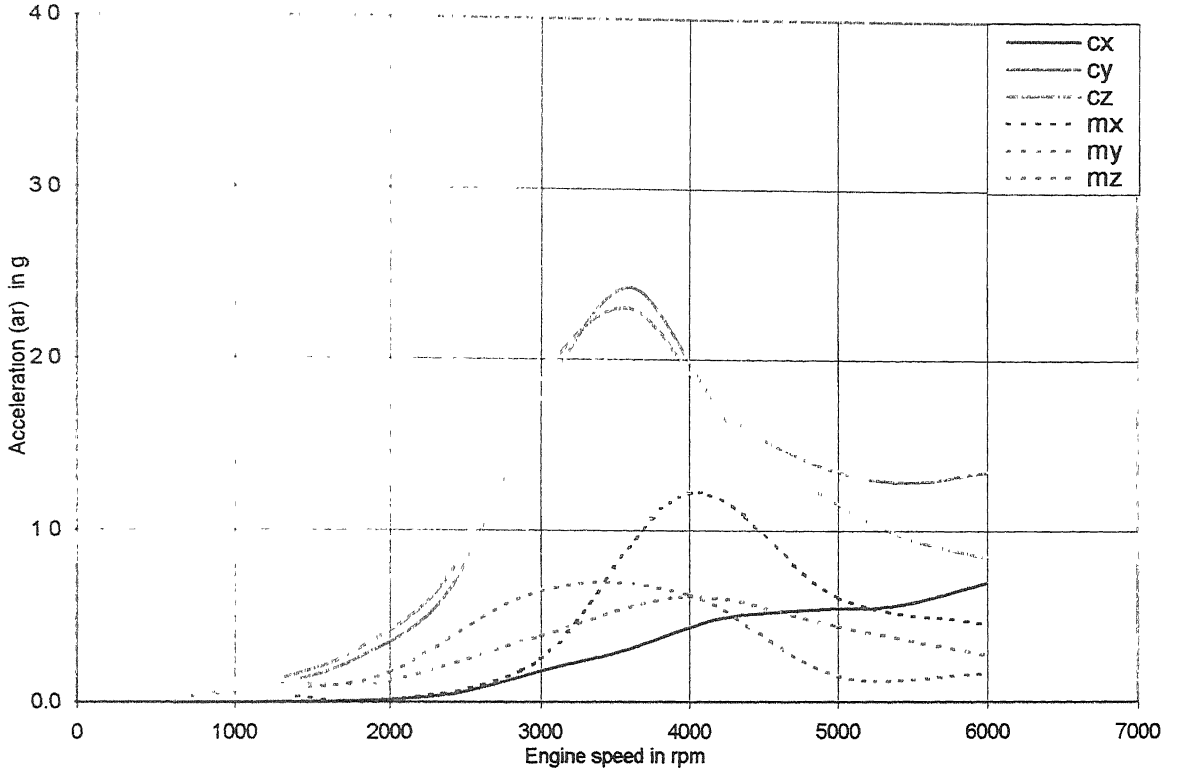

(i) : **Component accelerations**

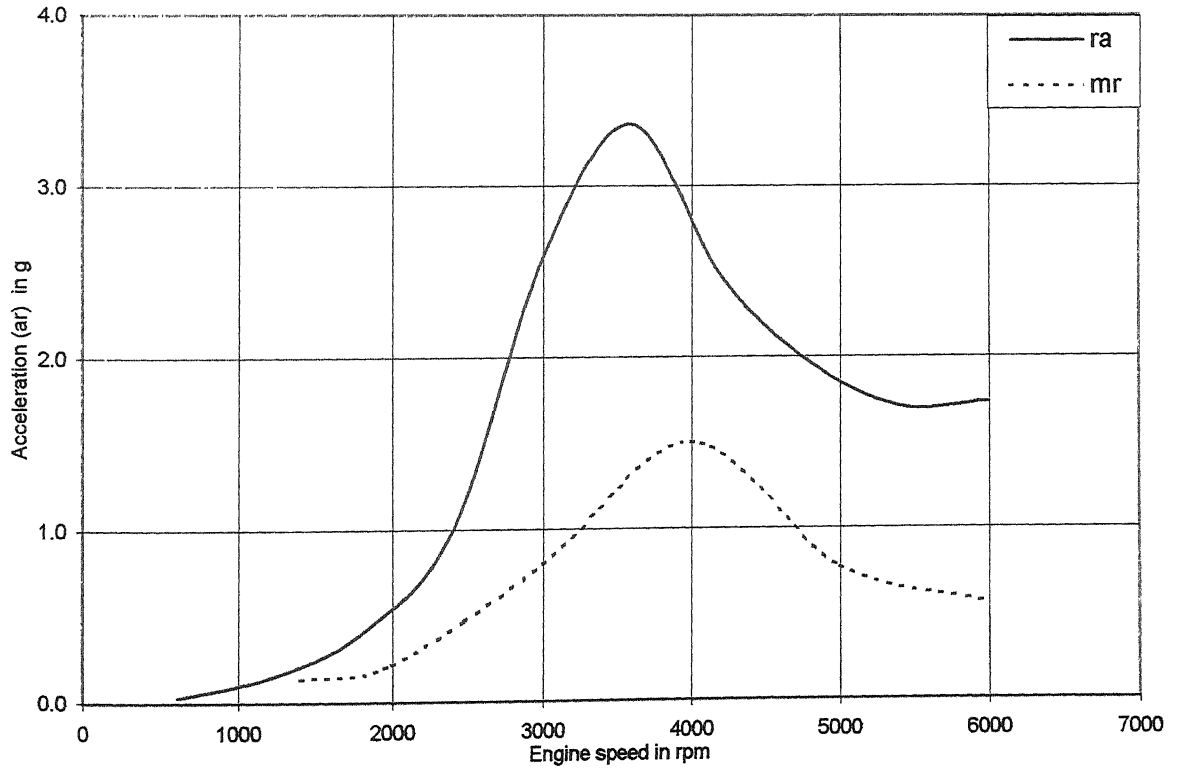

(j) : **Resultant accelerations**

FIGURE 3.15 – **Comparison with computational results**

3.8 Remarks

The experimental observations suggested that the engine performance of Vehicle Number 3 is good. From the current examination, it is clear that the steering-bar and seat mounting needs the modification for bettor riding comfort. It was decided to further investigate the possibility of structural improvement of the Steering- Bar during the present study.

Chapter - 4

STEERING BAR MODIFICATIONS FOR VIBRATION CONTROL

As mentioned in the previous chapter, the steering bar assembly is chosen to investigate the possibilities of structural modifications for improvement in its dynamic behavior. These investigations are carried out through finite element modeling. Five different configurations have been suggested. Each configuration further contains a couple of variations. Free and forced vibration characteristics of have been investigated for different cases and a comparison is presented.

The steering system of a motorcycle involves a complex configuration and possesses a rotational degree of freedom. A simplification is necessary to conduct an analysis for gaining insight into its dynamic behavior. For ease of modeling it was clamped with the frame at interfacing locations.

Earlier experiments and computational work have showed that the steering bar tips have high vibration with low natural frequencies. These natural frequencies lie in the normal speed of the engine and vehicle. Since the human body is very sensitive for low frequency vibrations, it is necessary to move these resonant away from the normal speed range or to reduce the amplitude of vibrations.

The objective of present work is to design the steering bar for controlled vibration parameters and minimize the vibration response of steering system using passive vibration control techniques. This section contains a brief discussion on the vibration control techniques.

4.1 Vibration Control Techniques

A vibration control generally follows five steps. First, identify the source excitation with its type. Second, define the vibration objective function. Third, choose the appropriate method for vibration control. Fourth, investigate performance through analytical, computational or experimental approach. Fifth, implement the best method, which meets the desired vibration levels and satisfies the design constraints. Reference can be made to Mallik (1990), Fuller et al (1996) and Mead (1998), for more detailed discussion on the subject.

In controlling the vibrations, initial effort is made to reduce the vibration input from the source. This is achieved by minimizing the net unbalanced engine shaking force, misalignment, clearances and use of proper lubrication in the rotating and reciprocating system. Flow-induced vibrations if any, are minimized by smoothening fluid flows. However once the engine design parameters are finalized, vibration is controlled in super -structure using active or passive vibration techniques.

Passive vibration control involves the modification of stiffness, mass and damping of the vibrating system to make the system less responsive to its vibratory environment. The modification takes the form of basic structural changes or addition of passive elements such as masses (concrete, metal pieces), springs (vibration isolators), and dampers (fluid and rubber). Active vibration control involves the use of active drives, which generate the anti vibration such that the initial vibration is cancelled. They require the sensors for detection of vibration, amplifiers for processing and driving the actuators.

Table 4.1 gives the summary of vibration control techniques for controlling the vehicle vibration.

TABLE 4.1 - **Vehicle vibration control**

Parameter	**Source control**	**Active control**	**Passive control**
Controlling quantity	High	Medium	Low
Development/ Maintenance cost	High and simple system	Complex Requires additional system leads maintenance cost	Simple and cheep
Controlling method	•Use of secondary balancer •Smoothening the flow passages	Use of mechtronic systems	• localized additions •Structural design change •use of suitable material •use of combined methods
Application	Engines	Suspension	Vibration control at super - structure

4.2 Steering Bar Modeling

Figure 4.1 shows the figure of steering arm without any auxiliary system. It represents a hollow steel tube bent in two planes with tube thickness 2.0 mm. The central portion of the tube is clamped at equal-distance.

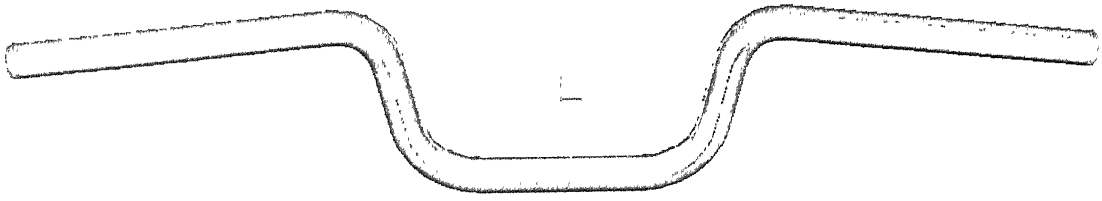

FIGURE 4.1 - **Model of existing steering bar**

The bar has been discretised as shown in the Fig. 4.2. The accessories have been localized and incorporated appropriately in elemental masses in the model. The bar tube is modeled with linear shell element at average radius. The insert handle bar is modeled using linear beam element along the centerline of the tube. This insert is connected to the handle bar shells using rigid element. The handle bar holder pieces are modeled using eight-noded brick elements. The handle accessory mass is modeled using mass element bracket mounting location.

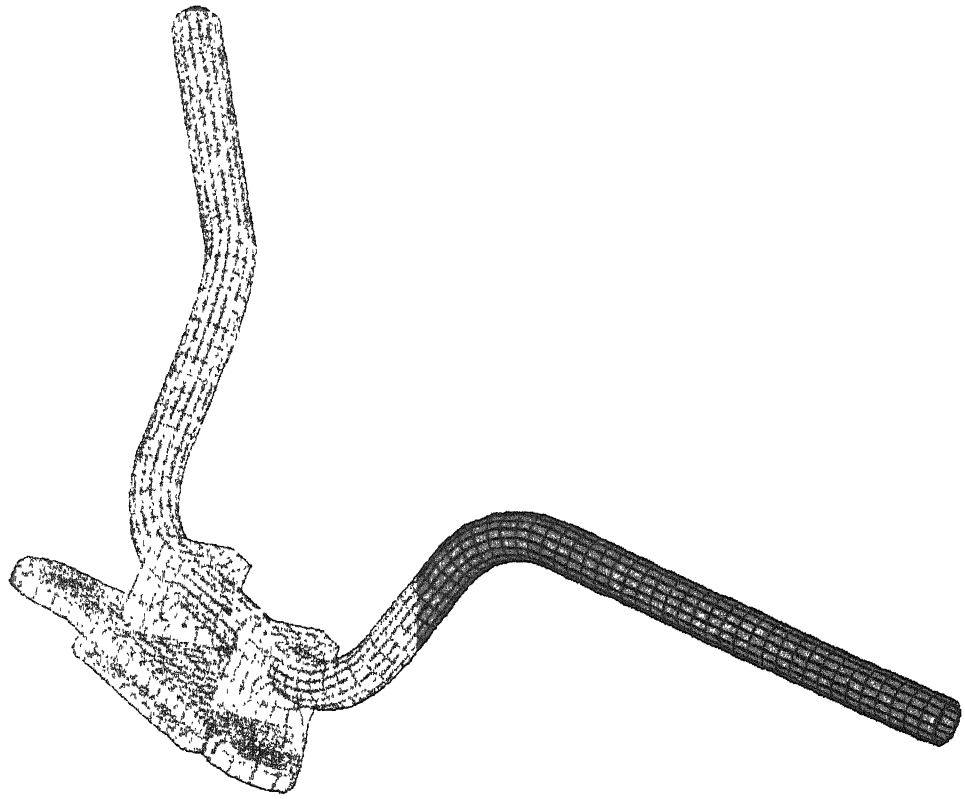

FIGURE 4.2 - **FE model of existing steering bar**

TABLE 4.2 – **Steering FE statistics**

Type	Element	Number
1	Shell	2172
2	Solid	128
3	Rigid	58
4	Mass	2

4.3 Free and Forced Vibration Characteristics

Vehicle mounting conditions as described in section 2.5 are used here. The first four natural frequencies are computed for laden conditions and tabulated in the Table 4.3. The corresponding mode shapes are shown in Fig.4.3.

TABLE 4.3 - **Resonant frequencies and modes**

Mode No.	Frequency Hz	Mode
1	53.99	Steering bar I lateral bending
2	56.17	Steering bar I vertical bending
3	57.87	Steering bar I longitudinal bending
4	65.02	Steering bar II vertical bending

Mode I : 53.99 Hz

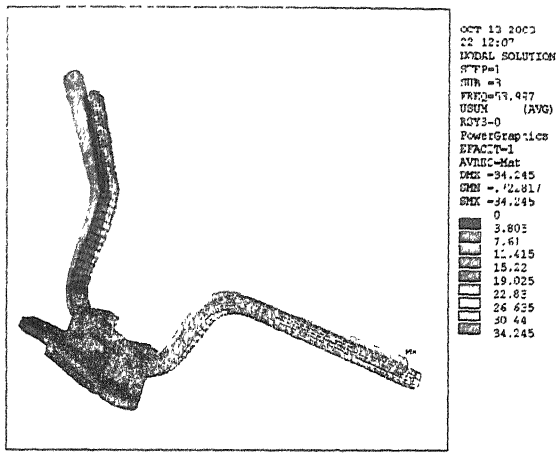

(a) : **Steering bar I lateral bending**

Mode II : 56.17 Hz

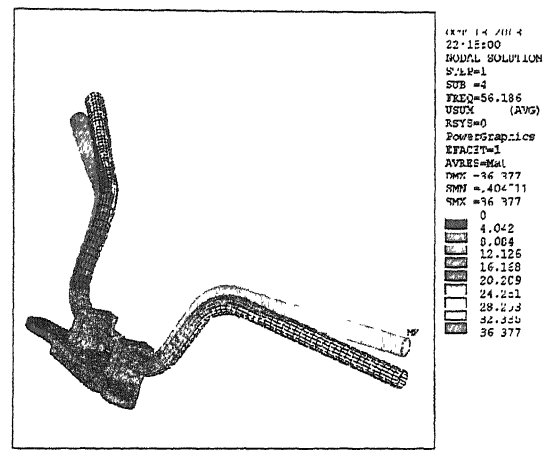

(b) : **Steering bar I vertical bending**

Mode III : 57.87 Hz

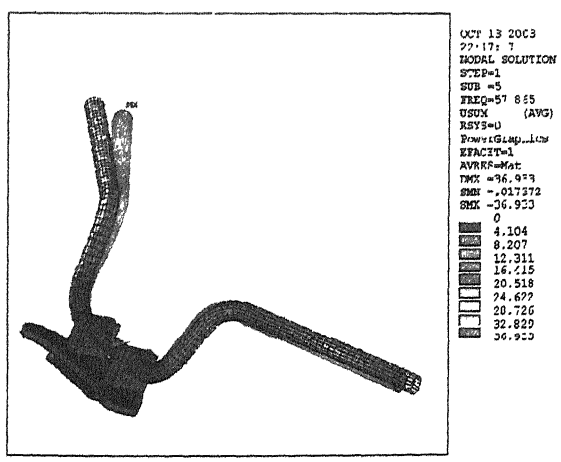

(c) : **Steering bar I longitudinal bending**

Mode IV : 65.02 Hz

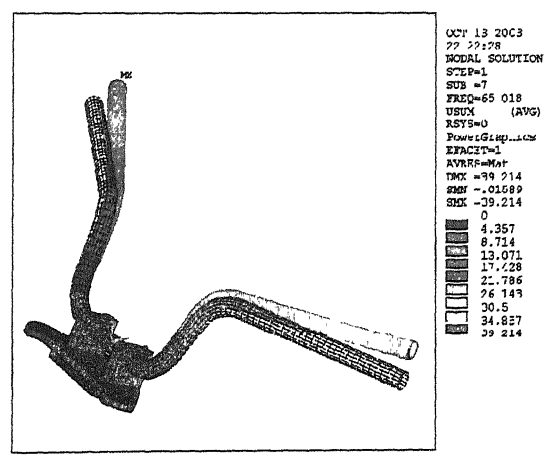

(d) : **Steering bar II vertical bending**

FIGURE 4.3 – **Steering bar mode shapes**

Only inertia load (as computed in Section 2.8.II) has been considered for forced vibration analysis. Damping is considered to be the same as that described earlier in Section 2.7.

Overall vibration characteristics were compared for three different locations on steering bar – (i) outer extreme point of bottom bend, (ii) outer extreme point of top bend and (iii) the mirror mounting location. Table 4.4 gives the coordinates of these locations

TABLE 4.4 – **Steering bar Vibration response locations**

Sl. No	Location	Co-ordinate, mm		
		X	Y	Z
1	Location No. 1	97.54	515.54	-464.54
2	Location No. 2	121.52	606.02	-405.50
5	Location No. 3	192.98	598.89	-369.86

Figure 4.4 shows the displacement and stress contours under inertia loading for engine excitation from 1200 to 6000 rpm.

Stage I : Engine Speed 1200 rpm

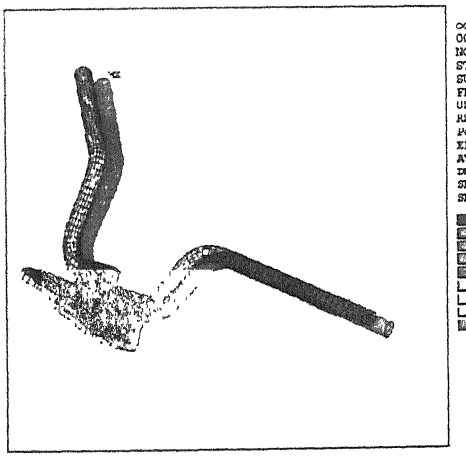

(a) : **Displacement contour**

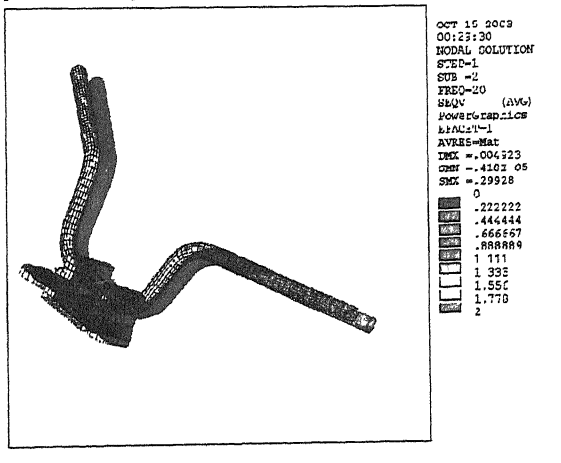

(b) : **Stress contour**

Stage II : Engine Speed 2400 rpm

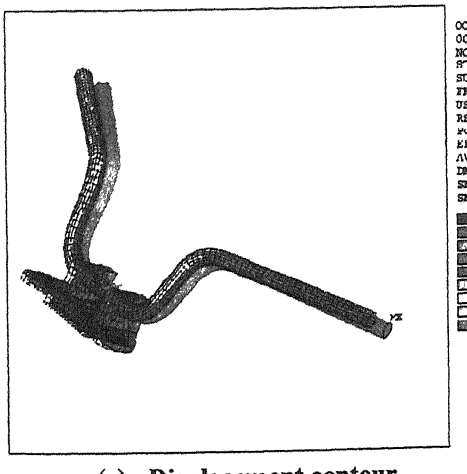

(c) : **Displacement contour**

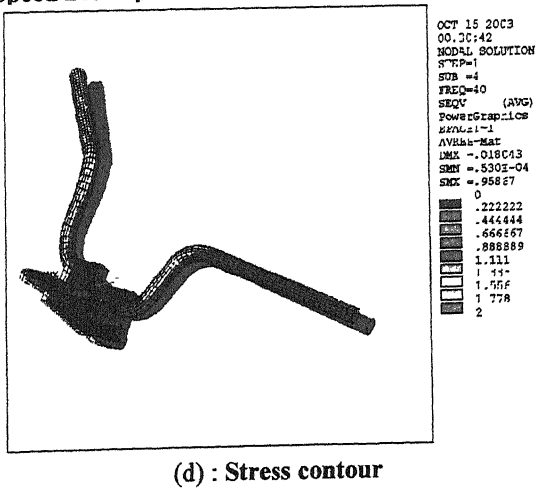

(d) : **Stress contour**

FUGURE 4.4 (a-d) – **Steering bar forced vibration response**

Stage III : Engine Speed 3600 rpm

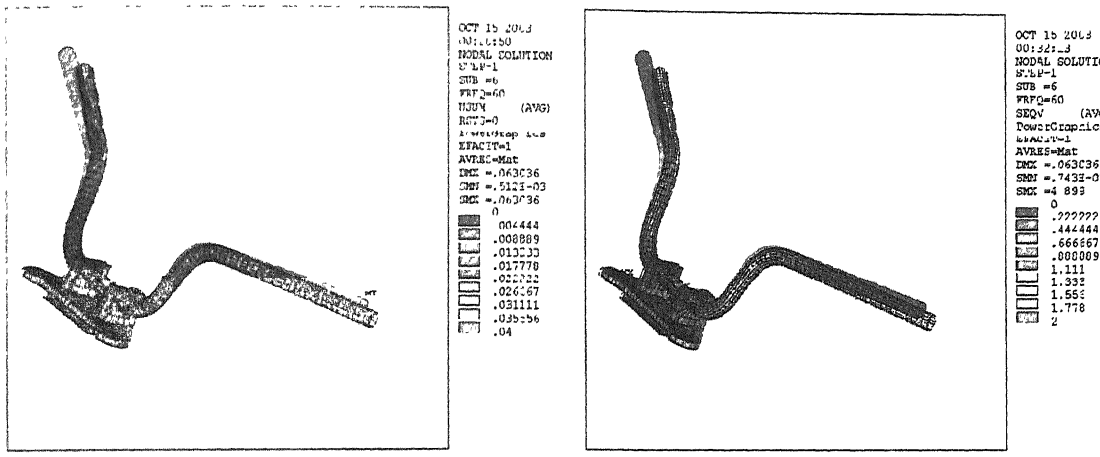

(e) : **Displacement contour** (f) : **Stress contour**

Stage IV : Engine Speed 4800 rpm

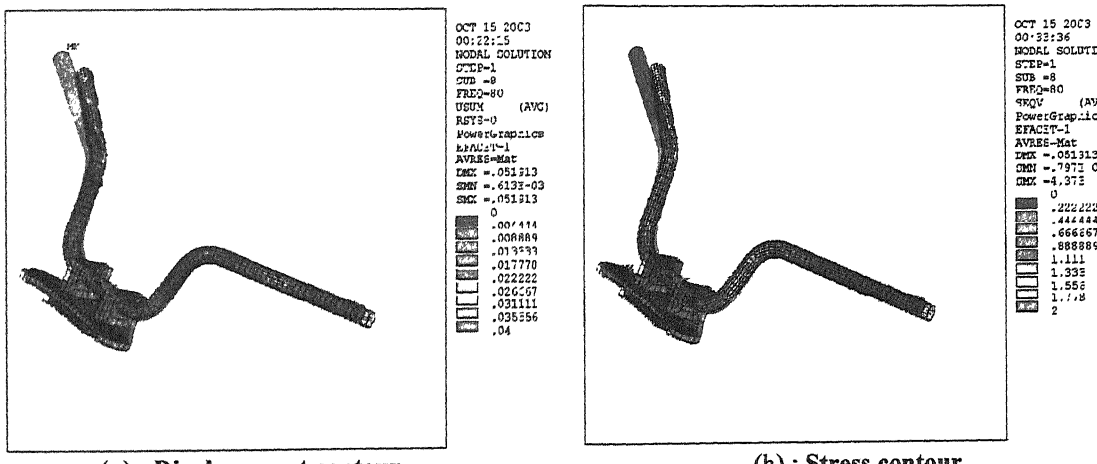

(g) : **Displacement contour** (h) : **Stress contour**

Stage V : Engine Speed 6000 rpm

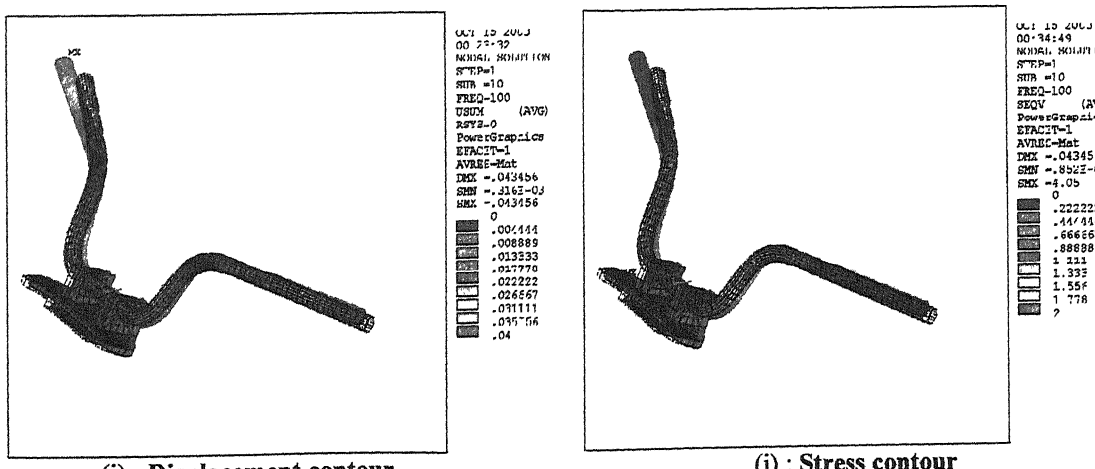

(i) : **Displacement contour** (j) : **Stress contour**

FUGURE 4.4 – **Steering bar forced vibration response**

The Frequency response function plots further developed from the forced vibration analysis are displayed in terms of acceleration and stresses for three measurement locations have been shown in Figs. 4.5.

The FRF plots reveal resonant vibrations at speeds 3600 rpm (Vehicle speed 40.5 kmph) of magnitude ranging from 0.15 g to 0.5 g. As expected the maximum vibrations are experienced at location number 3, which is the mirror mounting location. Vibration would be still higher at the free end of the bar. Comparison of overall vibration levels at the three measurement locations is given in Fig. 4.6.

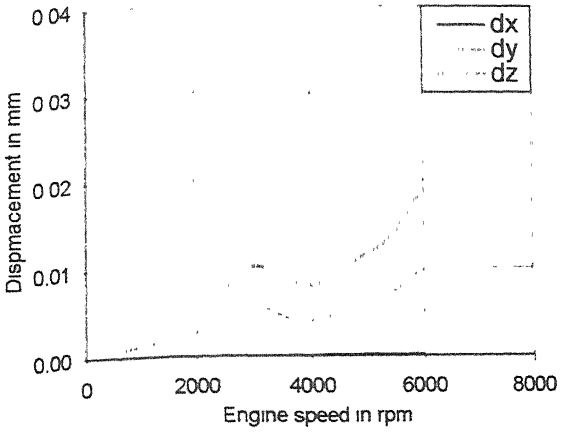

(a) : **Location No. 1 Displacement**

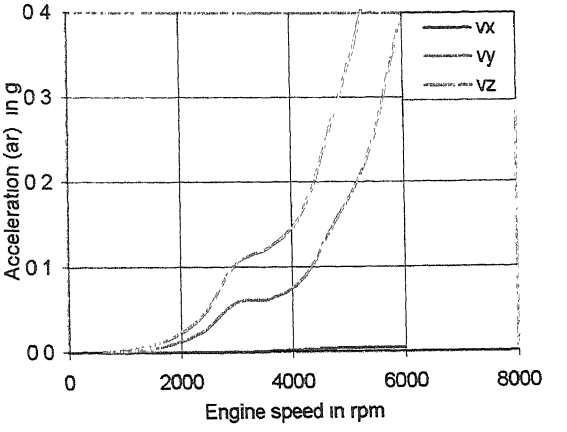

(b) : **Location No. 1 Acceleration**

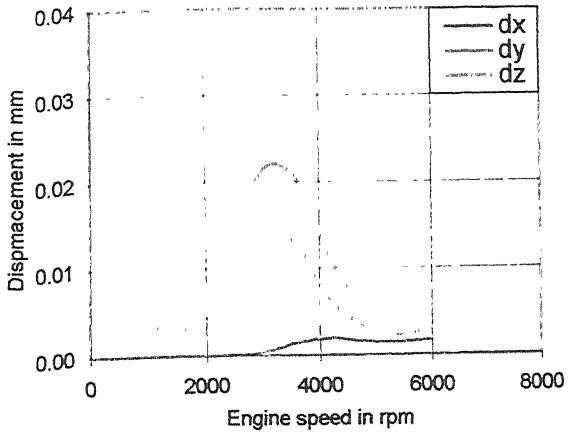

(c) : **Location No. 2 Displacement**

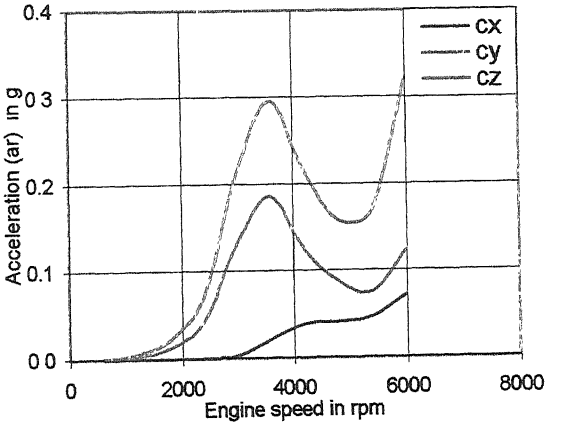

(d) : **Location No. 2 Acceleration**

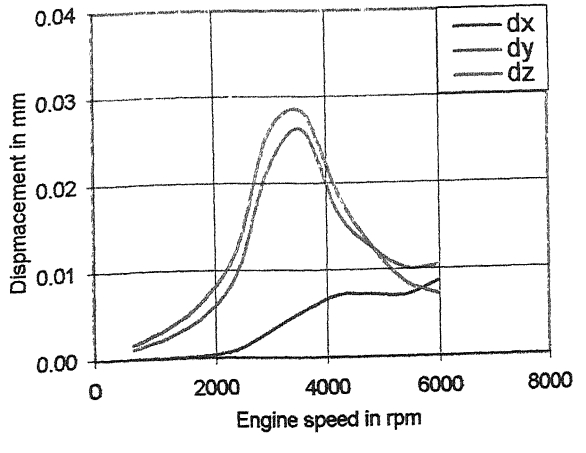

(e) : **Location No. 3 Displacement**

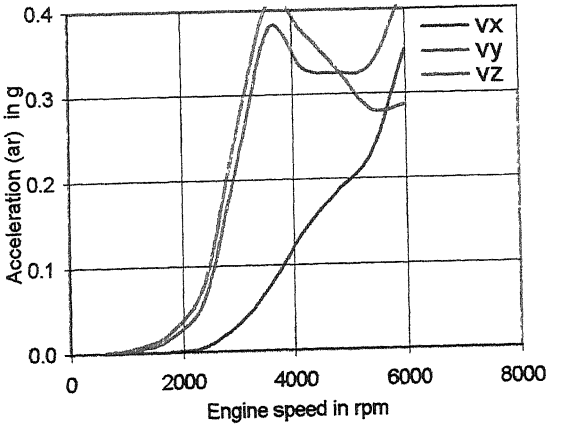

(f) : **Location No. 3 Acceleration**

FUGURE 4.5 – **FRF plots for existing steering bar**

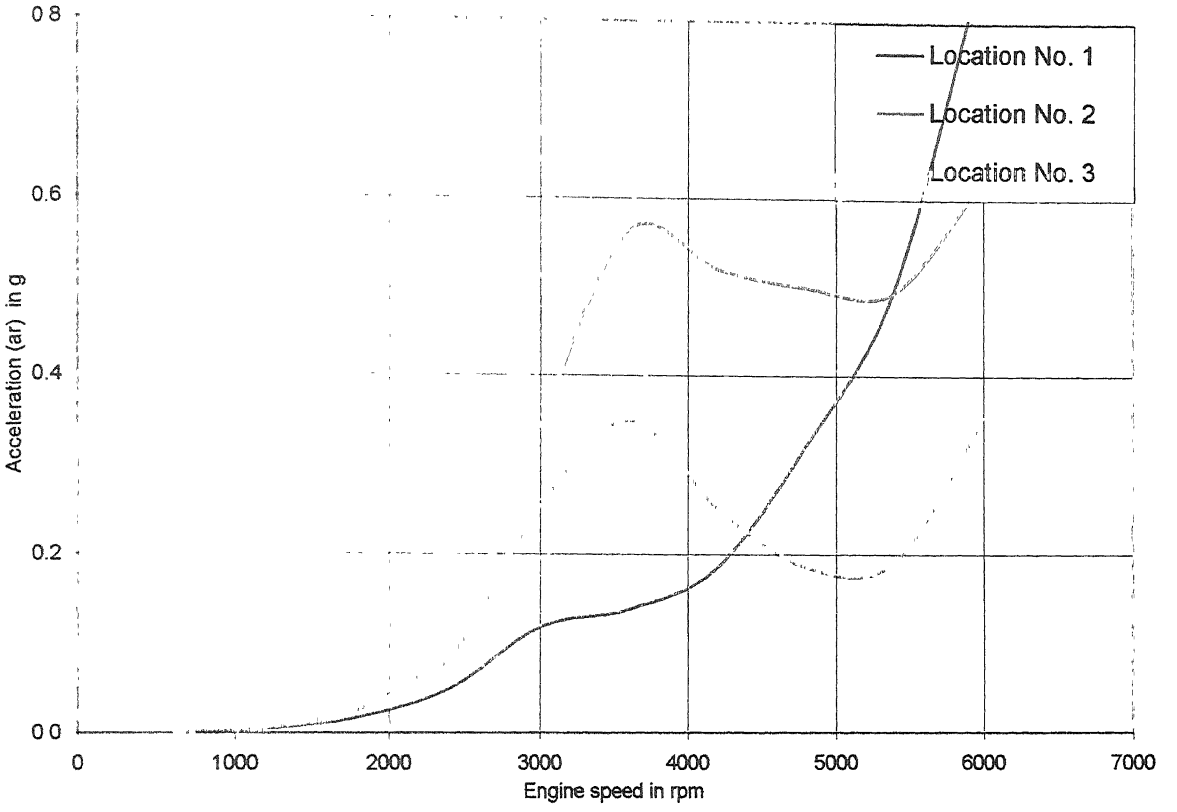

(a) : **Resultant acceleration**

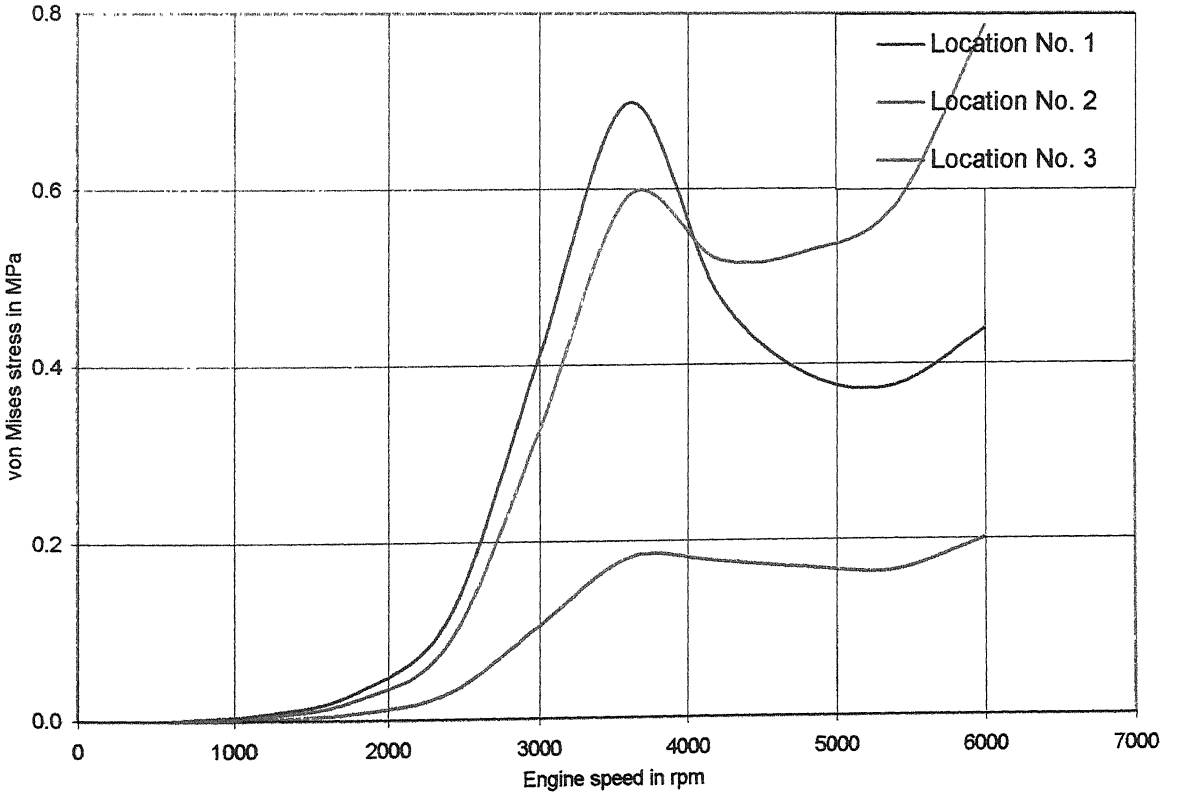

(b) : **von Mises stresses**

FUGURE 4.6 – **Overall vibrations of existing steering bar**

4.4 Steering Bar Modification Models for Vibration Control

Four different modified configurations of the steering bar are suggested here for reduction in vibration levels. These are discussed below:

(I) Vibration Control of Steering Bar by Stiffness Modification :

Three cases with different tube thickness in the range 1.5 to 3 mm were further investigated. The tube thickness 2.0 mm corresponds to the existing tube. These have been called Cases Number 1 (a), (b) and (c) and have been listed in Table 4.5.

TABLE 4.5 - **Structural design (Added stiffness) cases**

Case No.	Tube thickness, mm
1 (a)	1.5
1 (b)	2.5
1 (c)	3.0

Change in tube thickness involves both – alteration in mass and alteration in stiffness. Free vibration characteristics of the modified structures in these cases are given in Table 4.6. in Case Number 1 (a), where the thickness is less than the existing one, a lowering of natural frequencies has resulted, while in the other two cases, where the thickness are higher than existing, an increase in the natural frequency has resulted. This suggests that the modifications influence stiffness to a higher degree than mass.

TABLE 4.6 - **Added stiffness - natural frequencies in Hz**

Mode No.	Existing	Case No. 1 (a)	Case No. 1 (b)	Case No. 1 (c)
1	53.99	48.79	57.01	58.76
2	56.17	49.82	60.23	62.82
3	57.87	51.25	62.24	65.27
4	65.02	55.52	72.00	77.29

Forced vibration characteristics for these cases are plotted in Figs. 4.7. It can be seen that lower levels of vibration have been achieved (33%) in Case Number 1 (a), in contrast to the other two cases (-20%, -33%) that show higher vibration levels.

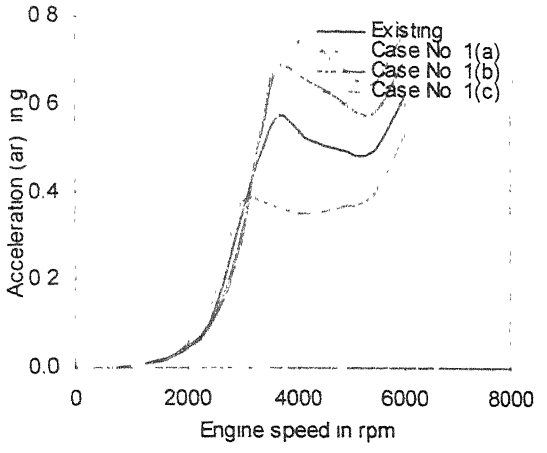

(a) : **Location No. 3 acceleration**

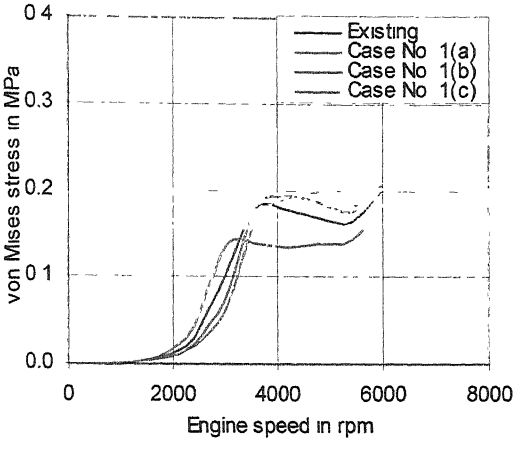

(b) : **Location No. 3 von Mises stress**

FUGURE 4.7 –**Effect of overall vibrations under added stiffness**

(II) Vibration Control by Addition of Masses at Various Locations:

This model involves vibration control through addition of localized mass of 250 gram. Models with masses added at three different locations have been shown in Figs. 4.8.

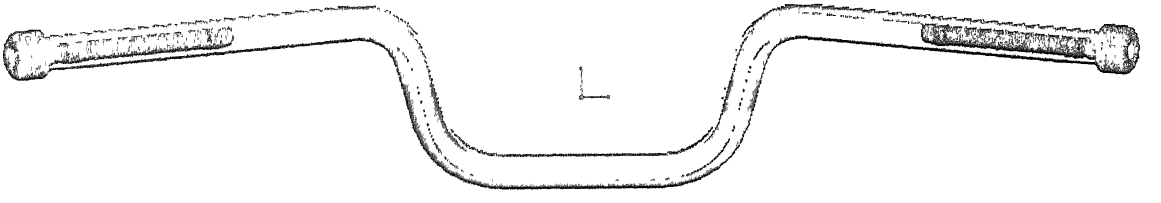

(a) : **Case No. 2 (a) - Localized mass at tip-out side**

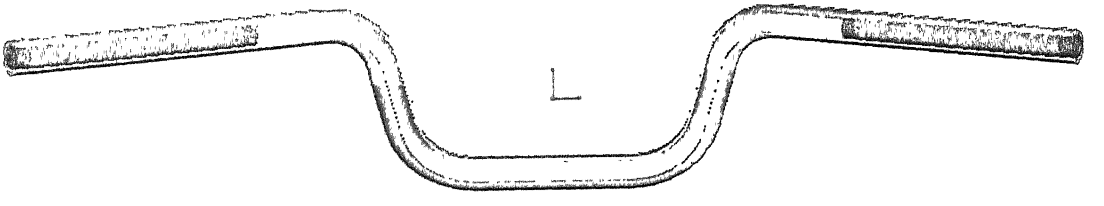

(b) : **Case No. 2 (b) - Localized mass at tip-in side**

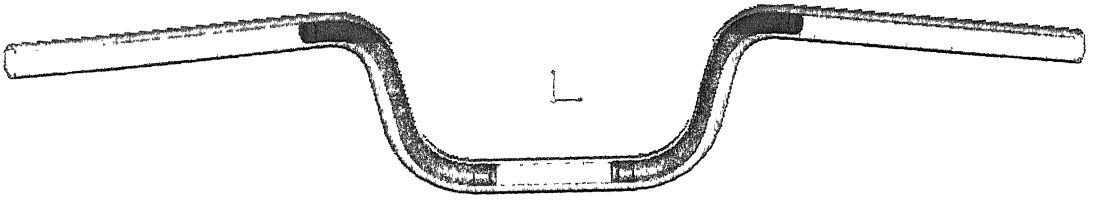

(c) : **Case No. 2 (c) - Localized mass in the entire bend**

FIGURE 4.8 - **Localized addition design cases**

The masses to be added have been visualized as solid cylindrical pieces, which can be readily inserted into the steering bars. The magnitude of the masses is mentioned in Table 4.7.

TABLE 4.7 - **Mass location selection cases**

Case No.	Magnitude, kg	Location
2 (a)	0.250	At Bar tip out side
2 (b)	0.250	At Bar tip in side
2 (c)	0.250	At Full bend

Free vibration analysis was carried out for all three cases. The natural frequencies are listed in Table 4.8. Comparison with the values of existing configuration reveal that the frequencies get reduced in Cases Number 2 (a) and (b), whereas they rise in Case 2 (c). This is due to the fact that addition of masses at the bends has resulted in an increase in stiffness also.

TABLE 4.8 - **Added mass location - natural frequencies in Hz**

Mode No.	Existing	Case No. 2 (a)	Case No. 2 (b)	Case No. 2 (c)
1	53.99	44.80	46.13	60.22
2	56.17	45.25	47.47	63.87
3	57.87	46.31	48.75	66.74
4	65.02	50.54	54.03	79.63

Forced vibration characteristics for the three cases are shown in Figs. 4.9.

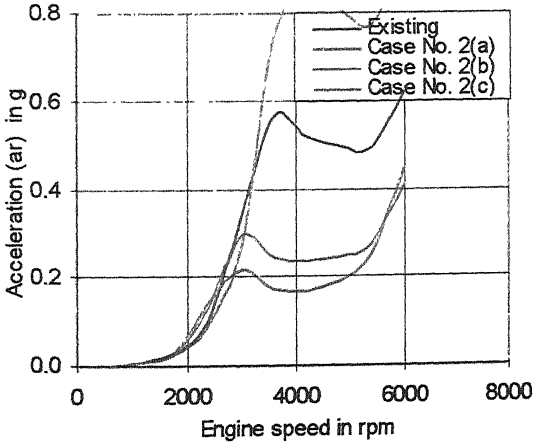

(a) : **Location No. 3 Acceleration**

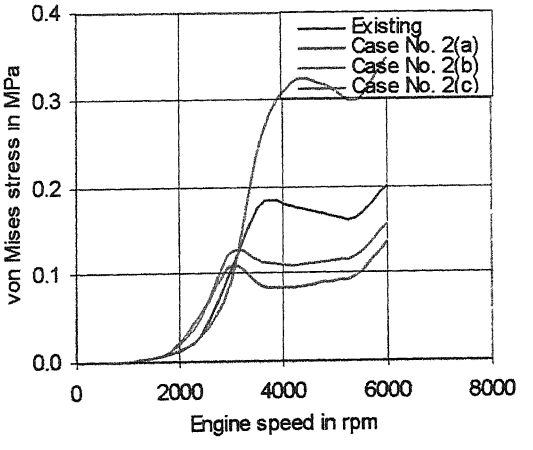

(b) : **Location No. 3 von Mises stress**

FUGURE 4.9 –**Effect of overall vibrations under added mass location**

It is clear from the plots that the vibration levels get reduced significantly for Case Number 2 (a) and (b) in comparison to the existing configuration for the first critical speed of 3700 rpm. It remains so for a large portion of the running speed range up to 6000 rpm. In cases No. 2 (c), the levels in this speed range are higher than the existing levels. The vibrations at the first critical speed were reduced by 61%, 48% and –55% respectively.

(III) Vibration Control by Material Selection:

In the modifications suggested in the previous sub-section, the material for the additional masses was chosen to be the same (steel) for all three cases. As a second set of design iteration three different materials were chosen for Case Number 2 (b), described previously. The materials chosen in these modifications are listed in Table 4.9. It is to be noted that Case Number 3 (b) is the same as Case Number 2 (c).

TABLE 4.9 : **Material selection cases**

Case No.	Material
3 (a)	Lead
3 (b)	Steel
3 (c)	Aluminum

Free vibration characteristics for these cases are listed in Table 4.10.

TABLE 4.10 : **Added material - natural frequencies in Hz**

Mode No.	Existing	Case No. 3 (a)	Case No. 3 (b)	Case No. 3 (c)
1	53.99	44.80	46.13	50.65
2	56.17	45.18	47.47	52.42
3	57.87	46.34	48.75	53.89
4	65.02	50.87	54.03	58.77

Figure 4.10 shows the frequency response curves for acceleration and stress for the above cases. These results show that Case Number 3(a) has shown 58% reduction in vibration levels, However Case Number 3(b) is also shown good reduction (48%) in the levels. The Case Number 3(c) has shown 25% reduction.

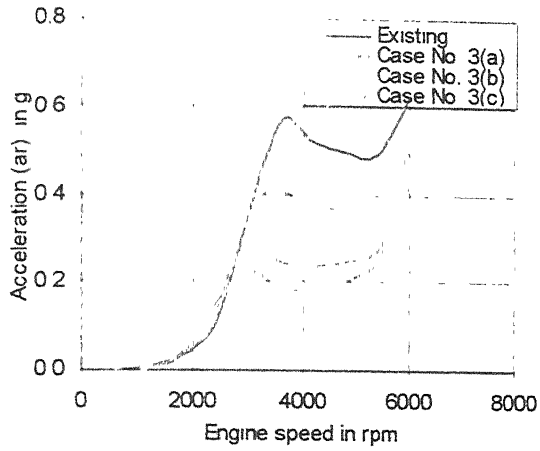

(a) : **Location No. 3 Acceleration**

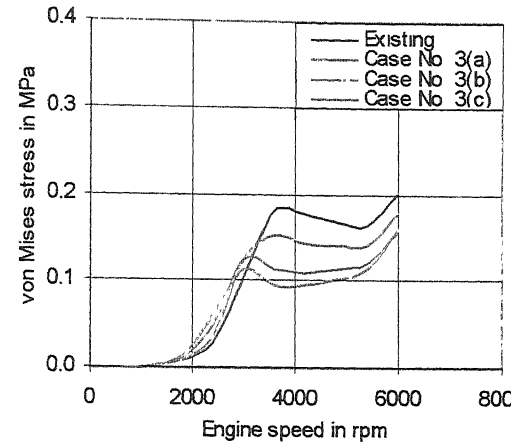

(b) : **Location No. 3 von Mises stress**

FUGURE 4.10 – **Effect of overall vibrations under added material**

(IV) Vibration Control by Addition of Masses of Various Sizes:

Three cases with different mass size in the range of 150 to 250 grams were further investigated at tip inside location (On case Number 2 (b). These have been called Cases Number 4 (a), (b) and (c) and have been listed in Table 4.11.

The masses to be added have been visualized as solid cylindrical pieces of various diameters and equal length, which can be readily inserted into the steering bars.

TABLE 4.11 - **Mass size selection cases**

Case No.	Magnitude, kg	Location
4 (a)	0.150	At Bar tip in side
4 (b)	0.200	At Bar tip in side
4 (c)	0.250	At Bar tip in side

Table 4.12 gives the natural frequencies under the free vibration analysis. Comparison with the values of existing configuration reveals that the frequencies get reduced in all cases. This is due to the fact that addition of masses at the tip has not altered the stiffness.

TABLE 4.12 - **Added mass size - natural frequencies in Hz**

Mode No.	Existing	Case No. 4 (a)	Case No. 4 (b)	Case No. 4 (c)
1	53.99	48.94	47.48	46.13
2	56.17	50.53	48.93	47.47
3	57.87	51.92	50.25	48.75
4	65.02	57.82	55.83	54.03

Forced vibration characteristics for the three cases are shown in Figs. 4.11.

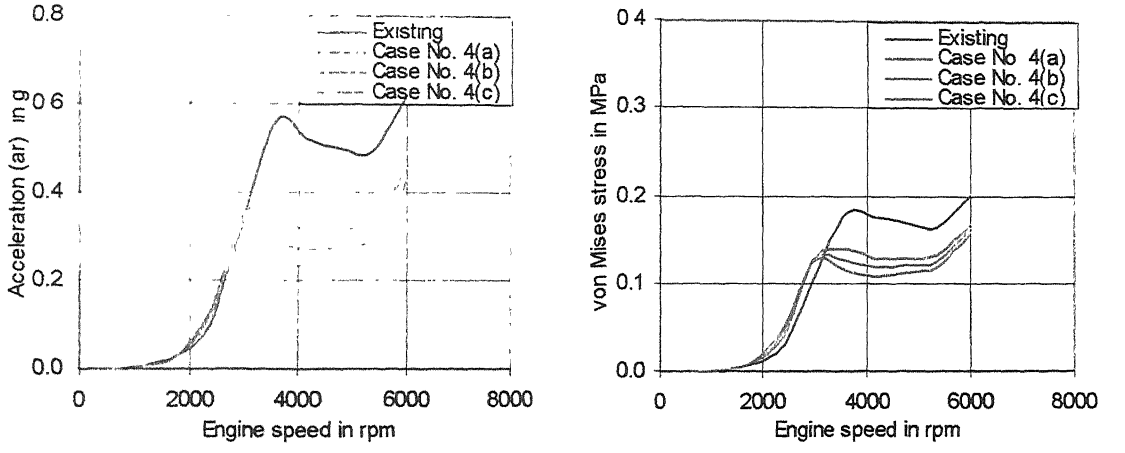

(a) : **Location No. 3 Acceleration** (b) : **Location No. 3 von Mises stress**

FUGURE 4.11 –**Effect of overall vibrations of steering bar under added mass size**

It is clear from the plots that the vibration levels get reduced significantly (48%) for Case Number 4 (c) in comparison to the existing configuration for the first critical speed of 3700 rpm, But in comparison with Case Number 4(a) reduced 32% and 4(b) reduced 42% case Number 4(a) has not shown much reduction in vibration and stress levels.

(V) Vibration Reduction Through Combined Approach

A combined approach is further selected for investigation. This involves changing the tube thickness for cases Number 2 (a) and 2 (b). These are now called Cases Number 5 (a), (b), (c) and (d) respectively and are listed in Table 4.13.

TABLE 4.13 - **Combined method cases**

Case No.	Mass added	Tube thickness, mm
5 (a)	Tip – Out side	1.5
5 (b)	Tip – Out side	2.0
5 (c)	Tip – In side	1.5
5 (d)	Tip – In side	2.0

Free vibration characteristics for these cases are given in Table 4.14. The natural frequencies have been lowered in the all cases.

TABLE 4.14 : **Added combined method - natural frequencies in Hz**

Mode No.	Existing	Case No. 5 (a)	Case No. 5 (b)	Case No. 5 (c)	Case No. 5 (d)
1	53.99	38.89	44.80	41.39	46.13
2	56.17	40.21	45.25	42.49	47.47
3	57.87	42.49	46.31	45.52	48.75
4	65.02	45.60	50.54	45.56	54.03

Forced vibration characteristics are shown in Figs. 4.12 for these cases. The plots show that the vibration levels are lowered in the Case No. 5(a) and (c) in larger extent.

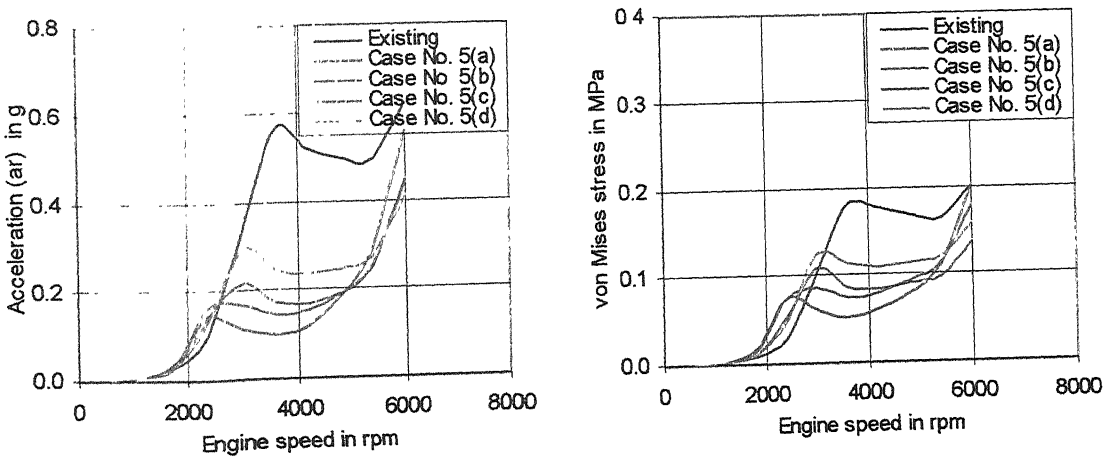

(a) : **Location No. 3 Acceleration** (b) : **Location No. 3 von Mises stress**

FUGURE 4.12 –**Effect of overall vibrations under combined method**

These results show that Case Number 5(a) has shown 71% reduction in vibration levels, However 5(b) is also shown reduction (61%) in the levels. The 5(c) and 5(d) has reduced the vibrations by 68% and 48% respectively.

Comparison of Overall Vibrations:

Figure 4.13 shows the resultant displacement, velocity, acceleration and von Mises stress Frequency Response Curves of the existing Steering Bar for location No. 3 along with all modifications - Case Number 1 to 5.

The figures are self-explanatory and show that the modification suggested in Case Number 5 (a) is the best 71%, while that of Case Number 2 (c) is the worst -55%. The maximum vibration reduced in Case Number 1 to 5 are , 33%, 61%, 58%, 48% and 71% respectively.

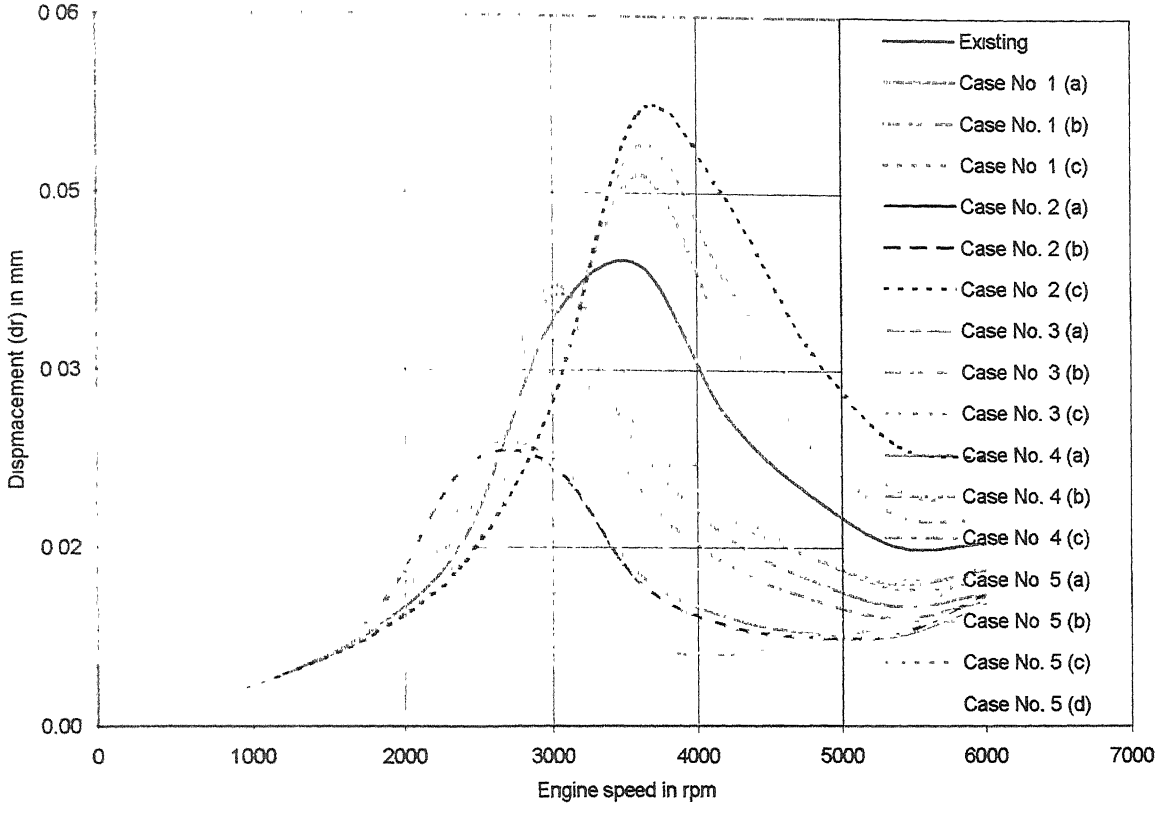

(a) : **Resultant displacements**

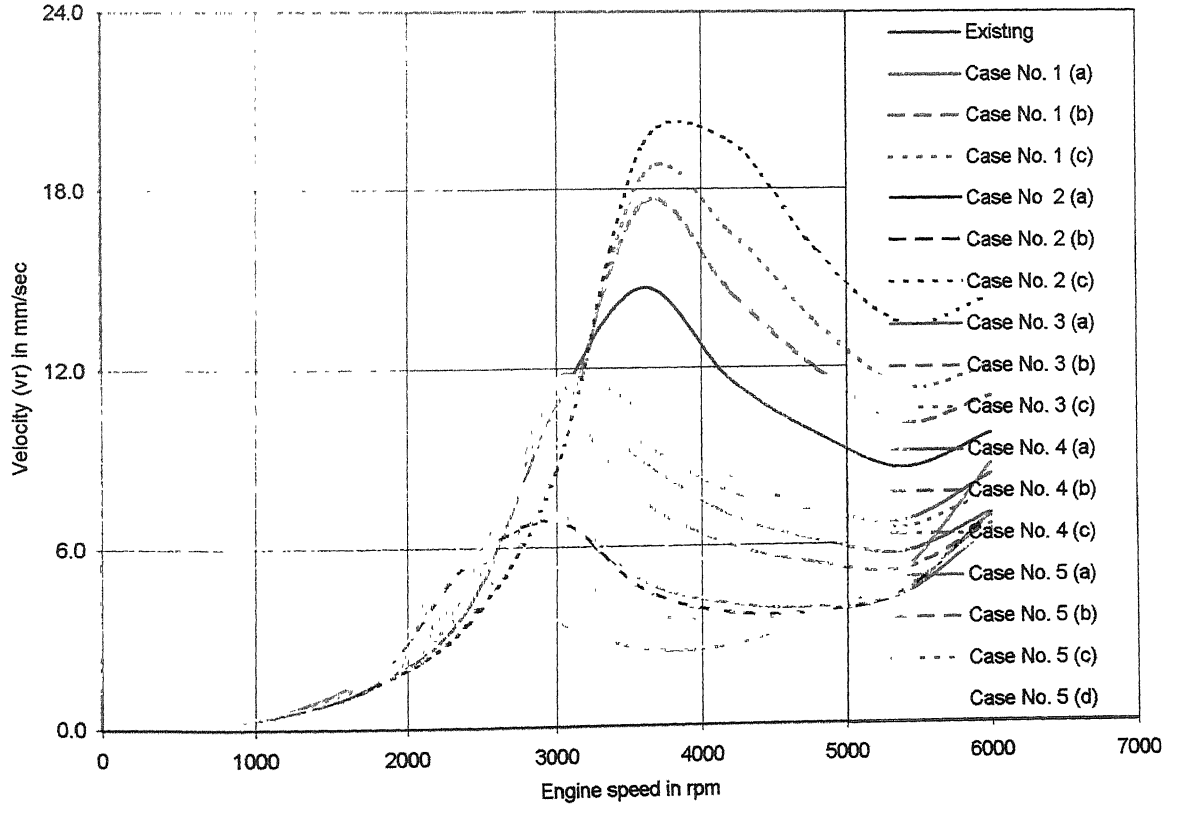

(b) : **Resultant velocities**

FUGURE 4.13 (a&b)–**Comparison of overall vibrations of steering bar due to added cases**

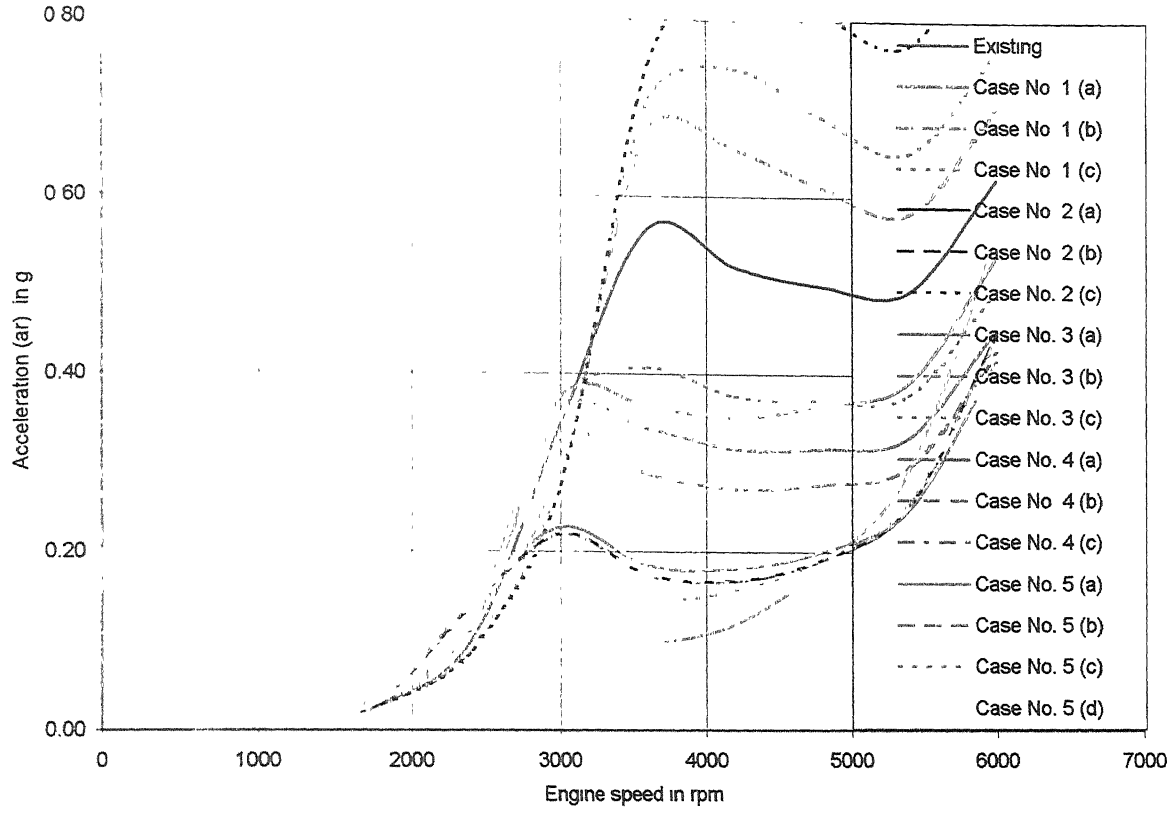

(c) : **Resultant acceleration**

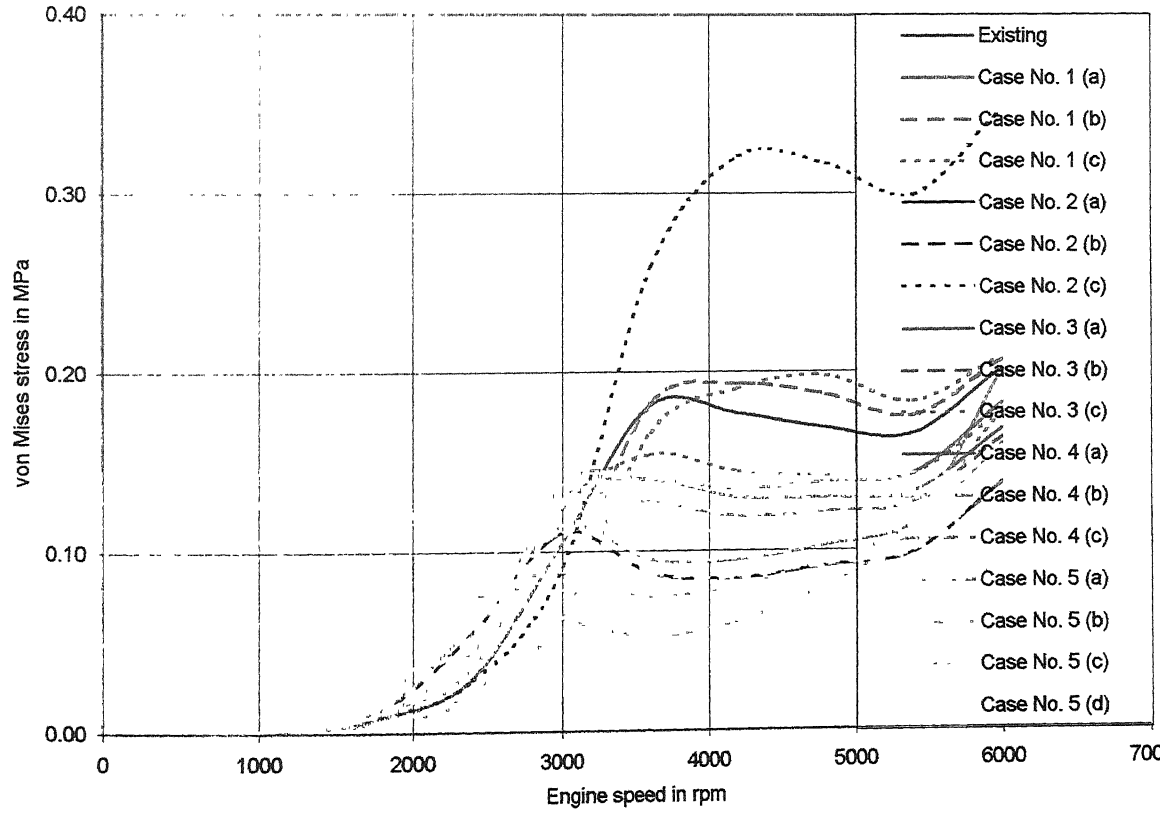

(d) : **von Mises stresses**

FUGURE 4.13 –**Comparison of overall vibrations of steering bar due to added cases**

Chapter - 5

CONCLUSIONS AND SCOPE FOR FUTURE WORK

Computational and experimental investigations have been carried out during the course of present study to understand motorcycle dynamics under engine excitation. The objective was to study vibration behavior of vehicles of a variety of makes and make suggestions on improving the performance characteristics of a specific component.

Motorcycle structural dynamics was simulated computationally through finite element method. The free vibration analysis was carried out and engine forces were calculated. The computed resonant stresses and vibration characteristics provide good information of dynamic behavior of the vehicle and critical speeds. Vibrations levels and overall information about vehicle vibration conditions were determined by making use of frequency response plots and FFT spectra. A good comparative picture of the vibration characteristics of different vehicles has also emerged.

The experimental observations suggested that the performance of the engine of the vehicle, which was computationally modeled, is good. The vehicle however showed large vibration levels on the steering-bar and seat mounting. Comparison between computational and experimental results showed that the finite element model was adequately good. Comparison is based on the assumption that the combustion and inertia force spectrum are sufficient to estimate the vibration levels computationally.

Passive vibration control techniques such as change in stiffness, addition of masses of various location, size, material, and combination of these, have shown improvements in the vibration characteristics of the steering bar. Stiffness reduction and addition of mass towards the tip of the steering bar, have shown improvements. The combined methods – mass addition and structural change have shown a greater reduction in vibration levels.

Further effort is required to identify the physical process corresponding to each harmonic of the measured FFT spectrums and their influence on different design cases. It is also necessary to study convergence aspects and optimum size of geometry in each design cases quantitatively. A study is also required on the selection of the range of engine excitation and appropriate number of influencing harmonics from FFT spectrums.

REFERENCES

1. J. Ben-Ari, G. deBotton, R. Itzhaki and E. Sher, "Fault Detection in Internal Combustion Engines by the Vibration Analysis Method", SAE -1999-01-1223.

2. G. deBotton, J. Ben-Ari and E. Sher, "Vibration Monitoring as a Predictive Maintenance Tool for Reciprocating Engines", Sproc Instn Mech Engrs Vol 214 Part D, ImechE –2000.

3. K. Senthil Kumar, S. Pal, R.C. Sethi, "Objective Evaluation of Ride Quality of Road Vehicles". Vechicle Research & Development Estiblishment, ARAI - 990055, 1999.

4. Robin S. Sharp "Motorcycle Steering Oscillations due to Road Profiling". Autumn Term – 2001, 2001.

5. C. Sujatha & V. Ramamurthi, "Modal and Vibration / Stress Analysis of a Passenger Vehicle by FEM", ARAI – 990003, 1999.

6. "Road Vehicles", ISO Standards Handbook Volume 1 and Volume 2, 1982.

7. "Acoustics Vibration and Shock" ISO Standards Handbook Volume 4, 1980.

8. Adil Jal Durukhanawala "Over Drive " Overdrive Publications, India, 2003.

9. D. J. Ewins, "Modal Testing Theory and Practice ", Research Studies Press Ltd 1984.

10. Jimin He and Zhi-Fang Fu. "Modal Analysis". Butterworth Heinemann, 2001.

11. Don H. Wright. "Testing of Automotive Materials and Components". Society of Automotive Engineers, Inc PA, 1999.

12. Robert C. Eisenmann, Sr., P.E. and Robert C. Eisenmann, Jr. "Machinery Malfunction Diagnosis and Correction". Prentice Hall PTR, New – Jersey, 1998.

13. J. S. Rao "Vibratory Condition Monitoring of Machines". Narosa Publishing House, New Delhi, 2000.

14. Hans B. Pacejka "Tire and Vehicle Dynamics". Butterworht Heinemann, MA, 2002

15. Gordon P. Blair. "Design and Simulation of Four Stroke Engines". Society of Automotive Engineers, Inc PA, 1999.

16. U. Kiencke, L. Nielsen. "Automotive Control Systems for Engine, Driveline and Vehicle". Socity of Automotive Engineers. PA. 2000

17. Shigle, J.E. and Uicker, J. J, "Theory of Machines and Mechanisms", McGraw – Hill, New York 1980.

18. A. R. Holowenko " Dynamic of Machinery " John Wiley and Sons, Inc. 1955.

19. Asok Kumar Mallik "Principles of Vibration Control" East – West Press Private Limited, New Delhi, 1990.

20. Denys J. Mead, "Passive Vibration Control" John Wiley and Sons Ltd. 1998.

21. C.R. Fuller, S.J. Elliott and P.A. Nelson. "Active Control of vibration", Academic Press Inc. California, 1996.

Date Slip

This book is to be returned on the date last stamped.